

The Theory of Spin Noise Spectroscopy: A Review

Nikolai A. Sinitsyn¹ and Yuriy V. Pershin²

¹Theoretical Division, Los Alamos National Laboratory, Los Alamos, NM 87545, USA

²Department of Physics and Astronomy and Smart State Center for Experimental Nanoscale Physics, University of South Carolina, Columbia, South Carolina 29208, USA

E-mail: nsinitsyn@lanl.gov

E-mail: pershin@physics.sc.edu

16 August 2016

Abstract. Direct measurements of spin fluctuations are becoming the mainstream approach for studies of complex condensed matter, molecular, nuclear, and atomic systems. This review covers recent progress in the field of optical Spin Noise Spectroscopy (SNS) with an additional goal to establish an introduction into its theoretical foundations. Various theoretical techniques that have been recently used to interpret results of SNS measurements are explained alongside with examples of their applications.

PACS numbers: 72.70.+m, 72.25.Rb, 78.67.Hc

Submitted to: *Rep. Prog. Phys.*

Contents

1 Introduction	3	7.2 Langevin Equation and Fluctuation-Dissipation theorem	30
2 Spin Correlators: Definition and Basic Properties	5	7.3 Cross-Correlation SNS and Multicomponent Spin Systems	31
2.1 2nd Order Correlator and Noise Power Spectrum	5	7.3.1 Off-Diagonal Correlators.	31
2.2 Higher Order Correlators	6	7.3.2 2D Dirac Materials.	32
3 Survey of Experimental Results and Systems	7	7.3.3 Mixtures of Hot Atomic Vapors.	33
3.1 Hot Atomic Vapors	7	7.3.4 Spatial Correlations.	33
3.1.1 Equilibrium SNS.	7	8 Methods II: Spin Noise of Conduction Electrons	34
3.1.2 Two-Color Spectroscopy.	9	8.1 Drift-Diffusion Approach	34
3.1.3 Beyond Equilibrium and Linear Response.	9	8.1.1 Spin Diffusion Equations	34
3.1.4 Quantum Effects in Atomic Spin Noise.	10	8.1.2 Average Spin Relaxation.	35
3.2 Conduction Electrons in GaAs	10	8.1.3 Spin Fluctuations.	35
3.3 Quantum Dots	11	8.2 Kubo Formula	36
3.4 Magnetic Impurities, Thin Magnetic Films, and Nanomagnets	13	8.3 Quantum Boltzmann Equation	37
3.5 Alternative SNS Techniques	14	8.4 Conduction Electrons Beyond Thermodynamic Equilibrium	38
3.6 Nuclear Spin Noise	14	8.5 Higher Order SNS and Stochastic Path Integral	39
4 Spin Correlators in Quantum Weak Measurement Theory	15	9 Methods III: Discrete Spin Models	39
4.0.1 Weak Measurements.	15	9.1 Symmetric Central Spin Model	39
4.0.2 Formulation Based on Kraus Operators.	16	9.2 Disordered Central Spin Problem	40
5 Faraday Rotation	17	9.3 Spin Cluster Model	41
5.1 Faraday Effect	17	9.4 Central Spin Problem at Higher Temperatures	41
5.2 Faraday Rotation Fluctuations due to Conduction Electrons	18	9.5 Spin Hopping Models	42
5.3 Faraday Rotation from Spins in Quantum Dots	19	9.6 Spin Diffusion in Disordered Spin Lattices	42
5.4 Spin Noise as a Probe of a Homogeneous Line-Width of an Optical Transition	21	10 Perspectives	43
6 Thermodynamic Constraints	23	10.1 Full Counting Statistics	43
6.1 Sum Rules for Integrated Noise Power	23	10.1.1 Phase Transitions in Rare Event Statistics.	43
6.2 Fluctuation-Dissipation Theorem	24	10.1.2 Quantum Entanglement Entropy and Entanglement Witness.	44
6.3 Higher Order Fluctuation Relations	25	10.2 Strongly Correlated Spin Systems	44
6.3.1 Higher Order Onsager Relations.	25	10.3 Extensions of Spin Noise Spectroscopy	45
6.3.2 Bochkov-Kuzovlev Type of Fluctuation Relations.	26	11 Conclusions	45
7 Methods I: Spin Noise Phenomenology	27		
7.1 Spin Fluctuation Dynamics	28		
7.1.1 Bloch Equation.	28		
7.1.2 Noise Power Spectrum in a Tilted Magnetic Field.	28		
7.1.3 Characteristic Sizes of Spin Fluctuations.	29		
7.1.4 Relaxation Time Anisotropy.	29		

1. Introduction

In experimental measurements, the noise is not necessarily a complication. From noise, one can often extract valuable information regarding its sources. Consider, for example, the circuit in Fig. 1(a) containing a resistor and battery. The standard way of measuring the resistance R is by application of a constant voltage V to the resistor and the measurement of average electric current, I . The resistance is then given by $R = V/I$. The noise-based measurement is a less invasive approach. It was shown as early as in 1928 [1, 2] that the resistance can be found from voltage fluctuations at the thermodynamic equilibrium (the Johnson-Nyquist noise [1, 2]) without application of any external voltage (see Fig. 1(b) circuit). Indeed, the fluctuation dissipation theorem states that the voltage variance (mean square) per Hertz of the bandwidth, is given by [3, 4]

$$\langle V^2 \rangle = 4k_B T R, \quad (1)$$

where k_B is the Boltzmann constant, T is temperature, and the average is taken over many repeated measurements. Equation (1) can be used to find the resistance R from measured voltage fluctuations and known temperature.

The above example shows that by studying equilibrium fluctuations we are able to obtain a single characteristic of a circuit component. However, we can achieve much more. By measuring higher correlators of noise (e.g., averages of higher powers of V) or by measuring the noise in a nonequilibrium regime, one can avoid restrictions imposed by the fluctuation-dissipation theorem and obtain the most detailed description of electron interactions [5, 6, 7]. For example, let's consider the case when the applied voltage induces a current, I , with mean and variance, $\langle I \rangle$ and $\text{var}(I) = \langle I^2 \rangle - \langle I \rangle^2$, respectively. The variance can be split into the equilibrium and nonequilibrium parts, $\text{var}(I) = \text{var}(I)_{eq} + \text{var}(I)_{neq}$. The nonequilibrium part carries considerable information about the physics of electrons. In particular, if electrons combine into

quasiparticles of charge e^* , then the ratio of the nonequilibrium variance to mean is proportional to e^* , i.e. $\text{var}(I)_{neq} / \langle I \rangle \sim e^*$ [5]. This observation was used in practice to obtain the long-sought experimental proof of the fact that the quasiparticles in the fractional quantum Hall effect have fractional charges [8, 9].

Unfortunately, the charge current noise has been very hard to study because of multiple parasitic effects induced, e.g., by contacts with leads, measurement devices, etc. The proof of the fractional charge of anyons is one of only a few transformative experimental results in the field of electron counting statistics, while theoretical developments were much more promising. Among them are predictions of new types of quantum phase transitions in rare fluctuations [10], approaches to measure the quantum entanglement entropy [11] and qubit states [12], and results in the area of full counting statistics of strongly correlated electron states [13, 14].

Spin noise spectroscopy (SNS) is an alternative route to obtain information about dynamics of various systems based on their *spin fluctuations*. This method was introduced in the pioneering work of Alexandrov and Zapasskii as early as in 1981 [15]. However, it took over two decades of instrumentation progress including development of real-time fast Fourier transformation (FFT) spectrum analyzers and ultrafast digitizers before this technique had become established as a powerful method to study spin dynamics in atomic gases [16], conduction electrons [17], and localized states in semiconductors [18]. It should be emphasized that currently, there is a large variety of available optical and non-optical spin noise measurement techniques targeting different applications. Some of the experimental methods, such as the resonance force microscopy [19] and NV-center magnetometry [20, 21, 22], have been introduced only recently and may experience considerable development in the near future.

In this review, we will focus on the frequently used optical approach based on the Faraday rotation spectroscopy, which has a relatively broad range of applications and has been the topic of many theoretical and experimental studies during the last decade. To

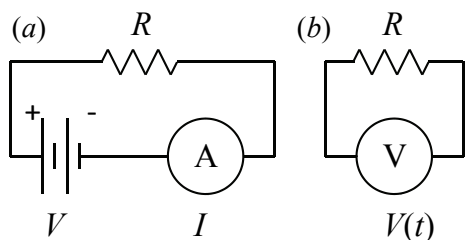


Figure 1. Circuits for (a) standard and (b) noise measurements of the resistance R . Here, A is the ammeter measuring the average current I and V is the voltmeter measuring voltage fluctuations $V(t)$. The constant voltage V across the battery in (a) is known.

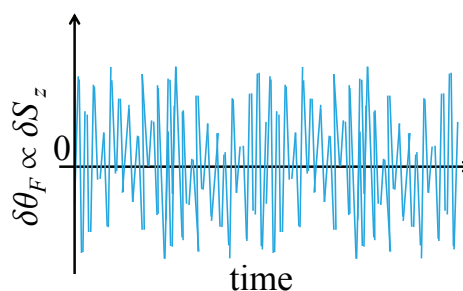


Figure 2. Faraday rotation noise signal in real time.

illustrate the main idea of this technique, let us consider an ensemble of spins in a small mesoscopic volume of an atomic gas or a semiconductor that contains N atoms or electrons with spins in a constant magnetic field B . Statistical fluctuations of N paramagnetic spins should generate spin fluctuations of the order of \sqrt{N} , even in a zero magnetic field at equilibrium [16]. Optically, such fluctuations are measured by detecting the Faraday rotation (Fig. 3(a)) of the polarization axis of a linearly polarized beam ($\sim 1\text{-}100\ \mu\text{m}$ diameter) passing through a sample ‡. A typical experimental setup is shown in Fig. 2.

The polarization rotation angle is proportional to the local instantaneous magnetization of the illuminated region and its fluctuations can be traced with sub-nanosecond resolution in time [23, 24, 25, 26], thus providing considerable statistical data about local magnetization dynamics. The spin noise power spectrum is found as FFT of the autocorrelation function $\langle S_z(t)S_z(0) \rangle$ (for an example, see Fig. 3(b)). The position and shape of the spin noise peaks are used to extract physical parameters of a particular system. Importantly, the frequency of the measurement beam can be detuned from system resonances so that dissipative effects during measurements are minimized. Therefore, spin fluctuations can be studied in spin systems at the thermodynamic equilibrium without inducing undesired extrinsic excitations. Potentially, this technique can be applied to any material that demonstrates measurable Faraday or Kerr rotations induced by partial spin polarization. These include most known semiconductors, topological insulators, unconventional superconductors, as well as atomic gases.

The research on SNS is highly interdisciplinary with diverse applications in the areas of atomic gases, conduction electrons, spintronics, optoelectronics, semiconductor quantum dots, spin glasses, and micromagnetics. By itself, SNS essentially differs from the traditional methods used in materials science. Moreover, the very type of data that SNS deals with is unusual for condensed matter physics. SNS works with *stochastic signals* that often have to be processed with a rate of gigabytes per second, sometimes during days or longer [27, 28].

Several reviews have been already written about SNS with the focus on experimental developments [29, 30, 31, 32, 33, 34]. The goal of the present review is different. Despite diverse applications, there are established theoretical methods and results that can be useful for theorists entering or working in this field. We wrote our review to provide an introduction to SNS from the theoretical point of view minimizing

‡ Note that the relative fluctuations $\sim \sqrt{N}/N = 1/\sqrt{N}$ increase with decreasing the beam diameter.

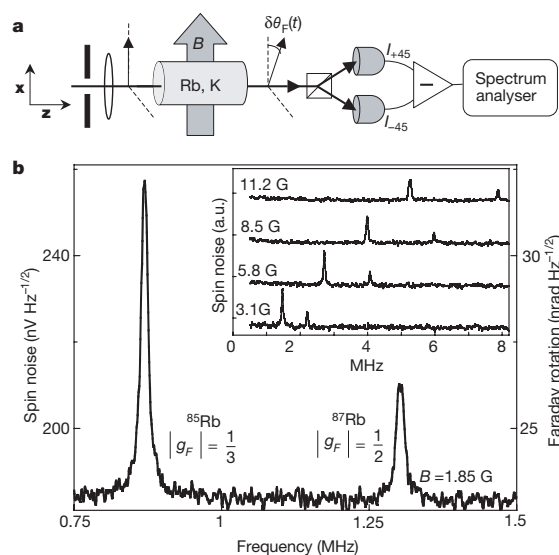


Figure 3. SNS of Rb vapor [16]: (a) The experimental setup: a linearly polarized laser beam ($\sim 1\text{-}100\ \mu\text{m}$ diameter) passes through a small volume of gas. The outgoing beam experiences measurable Faraday rotation of polarization, $\delta\theta_F$, proportional to the instantaneous gas magnetization in the volume. (b) The noise power spectrum from Rb vapor showing two peaks from ^{85}Rb and ^{87}Rb at corresponding Larmor frequencies. For more details, see Ref. [16]. Reprinted with permission from Macmillan Publishers Ltd: Nature 431, pp. 4952, 2004, Copyright ©(2004) [16].

the discussion of instrumentation. Thus, our main attention is focused on the theoretical justification of the technique, theoretical methods to study spin noise, and the problems that will likely benefit from advances in the theory of SNS in the future.

Our review is organized as follows. In Sec. 2, we define various spin correlators and discuss their elementary properties. In Sec. 3, we review available experimental results from the theoretical perspective, illustrating theoretical problems and providing examples of elementary theoretical calculations. Moreover, in order to place the optical SNS into a broader context, subsection 3.5 contains a brief review of several alternative spin noise characterization techniques. In Sec. 4, we provide quantum theory of spin correlators in the weak measurement framework. Section 5 contains an introduction to the theory of measurement based on the Faraday rotation effect. Section 6 is devoted to sum rules that are applicable practically to all spin systems studied by SNS. Sections 7-9 review theoretical methods that are frequently used in the research on SNS. Section 10 reviews possible future research directions and extensions of SNS.

Different sections of this review are written at different levels of complexity. Sections 2-3 set the framework of problems for the rest of the review and provide introduction to the SNS at a nonspecialist

level. Sections 4-7 contain introductions to different theoretical aspects of the optical SNS with many worked out examples. Although there are occasional cross-references between these sections, they are independent of each other and can be read in an arbitrary order. Subsections 8.1 and 8.2 are written in the same style but they should be more accessible to readers with prior experience in spin drift-diffusion equation and Kubo formula. In sections 8.3-10, we return to the “review” mode in order to cover a large variety of other, more specified, theoretical ideas without attempting to provide a detailed introduction.

2. Spin Correlators: Definition and Basic Properties

2.1. 2nd Order Correlator and Noise Power Spectrum

The simplest characteristic that describes correlations of a signal in SNS is the spin-spin correlator

$$g_2(t_2, t_1) \equiv \langle S_z(t_2)S_z(t_1) \rangle, \quad (2)$$

where $S_z(t)$ is the time-dependent spin polarization in the observation region and z is the measurement axis. Generally, this correlator is a function of two time arguments, however, if measurements are performed in the steady state then (due to the translation invariance in time) this correlator depends only on the time difference t :

$$g_2(t) = \langle S_z(t)S_z(0) \rangle. \quad (3)$$

In many (but not all [35]) experimental setups, it is much more convenient to process signals in the frequency domain. Let’s consider first the straightforward way to calculate the correlator (3) from an experimentally measured “trajectory” $S_z(t)$. In order to obtain (3), the total measurement time interval should be divided into relatively long time intervals $T_m \gg \tau_s$, where τ_s is the characteristic spin relaxation time. Each time interval of size T_m also consists of $N_m \gg 1$ elementary intervals of size $dt \ll \tau_s$. Naively, one may think that in order to obtain (3), one should take all pairs of time moments, t_i and t_{i+j} , within the same time interval of size T_m , and calculate all possible products of measurement results $S_z(t_{i+j})S_z(t_i)$. Then, the average over i provides $\langle S_z(t_j)S_z(0) \rangle$. Additional averaging over the large time intervals of size T_m further increases the precision of calculations. This straightforward process, however, is not optimal as N_m measurement points in the interval T_m require the calculation of $\sim N_m^2$ products $S_z(t_{j+i})S_z(t_i)$ in order to estimate correlator (3) for all different t . For measurements performed with, e.g., a nanosecond resolution, continuous data processing imposes very strict hardware requirements that are difficult to satisfy.

The widely used approach is based on the Fourier transform of the recorded trajectory during the measurement interval T_m

$$a(\omega) = \frac{1}{\sqrt{T_m}} \int_0^{T_m} dt e^{i\omega t} S_z(t). \quad (4)$$

A typical FFT algorithm (e.g., the Cooley-Tukey FFT algorithm) requires $t \sim N_m \log(N_m) \ll N_m^2$ steps to perform. Note that since the measured trajectory $S_z(t)$ is real, $a(-\omega) = a^*(\omega)$. For a system in the steady state, $\langle a(\omega) \rangle = 0$ at $\omega \neq 0$, where the average is considered over repeated time intervals of size T_m under identical experimental conditions §.

The most accessible physically interesting characteristic in the frequency domain is the *noise power spectrum*, defined as

$$C_2(\omega) = \langle |a(\omega)|^2 \rangle. \quad (5)$$

One can easily prove that, due to the translation invariance in time,

$$\langle a(\omega)a(\omega') \rangle = 0, \quad \text{for } \omega \neq -\omega'.$$

It is crucial for fast signal processing that $C_2(\omega)$ depends only on a single argument, so that its calculation for all independent values of ω scales as $\sim N_m$ for a discretized signal, as desired, so the slowest step in determining $C_2(\omega)$ is application of the FFT algorithm.

Another important property of the noise power spectrum is the additivity, namely, the contributions from independent noise sources add to each other. Indeed, suppose that the measured Fourier transform of the signal is given by $a(\omega) = a_{\text{ph}}(\omega) + \zeta(\omega)$, where $a_{\text{ph}}(\omega)$ is the physical spin noise signal and $\zeta(\omega)$ is an uncorrelated from $a_{\text{ph}}(\omega)$ background noise that originates, e.g., from an amplifier or represents the photon shot noise. In such a case $\langle a_{\text{ph}}(\omega)\zeta(\omega) \rangle = 0$, so

$$C_2(\omega) = \langle |a_{\text{ph}}(\omega)|^2 \rangle + \langle |\zeta(\omega)|^2 \rangle. \quad (6)$$

It is possible then to get rid of the background part by measuring it separately. The most popular way to do this is to measure the spectrum in a large external magnetic field applied in the transverse direction to the measurement beam. This field induces fast spin precessions that move the physical part of the noise power to very high frequencies. By measuring the background level in such a field, the physical noise is obtained by subtracting $\langle |\zeta(\omega)|^2 \rangle$ from (6).

The noise power spectrum is also often easier to interpret than the spin-spin correlator in real time.

§ Generally, $S_z(t)$ may have a constant component, so that $\langle S_z(t) \rangle = 0$ is not required.

However, if correlators are needed in the time domain, there is the following important theorem that relates the noise power spectrum to the time correlator $g_2(t)$:

Wiener-Khinchine theorem [36]: In the steady state, the noise power spectrum and the spin-spin correlator are related by the Fourier transform:

$$C_2(\omega) = 2 \int_0^{\infty} dt \cos(\omega t) \langle S_z(t) S_z(0) \rangle. \quad (7)$$

This theorem requires several conditions, such as the requirement that the measurement time is much longer than the spin relaxation time ($T_m \gg \tau_s$), which are discussed in more detail, e.g., in [36, 37]. Apart from these details, the proof is straightforward: Substituting the definition of the Fourier transformed trajectory (4) into (5), and using the property $g_2(t_1, t_2) = g_2(t_1 - t_2)$ and the fact that, since $S_z(t)$ is real, $a^*(\omega) = a(-\omega)$, we find

$$C_2(\omega) = \frac{1}{T_m} \lim_{T_m \rightarrow \infty} \int_{-T_m/2}^{T_m/2} dt_1 \int_{-T_m/2}^{T_m/2} dt_2 e^{i\omega(t_1 - t_2)} \times \langle S_z(t_2) S_z(t_1) \rangle = \int_{-\infty}^{\infty} dt e^{i\omega t} \langle S_z(t) S_z(0) \rangle. \quad (8)$$

Taking into account that $S_z(t)$ is the real valued signal, i.e. it is not an operator, we can use the property $\langle S_z(-t) S_z(0) \rangle = \langle S_z(t) S_z(0) \rangle$, which demonstrates that the last integral in (8) coincides with (7). This proves the theorem.

The optical SNS is not restricted to measurements of a single spin component or to fluctuations in homogeneous spin systems. In such situations, one can consider cross-correlations of spin densities with different indexes, e.g.,

$$C_{AB}(\omega) = \int_{-\infty}^{\infty} dt e^{i\omega t} \langle S_A(t) S_B(0) \rangle, \quad (9)$$

where A and B are indexes that may correspond to different atomic species in an interacting gas mixture or different spin projections probed by noncollinear beams. Generally, the cross-correlator $C_{AB}(\omega)$ is not positive definite. Moreover, it can have both real and imaginary components.

An example of the experimentally measured noise power spectrum is shown, e.g., in Fig. 3(b). Typically, the spectrum consists of one or several peaks. Two types of peaks are most frequently encountered: the Lorentzian shaped peaks

$$C_2^L(\omega) \sim \frac{1}{(\omega - \omega_L)^2 + \Gamma^2}, \quad (10)$$

and Gaussian shaped peaks

$$C_2^G(\omega) \sim e^{-\frac{\omega^2}{2\Gamma^2}}, \quad (11)$$

where Γ is a characteristic spin relaxation rate. Performing the inverse Fourier transform, one can verify that, in the time domain, the Lorentzian shape corresponds to the exponentially damped spin precession

$$g_2^L(t) \sim e^{-\Gamma|t|} \cos(\omega_L t). \quad (12)$$

The Fourier transform of the Gaussian function remains the Gaussian one:

$$g_2^G(t) \sim e^{-\Gamma^2 t^2 / 2}. \quad (13)$$

The exponential relaxation (12) is usually associated with processes involving numerous fast mutually-uncorrelated microscopic interactions, such as atomic collisions, that contribute to the observed relaxation. The relaxation according to the Gaussian law (13) usually indicates the presence of dephasing processes, as in the case of an ensemble of similar systems with a Gaussian distribution of time-independent parameters.

2.2. Higher Order Correlators

A spin system's n -th order time-correlator is the average of a product of n results of the spin polarization measurements taken at different moments of time. The information content of 2nd order correlators is intrinsically limited. Actually, this is not surprising as the noise power spectrum tells us only the weight of each frequency in the dynamics of spin polarization without providing any information regarding correlations among different frequencies. The complete information about an interacting spin system is contained in the full set of all-order correlators [38]. Hence, the *higher order* SNS is very interesting direction for future research.

Higher order correlators depend on more than one frequency, therefore, they are usually represented by multidimensional data, e.g. in the form of 2D or 3D density plots, that contain additional and, possibly, considerably larger amount of information about the system than the noise power spectrum [39]. This information can be particularly useful when the studied spin system experiences fluctuations at different time scales, such as in the case of a qubit interacting with a slowly changing configuration of nuclear spins and simultaneously fast fluctuating spin-orbit fields due to interactions with phonons. In other words, higher order correlators are sensitive to the homogeneous broadening even in a strongly inhomogeneously broadened system, i.e. they can be used to separate the effect of a static disorder from the intrinsic spin dynamics.

Another interesting property of higher order correlators is their intrinsic “quantumness”: Quantum measurements at intermediate time moments generally break the unitarity of evolution during the observed time interval. This fact may strongly influence higher order correlators, as it was demonstrated in a recent experiment [40], which extracted the quantum life time from an inhomogeneously broadened spectrum of a quantum dot spin qubit by using quantum properties of the 3rd order correlator of spin projection operators.

To define higher order cumulants in the frequency domain, let us introduce the normalized spin polarization

$$\delta S_z(t) = S_z(t) - \langle S_z \rangle, \quad (14)$$

and consider its Fourier transform $a(\omega)$. Similarly to the 2nd order correlator, in the steady state, only the products of $a(\omega_i)$ with $\sum_i \omega_i = 0$ remain non-zero after the averaging. Hence, the next nearest nontrivial correlator of $a(\omega)$ is the 3rd order one given by

$$C_3(\omega_1, \omega_2) = \langle a(\omega_1)a(\omega_2)a^*(\omega_1 + \omega_2) \rangle. \quad (15)$$

A specific property of C_3 is that it is zero in a system with time-reversal symmetry because spin variables are odd under the time reversal. Note also that the 3rd order correlator (15) is generally complex-valued.

In the steady state, the 4th order cumulant is generally a function of three independent frequencies. Its definition depends on whether the sum of any two of these frequencies is zero or not. If the latter is the case, the 4th cumulant in the frequency domain can be defined as

$$C_4(\omega_1, \omega_2, \omega_3) = \langle a(\omega_1)a(\omega_2)a(\omega_3)a^*(\omega_1 + \omega_2 + \omega_3) \rangle. \quad (16)$$

In the case of $\omega_1 = -\omega_3 \neq \omega_2$, the 4th order cumulant is defined as

$$C_4(\omega_1, \omega_2) \equiv \langle |a(\omega_1)|^2 |a(\omega_2)|^2 \rangle - \langle |a(\omega_1)|^2 \rangle \langle |a(\omega_2)|^2 \rangle. \quad (17)$$

Note that (17) cannot be obtained as a special case of (16). The choice of the form of cumulants at equal values of some frequency parameters is dictated by the requirement that such cumulants should be zero for Gaussian fluctuations of $a(\omega)$, so that the higher order cumulants do not duplicate the information that can be obtained from the lower ones. The correlators that depend on two frequencies, such as the 3rd order correlator (15) or the correlator (17), are often called the *bispectra*. A bispectrum indicates how spin noise components at two different frequencies “talk” to each other. For example, if $C_4(\omega_1, \omega_2)$ is negative, one can conclude the presence of anti-correlations, i.e. the observation of a strong signal at one frequency means that another frequency is likely suppressed, etc. An illustrative example of the experimental measurement

of the correlator (17) can be found in [41]. Moreover, for $\omega_1 = \omega_2 = -\omega_3 \equiv \omega$, the 4th cumulant is given by:

$$C_4(\omega) \equiv \langle |a(\omega)|^4 \rangle - 2\langle |a(\omega)|^2 \rangle^2. \quad (18)$$

Finally, there is a generalization of the correlator (17) called the “noise of susceptibility” [42, 43]. In the correlator (18), the product of 4th order spin variables is averaged over repeated time intervals of duration T_m . Instead, one can measure the noise powers, $|a(\omega_1)|^2$ and $|a_T(\omega_2)|^2$, of *different* time intervals separated by a given duration T , e.g., $(t, t+T_m)$ and $(t+T, t+T+T_m)$. One can then consider their product averaged over all such pairs of intervals with different t , separated by time T :

$$\begin{aligned} \chi^{(4)}(\omega_1, \omega_2|T) &= \\ &= \langle |a(\omega_1)|^2 |a_T(\omega_2)|^2 \rangle - \langle |a(\omega_1)|^2 \rangle \langle |a_T(\omega_2)|^2 \rangle. \end{aligned} \quad (19)$$

3. Survey of Experimental Results and Systems

3.1. Hot Atomic Vapors

Hot atomic vapors are usually evaporated gases of atoms, such as K, Rb, Cs, above the room temperature (e.g., at 400K). Atoms in a hot vapor are relatively energetic, so that the average occupancy of states in these vapors is small ($\ll 1$). In this regard, hot atomic vapors are different from ultra-cold gases, in which atoms tend to occupy the lowest energy levels.

Hot atomic vapors have broad applications in magnetometry and isotope separation techniques [44, 45]. As spin fluctuations limit the precision of these applications, future advances in these fields will likely depend on our understanding of spin noise and our ability to control it. In fact, strategies to suppress unwanted spin fluctuations by a feedback control have been recently demonstrated [46, 47]. We also mention that a random number generator based on the atomic spin noise was recently proposed [48].

3.1.1. Equilibrium SNS. The nowadays interest in spontaneous spin fluctuations at the thermodynamic equilibrium originates from the pioneering experiments on Rb and K atomic vapors [16]. These experiments clearly resolved spin noise power peaks (Fig. 3(b)) and explored the strategies for digital signal processing. The noise power peaks were associated with resonances of hyperfine coupled electronic spins. This work has clearly demonstrated that spin interactions can be studied at the thermodynamics equilibrium without externally exciting a system.

Consider the atomic vapor of ^{41}K that was investigated by SNS in Refs. [50, 51]. Figure 4 shows the experimental setup and the equilibrium noise power spectrum of this vapor measured in the

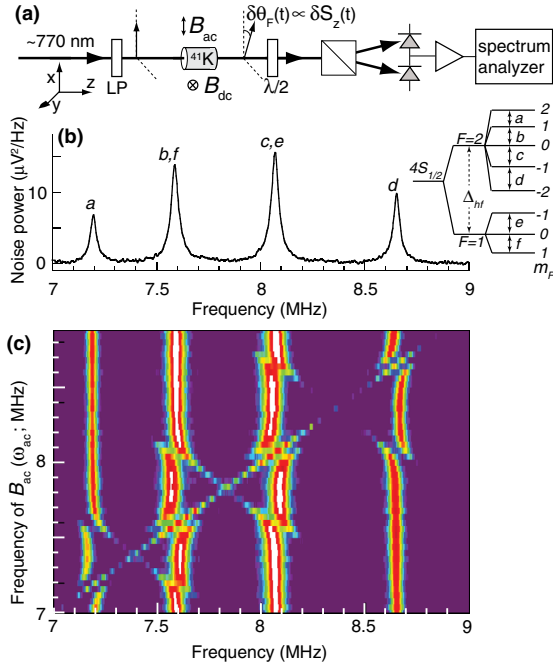


Figure 4. Spin noise spectroscopy of ^{41}K vapour subjected to a dc and weak ac magnetic fields. (a) The measurement setup. (b) The equilibrium noise power spectrum of ^{41}K atomic vapor ($B_{ac} = 0$). (c) The density plot of the noise power spectrum vs frequency of an ac-magnetic field applied in the transverse to the measurement beam direction. Simultaneous response of more than one peak to such external perturbation reveals cross-correlations between different spin resonances. Reprinted figure with permission from P. Glasenapp, et al., Physical Review Letters 113, p. 156601, 2014 [49]. Copyright ©(2014) by the American Physical Society.

applied magnetic field. The spectrum consists of four Lorentzian peaks centered at different frequencies.

In ^{41}K atoms, the uncompensated electronic spin with $S = 1/2$ couples relatively strongly with a nuclear spin of $I = 3/2$. The eigenstates of the exchange Hamiltonian $\hat{H}_0 = \hat{\mathbf{S}} \cdot \hat{\mathbf{I}}$ split into two multiplets with the total angular momentum $F = 1$ and $F = 2$. The hyperfine splitting between the two multiplets is about 254 MHz, which is much higher than the frequency range of the spectrum shown in Fig. 4(b). The external magnetic field $\mathbf{B} = B\hat{y}$ modifies the Hamiltonian: $\hat{H} \approx \hat{H}_0 + g\mathbf{B} \cdot \hat{\mathbf{S}}$. Figure 5 shows that the magnetic field \mathbf{B} splits each multiplet into energy levels characterized by the projection of the total angular momentum M on the field axis. Different pairs of nearest levels generally experience a different size of splitting. We also note that the temperature of the atomic gas $T \sim 400\text{K}$ is orders of magnitude higher than the splitting between any pair of energy levels in Fig. 5. Therefore, one can consider that these levels are occupied with equal probabilities.

Let us assume that the measurement axis is

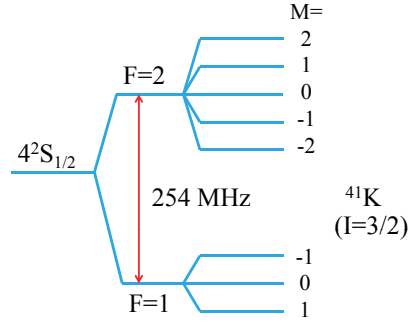


Figure 5. $4^2S_{1/2}$ level diagram for ^{41}K atom in a constant magnetic field.

transverse to the magnetic field direction as shown in Fig. 4(a). The optical beam couples to the electron spin operator \hat{S}_z that has nonzero matrix elements only between the pairs of states with $\Delta M = \pm 1$, where M is the angular momentum projection on the magnetic field axis. The spin-spin correlator in real time can then be estimated as

$$\begin{aligned} \langle S_z(t)S_z(0) \rangle &\sim \sum_i \langle E_i | e^{i\hat{H}t} \hat{S}_z e^{-i\hat{H}t} \hat{S}_z | E_i \rangle = \\ &= \sum_{i,j=i\pm 1} e^{i(E_j - E_i)t - \gamma_{ij}t} |\langle E_i | \hat{S}_z | E_j \rangle|^2, \end{aligned} \quad (20)$$

where E_j are the energies of the levels and index i runs through all states. Note that in Eq. (20), for each resonance with the energy difference $E_j - E_i$, we introduced a phenomenological relaxation rate γ_{ij} .

Equation (20) shows that each pair of adjacent energy levels within each multiplet in Fig. 5 contributes to the correlator with a damped oscillatory term $\sim e^{-\gamma_{ij}t} \cos([E_i - E_j]t)$. After taking the Fourier transform, each such a term produces a Lorentzian peak, each such a term produces a Lorentzian peak, each such a term produces a Lorentzian peak with the energy difference $E_j - E_i$ (for $\omega > 0$) with the width determined by the relaxation rate γ_{ij} . Hence, the positions of these peaks can be used to find characteristic splittings between the energy levels, while their widths can be used to extract the relaxation rates. Moreover, Eq. (20) shows that the amplitudes of the peaks contain information about the matrix elements $\langle E_i | \hat{S}_z | E_j \rangle$.

Finally, we note that energy splittings between the levels with $M = 0, 1$ for $F = 1$ and $F = 2$, as well as between the levels with $M = -1, 0$ for $F = 1$ and $F = 2$, are degenerate. This explains the only four peaks observed in Fig. 4(b) instead of six peaks as Fig. 5 suggests. Consequently, each of the two central peaks in Fig. 4(b) is the result of the overlap of two peaks from different resonances. This partly explains the relatively high amplitudes of the central peaks.

Relative heights of the peaks and their behavior in external fields in relation to the matrix elements

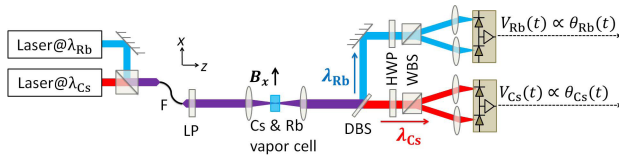


Figure 6. Two probe beams measure fluctuations of spins of different atomic species. Cross-correlations between spin fluctuations of different spin species provide information regarding interactions between these different types of spins. Reprinted with permission from Macmillan Publishers Ltd: Scientific Reports 5, article number: 9573, 2015, Copyright ©(2015) [66].

of the measured electronic spin operator at different moments of time were discussed in [50, 51]. In [52], an SNS-based approach to high precision relaxation time measurements was developed. In [53], the effect of the probe beam frequency on the spin noise spectrum was explored. Peculiarities of near the resonance response were attributed to collective effects. Atomic gases were also used as a simple testbed to improve SNS instrumentation [54] and to demonstrate extensions of this technique [41, 55].

Experiments with hot atomic gases are relatively simple. They do not require cryogenic equipment. Statistical filtering of physical spin correlators from the background noise in hot atomic gases, such as ^{41}K , can be achieved within few seconds. Moreover, the electronic quantum states of different atomic isotopes have been extensively studied by atomic physicists throughout the 20th century and can be considered very well understood. Due to this simplicity, a methodology to teach the basics of SNS in undergraduate laboratories was proposed in [56]. Hot atomic vapors are also ideal for testing new measurement approaches and producing artificially correlated spin systems. Below, we discuss a few such examples.

3.1.2. Two-Color Spectroscopy. Electron spins cannot be generally considered identical even in the same observation region. They can be localized near different impurities, inside different quantum dots, etc. There are numerous natural and engineered systems in which interactions between “spins of different kind” are important. Examples include the Kondo-lattices in correlated-electron materials [57, 58], decoherence of solid-state spin qubits by a nuclear spin bath [59, 60, 61, 62], ferromagnetism in diluted magnetic semiconductors [63, 64], and spin-exchange pumping of noble gas nuclei for medical imaging [65].

In [66], cross-correlations between spins of different kind were effectively characterized by multi-probe SNS. The idea of this experiment is shown schematically in Fig. 6, wherein two atomic vapors,

Cs and Rb, interact by the direct spin exchange at the thermal equilibrium. In this experiment, the spin fluctuations from Cs and Rb are independently detected, and signatures of spin interactions are observed in the cross-correlator (9) of these two spin noise signals. The authors of [66] have demonstrated that the spin relaxation and spin exchange rates can be measured separately without ever perturbing the gas mixture from the thermodynamic equilibrium.

3.1.3. Beyond Equilibrium and Linear Response.

One of the central results in statistical physics – the fluctuation-dissipation theorem – tells us that the information provided by the 2nd order correlators taken at the thermodynamic equilibrium is equivalent to the information that can be obtained by measuring a macroscopic linear response characteristic, such as the spin susceptibility. In this sense, the 2nd order correlator of spin fluctuations at the thermodynamic equilibrium does not provide any new information compared to the information that can be obtained, e.g., by the well developed pump-probe technique [67], at least in principle.

However, the 2nd order correlator measured at *nonequilibrium* conditions is generally independent of the linear response characteristics. The authors of [49] have explored the spin noise in the presence of a weak radio frequency magnetic field, which was transverse both to the measurement and constant field axes. This work demonstrated the possibility of a *multidimensional* SNS [38, 68], in which the noise power spectrum is represented as a function of both intrinsic and driving field frequencies in a 2D density plot (as an example see Fig. 4(c)). Such multidimensional data show underlying patterns of correlations between different frequencies and reveal numerous effects at the fluctuation level beyond the equilibrium and linear response.

The multidimensional plots, such as Fig. 4(c), can be interpreted within the so called “dressed state” Hamiltonian

$$\hat{H}_d = \hat{H} + \hat{H}_{EM} + \hat{V} \quad (21)$$

that describes the interaction of an atom with a coherent state of the electromagnetic field. Here \hat{H} is the unperturbed atomic Hamiltonian, \hat{H}_{EM} is the secondary quantized Hamiltonian of the magnetic ac-field

$$\hat{H}_{EM} = \omega_{ac} \hat{a}^\dagger \hat{a}, \quad (22)$$

where \hat{a}^\dagger and \hat{a} are the creation and annihilation operators of the photons corresponding to this field mode, and

$$\hat{V} = \sum_i \tilde{\mu}_i B_{ac} (|E_i\rangle \langle E_{i+1}| (\hat{a} + \hat{a}^\dagger) + \text{h.c.}) \quad (23)$$

is the term describing the coupling of the radio frequency field of the amplitude B_{ac} to the atomic spin states.

The electron spin-spin correlator of such a system can be calculated similarly to Eq. (20) with the only difference that the index i runs now throughout the eigenstates of the total Hamiltonian (21). For a weak ac-field, the interaction term (23) can be treated as a perturbation. In the first order in \hat{V} , the off-resonance values of the ac-field do not influence the spectrum. However, if ω_{ac} is in resonance with any of the peaks then the corresponding peak splits into the so-called Mollow triplet [69] of three peaks. Moreover, if such a resonance shares a quantum level with another resonance, the latter also splits in the so-called Autler-Townes doublet [70] of two peaks. The distance between such splitted peaks is linear in the ac-field amplitude, B_{ac} . Higher ac-field amplitude leads to clearly observable nonlinear effects in the noise power spectrum, such as the appearance of the spin noise power peak centered at $\omega = \omega_{ac}$, additional splittings of other peaks, shifts of their positions, etc. [49].

The theory of dressed states is very well developed and cannot be reviewed here in detail. Fortunately, fairly complete and comprehensive introductions into this topic already exist (we refer to Refs. [71, 72] for further information). It should be emphasized that the importance of the work [49] stems from the fact that for the first time the rich physics of dressed states was observed at the fluctuation level without applications of pump laser pulses [49].

The experimental demonstration of spontaneous spin fluctuations under steady nonequilibrium conditions in atomic vapors [49] was followed by several theoretical studies suggesting a broad range of applications for *non-equilibrium* SNS. In particular, it was proposed to use an ac-magnetic driving to identify spin relaxation rates when the spin noise power spectrum is inhomogeneously broadened (the quantum dots case) [73]. In the case of electronic transport, several effects (related to spin noise) were predicted both in the linear response regime [74, 75] and far from equilibrium [76]. The optical pumping can also be used to create nonequilibrium conditions. Spin noise of optically induced excitons in semiconductors was explored theoretically in [77].

3.1.4. Quantum Effects in Atomic Spin Noise. Squeezed spin states can be less susceptible to quantum projection noise and thus can be used to increase the sensitivity of magnetometers [78]. Experimental studies of quantum projection noise and other spin fluctuations in such artificially correlated atomic systems were reported in [79, 80, 81, 82, 83]. The magnitude of artificially introduced correlations makes

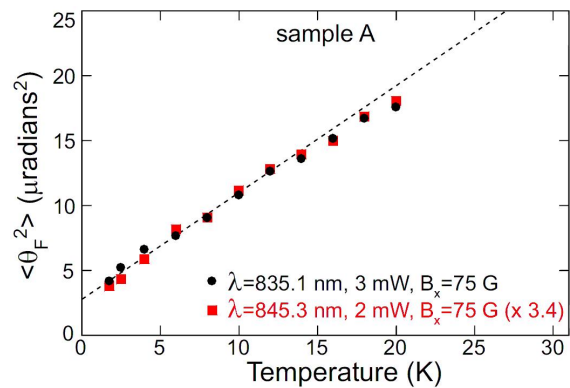


Figure 7. The integrated noise power $P_{\text{int}} = \int C_2(\omega)d\omega$ of electronic spins in GaAs as a function of temperature. Linear scaling is in good agreement with predictions of the Fermi liquid theory. A finite offset, however, indicates either localization effects or the presence of other spin noise sources in the sample. Reprinted figure with permission from S. A. Crooker et al., Physical Review B 79, p. 035208, 2009 [86]. Copyright ©(2009) by the American Physical Society.

possible observing their higher order spin cumulants experimentally [84].

We anticipate numerous applications of the optical SNS in atomic Bose-Einstein condensates and other ultracold atomic and molecular systems. Currently, however, we are still at the very early stage in investigations of the spontaneous equilibrium spin fluctuations in these systems using the optical SNS. In fact, the proof-of-principle experiment was reported [85]. This work communicates time-dependent spin fluctuations in a cold atomic Fermi gas paying attention also to quantum measurement effects.

3.2. Conduction Electrons in GaAs

The first proof-of-principle measurements of the noise power spectrum of conduction electron spins in GaAs revealed a much weaker useful signal in comparison to atomic gases [17]. Nevertheless, considerable improvements at the instrumentation and software levels [27, 86, 87] have quickly enabled numerous SNS applications:

- The temperature-dependent spin relaxation rate and the Lande g -factor at the thermodynamic equilibrium were studied in [86]. The dependence of the spin noise power spectrum on the doping concentration level was explored in [88, 89]. The influence of optical excitations on spin noise in semiconductors was investigated in [90].
- Measurements of spin noise with *picosecond* time resolution were reported in [23]. Such a *high bandwidth spectroscopy* was used to observe inhomogeneous broadening of the spin noise peak

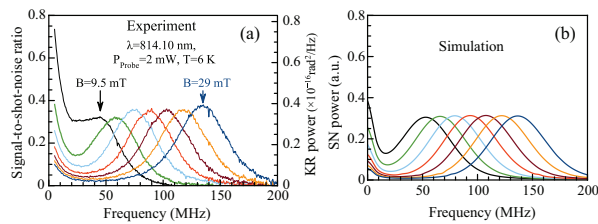


Figure 8. Spin noise from a single GaAs quantum well embedded into a microcavity [94]. (a) Measured noise power spectrum of conduction electrons. (b) Predictions of the theoretical model in [94] that includes exciton effects. Reprinted figure with permission from S. V. Poltavtsev et al., *Physical Review B* 89, p. 081304, 2014 [94]. Copyright ©(2014) by the American Physical Society.

of conduction electrons in a relatively large magnetic field [23].

- The inverse Faraday effect [91], i.e. the appearance of an effective magnetic field induced by a circularly polarized light, was observed at the spin noise level [92].
- The observation of a slow evolution of the noise power spectrum of electrons interacting with polarized nuclear spins was reported in [93].

Spin dynamics of conduction electrons in n -doped materials has been relatively well understood prior to the appearance of SNS. However, some features of spin noise in GaAs are still obscure. One such observation [86] concerns the behavior of the integrated noise power, $P_{\text{int}} = \int P(\omega)d\omega$, as function of temperature T . The Fermi liquid theory predicts its linear scaling $P_{\text{int}} \sim T$ at low temperatures. However, the experiment [86] showed rather a linear scaling with an offset, $P_{\text{int}} = a + bT$, where a and b are constants (Fig. 7). The origin of this offset is not quite understood. It can be due to the conduction electron localization or presence of deep donor bound states.

Another not fully explained feature of the noise power spectrum is a small peak centered at zero frequency that persists even in presence of an in-plane magnetic field (Fig. 8). The magnetic field shifts most of the noise power to the major Lorentzian peak centered at the Larmor frequency but a small fraction of the noise power remains peaked at $\omega = 0$. Different explanations of this phenomenon have been proposed. For example, a small ellipticity of the probe beam polarization can lead to the inverse Faraday effect [91], which does lead to a zero frequency peak [93]. Another possible explanation is the presence of localized states, which contribution to the spin noise power is usually centered at zero frequency at weak external fields [18]. There has also been a proposal to relate this effect to excitons [94].

An important future goal is to extend SNS to conduction electrons in other materials. New

measurement schemes have been proposed to increase the useful signal-to-background ratio [35, 95, 96]. A big step in this direction was an experiment on placing a 2D electron system in a microcavity that considerably enhanced coupling of the probe beam to spins of conduction electrons [94]. This geometry increased the useful signal by orders of magnitude and allowed studies of spin noise from only a few hundreds of electrons instead of millions in early experiments. Such micro-cavities can also be used to produce strongly correlated spin-photon states, which can be revealed by spin noise measurements [97].

3.3. Quantum Dots

Prior to the advances in SNS, the experimental studies of decoherence and relaxation of quantum dot spin qubits could not verify numerous theoretical predictions. Earliest applications of the SNS to hole-doped InGaAs quantum dots showed a relatively strong useful signal per spin [18, 98]. Subsequent studies of the spin noise power spectrum of quantum dots have not only verified some of the theories but also revealed some unexpected behavior. It was clearly demonstrated that SNS is capable of resolving important questions in materials science and uncover new physical phenomena.

When GaAs samples are grown with an admixture of indium atoms that substitute gallium, indium does not dissolve in the lattice uniformly but rather creates InAs “droplets” of a few tens of nm diameter and several nm height (shown in Fig. 9(a)), which are called the self-assembled quantum dots (QD). QDs provide a confining potential for a localized single electron or hole state with an uncompensated spin.

In a relatively strong in-plane magnetic field, the spin noise power spectrum of hole-doped QDs was found to be in a good agreement with theoretical expectations [18]. The spectrum consists of a shallow Gaussian peak, which indicates the presence of the Larmor precession with a strong inhomogeneous broadening due to different values of the Lande g -factor of hole spins in different QDs. Moreover, the measured anisotropy of the g -factor was in a good agreement with theoretical predictions [18]. At zero magnetic field but relatively high temperatures, $T > 7\text{K}$, the experimental observations also agreed well with a theoretical expectation of phonon-induced spin relaxation [62]. It was found that at lower temperatures, $T < 7\text{K}$, the spectrum no longer depended on T , which ruled out the phonon origin of spin relaxation and indicated the transition to the regime where the spin relaxation was dominated by the coupling to the nuclear spin bath.

An unexpected behavior was observed at $B = 0$ and low temperature. It was found that the

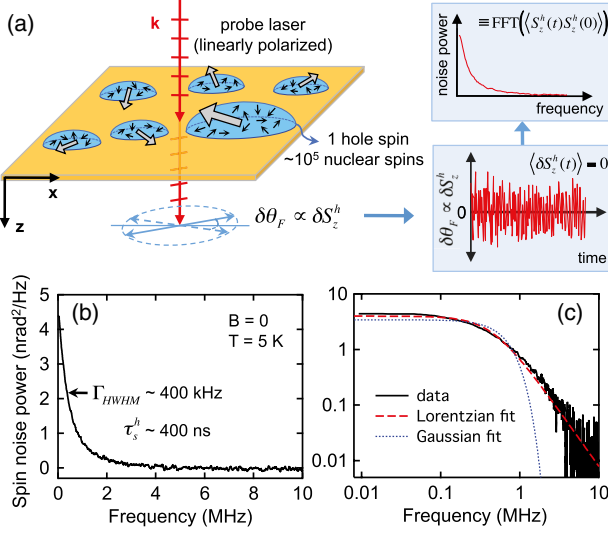


Figure 9. Spin noise from holes coupled to nuclear spin baths in (In, Ga)As quantum dots [62]. (a) Experimental setup, (b) typical spin noise power spectrum of the resident holes at a low temperature (5 K) and zero applied magnetic field ($B = 0$), and (c) the same spectrum on a log-log scale. The noise line shape closely follows a Lorentzian, indicating exponentially decaying hole spin correlations [62]. Reprinted figure with permission from Y. Li et al., Physical Review Letters 108, p. 186603, 2012 [62]. Copyright ©(2012) by the American Physical Society.

spectrum of hole-doped QDs consists of a single narrow Lorentzian peak (Fig. 9(b)), indicating an exponential relaxation of hole spins within $\sim 0.4 \mu\text{s}$ [62, 99]. To understand why this behavior was unexpected, consider the Hamiltonian that describes the hyperfine coupling of the central spin to a nuclear spin bath:

$$\hat{H}^{\text{hf}} = \sum_{i=1}^N g_{\parallel}^i \hat{S}_z \hat{s}_z^i + \sum_{i=1}^N g_{\perp}^i (\hat{S}_x \hat{s}_x^i + \hat{S}_y \hat{s}_y^i), \quad (24)$$

where \hat{S}_{α} , \hat{s}_{α}^i are the components of the central and nuclear spin operators, respectively, g_{\parallel}^i and g_{\perp}^i are the out-of-plane and in-plane hyperfine coupling constants describing the central spin and i th nuclear spin interaction. Typically, the number of nuclear spins in an InGaAs quantum dot is $N \sim 10^5$. The hyperfine coupling is almost isotropic for electron-doped QDs with $\langle g^i \rangle \sim 1$ MHz. It is usually an order of magnitude smaller and has a relatively strong out-of-plane anisotropy for hole-doped QDs: $g_{\perp}^i / g_{\parallel}^i \sim 0.2 - 0.5$.

Due to the large number of nuclear spins, one can justify the mean field approximation, in which the effect of the nuclear spin bath on the central spin is described by an effective field, called the Overhauser field \mathbf{B}_O [100]:

$$\hat{H}_{\text{eff}}^{\text{hf}} = \mathbf{B}_O \cdot \hat{\mathbf{S}}. \quad (25)$$

One can assume that this field points in a random

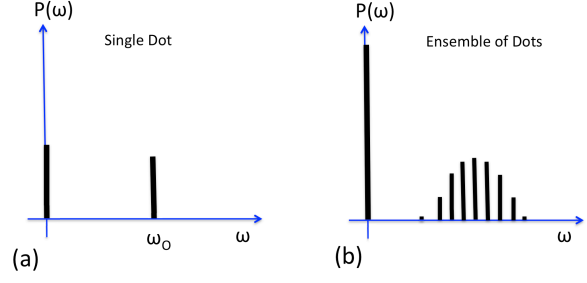


Figure 10. (a) The expected spin noise power spectrum for a single quantum dot (as follows from Eq. (27)). (b) Inhomogeneous broadening of the finite frequency peak in an ensemble of quantum dots.

direction, which is different in different QDs. The components of the Overhauser field are described by the Gaussian distribution, such that $\sqrt{\langle B_{O,z}^2 \rangle} \sim g_{\parallel} \sqrt{N}$ and $\sqrt{\langle B_{O,x}^2 \rangle}, \sqrt{\langle B_{O,y}^2 \rangle} \sim g_{\perp} \sqrt{N}$.

The size of the Overhauser field sets the frequency of precession of the central spin around this field: $\omega_O \approx g_{\parallel} \sqrt{N} \sim 10$ MHz for hole-doped QDs. Let θ be the angle between the Overhauser field and the measurement z -axis. A coherent spin polarization precession around such a field is described by the correlator

$$\langle S_z(t) S_z(0) \rangle = \cos^2(\theta) + \sin^2(\theta) \cos(\omega_O t), \quad (26)$$

where we normalized the correlator to 1 at $t = 0$. While the spin polarization component along the measurement axis remains constant, the other part oscillates [100]. The Fourier transform of this correlator produces two delta-functions (Fig. 10(a)): one at zero frequency and another at ω_O :

$$P(\omega) \equiv C_2(\omega) = \cos^2(\theta) \delta(\omega) + \sin^2(\theta) \delta(\omega - \omega_O). \quad (27)$$

If measurements are performed on an ensemble of a large number of quantum dots, Eq. (27) should be averaged over the distribution of the Overhauser field. Each quantum dot then still contributes to the δ -function at $\omega = 0$ and, in addition, produces a finite frequency contribution at its individual ω_O , so that the high frequency peak is expected to be broadened and have the Gaussian shape, as shown in Fig. 10(b). The maximum of this peak is expected to be at $\omega \approx g_{\parallel} \sqrt{N} \sim 10$ MHz. There have been debates in theoretical literature about the role of the slow dynamics of the Overhauser field. This dynamics is responsible for the broadening of the zero frequency peak. Numerical studies [101, 102, 103] have shown that, within the model (24), this dynamics is very slow so that only a small power-law broadening of the zero frequency peak is expected, not exceeding the transverse hyperfine coupling frequency scale $g_{\perp} < 0.1$ MHz.

Apparently, the experimental observation [62] of a single Lorentzian peak with a width of ~ 1 MHz (Fig. 9(b)) strongly contradicts the above expectation. Not only the shape of the peak but also its characteristic width could not be explained by the above mentioned theory. Moreover, this result can not be related to an unusual inhomogeneous broadening. In fact, it was possible to make an experiment in which all but one quantum dots were shielded from the probe beam so that the Faraday rotation noise spectrum of a *single spin* was detected [104]. At zero magnetic field, no deviations in measurement results for a single quantum dot from the results for an ensemble of quantum dots were found.

The experimental observations reported in [62, 99] were explained theoretically in Ref. [103] by the presence of quadrupole couplings, whose importance had been clearly exposed earlier in Ref. [105]. A more realistic Hamiltonian is written as

$$\hat{H} = \hat{H}^{\text{hf}} + \sum_{i=1}^N \frac{\gamma_q^i}{2} (\hat{\mathbf{s}}^i \cdot \mathbf{n}^i)^2, \quad (28)$$

where \hat{H}^{hf} is defined by Eq. (25), γ_q^i is the strength of the quadrupole coupling of the i th nuclear spin, $\hat{\mathbf{s}}^i$ is the nuclear spin operator, and \mathbf{n}^i is the unit vector along the direction of the local quadrupole coupling anisotropy. The last term in Eq. (28) becomes nontrivial, i.e., different from a constant when $s^i > 1/2$. In fact, the most abundant isotopes of Ga and In are characterized by $s = 3/2$ and $s = 9/2$, respectively. The assumption [103] of a broad distribution of \mathbf{n}^i inside self-assembled quantum dots helped to explain the experimental observations.

An analytical solution to the system described by the Hamiltonian (28) can be found in the limit of a large quadrupole coupling, which is relevant to the hole-doped dots. In this case, the nuclear spin dynamics is dominated by the last term in (28), which induces fluctuations of the Overhauser field with a typical amplitude $\sim g_{\parallel} \sqrt{N}$ and correlation time $\sim \gamma_q s / 2$. The dynamics of the central spin subjected to such a fluctuating Overhauser field was investigated in [103], where it was shown that in hole-doped InGaAs quantum dots the central spin relaxes exponentially. In the case of electron-doped dots, numerical simulations [103, 106] predict that the basic physics leading to Fig. 10(b) is correct except the zero frequency peak is broadened by the quadrupole coupling effects. This difference from the hole-doped quantum dots follows mainly from order of magnitude stronger hyperfine coupling, which reduces the relative role of the quadrupole coupling effects. Recent optical measurements of spin correlators in electron-doped dots [107, 106] and spins confined near impurities [93] have confirmed this prediction. Moreover, experiments

with a single quantum dot revealed an additional oscillation in the spin correlator in the time-domain, which was also explained by the quadrupole coupling effect [107].

3.4. Magnetic Impurities, Thin Magnetic Films, and Nanomagnets

The spin noise power spectrum of localized electrons bound to impurities has been observed in [108]. The noise from such bound electrons is similar to the noise from electrons confined in quantum dots. This is explained by the same spin relaxation mechanism at low temperatures: the electron spin interaction with local nuclear spins. Importantly, impurities have a reproducible confining potential. Consequently, the resulting spin noise is less influenced by inhomogeneous broadening, which can be very strong in quantum dots.

The spin noise power measurements of magnetic Mn ions in CdTe quantum wells were reported in [109]. In this system, the spin noise power spectrum has a relatively complex form explained by multiple resonances of spin-5/2 Mn ions.

The authors of [93] have communicated the spin noise power spectrum of electrons bound to Si impurities in GaAs. The measured noise power spectrum contains two clear peaks - one centered at zero and another one centered at the characteristic frequency of the Overhauser field. The application of the external magnetic field removes the zero frequency peak and produces a Gaussian broadened peak at the Larmor frequency, as expected. The spin dephasing and relaxation times of electrons bound to Si impurities in GaAs are longer compared to these in InGaAs quantum dots.

In [110], the Kerr rotation spectroscopy was applied to detect ferromagnetic fluctuations and random thermal motion of domain walls in a thin film made of magnetic Co atoms. The width of the film varied so that the magnetization fluctuations could be studied in different phases near the ferromagnetic phase transition. Due to the large size of the domain walls, both temporal and spatial noise characterization was performed.

In [111], the optical SNS was applied to study fluctuations of the magnetization in molecular nanomagnets. The latter are molecules with uncompensated spins of magnetic ions. Typically, spins of nanomagnets experience magnetic crystal anisotropy, in which they have two or several degenerate ground states. This degeneracy is lifted by spin tunneling and interactions of nanomagnets with each other and with nuclear spins. Fluctuations of the magnetization of nanomagnets can be used for precise parameter estimation of these technologically interesting nanostructures.

3.5. Alternative SNS Techniques

Non-optical SNS methods usually do not probe the spin polarization directly but rather detect fluctuations of the local magnetic field produced by flipping spins. The sensitivity of such techniques to the relative position of probe and noise sources complicates the interpretation of the signal. At the same time, this can be used as an advantage in situations when a better spatial resolution is needed.

Barkhausen noise. Studies of fluctuations in magnetic systems take roots in the work of Heinrich Barkhausen who proved already in 1919 that the magnetic hysteresis curve is not continuous, but is made up of small random steps caused when the magnetic domains move under an applied magnetic field [112]. This noise can be characterized by placing a coil of a conducting wire near the sample. Motion of ferromagnetic domain walls produces changes in the magnetization that induces noisy electrical signals in the coil. Studies of Barkhausen noise have been used in practice as a nondemolition tool to characterize distribution of elastic stresses and the micro-structure of magnetic samples [113].

SQUID-based spectroscopy. Superconducting quantum interference devices (SQUIDs) have been the method of choice for studies of magnetic field fluctuations in superconductors [114], spin glasses [115, 115, 116], ferroelectric liquid crystals [117], and nanomagnets [118]. In this approach, the sample is placed directly in the vicinity of a dc-SQUID chip with integrated pickup loops and field coils that detects magnetic field fluctuations that originate from flipping magnetic moments. The frequency bandwidth of SQUID devices is relatively small in comparison to optical SNS setups. It is most suitable for materials made of ferromagnetic grains or large spins, such as nanomagnet arrays. Strong disorder, dipole interactions, and anisotropy fields lead to a broad distribution of spin relaxation rates in such samples so that the measured noise power spectra usually were reported to have the form of $\sim 1/f$ or $\sim 1/f^\alpha$ noise. Yet, the dependence of such spectra on temperature and the magnetic field could be used to extract important physics. A number of theoretical publications have been devoted to this field, e.g., to the origin of the power laws and violation of the fluctuation-dissipation theorem in spin glasses [119, 120, 121, 122].

Cantilever-based spectroscopy. Local fluctuations of spins can also be probed with a nanomechanical resonator [19, 123]. In this approach, fluctuations of the magnetization are detected via measuring their mechanical force that the time-dependent spin polarization produces on a small permanent magnet attached to the end of a sensitive silicon cantilever.

This technique was successfully applied to ensembles of electronic localized spins [19], molecular nanomagnets [123], and nuclear spins [124]. Currently, the allowed frequency bandwidth is comparable to the optical techniques, while cantilever-based spectroscopy has a better spatial resolution and is not restricted to optically sensitive materials. Its applications are restricted, however, to spins near the surface of a sample. Interpretation of the data can be complicated by complex distribution of forces with which spins at different locations act on the probe mechanical resonator.

STM-based spectroscopy. Measuring fluctuations of a spin polarized tunneling current from an STM tip can be used to extract spectroscopic information on the temporal susceptibility of a single magnetic atom. This technique has an exceptional time and atomic-scale spatial resolution. However, its applications are restricted to surface spins. Moreover, technical problems such as the lack of a good control of the magnitude of the tunneling current remain to be resolved. For a detailed discussion of this method, we refer the reader to a recent review [125] and theoretical papers [126, 127, 128, 129].

X-ray photon correlation spectroscopy. This experimental technique has been used for many different purposes including studies of domain wall fluctuations in antiferromagnets at short wavelengths [130, 131]. In this application, a coherent beam reflected from a sample surface (chromium (111) surface in Ref. [130]) creates an interference pattern known as speckle [132, 133] (see Fig. 11 for a speckle example). The sensitivity of the speckle to the domain wall structure was used to obtain information regarding the microscopic dynamics of antiferromagnetic domains [130]. In the speckle data analysis, the autocorrelation function $g_2(t) = \langle I(\tau)I(\tau+t) \rangle_\tau / \langle I(\tau) \rangle_\tau^2$ is found for a given pixel and used to extract relevant time scales. The theory of coherent light propagation in disordered media and speckle statistics was developed in [134].

The chromium antiferromagnetism is a complex phenomenon associated with spin- and charge-density waves of different periods. In Ref. [130], the spin-density wave dynamics was tested indirectly at a charge-density wave Bragg reflection angle. It's interesting that the reflection at the spin-density wave angle contains just a single stationary peak [131]. Therefore, we feel that there is a need of better understanding of co-existence of the spin- and charge-density waves in chromium, and their coupling to light.

3.6. Nuclear Spin Noise

The nuclear magnetic fields from mesoscopic volumes at equilibrium are extremely weak. Nevertheless, it is

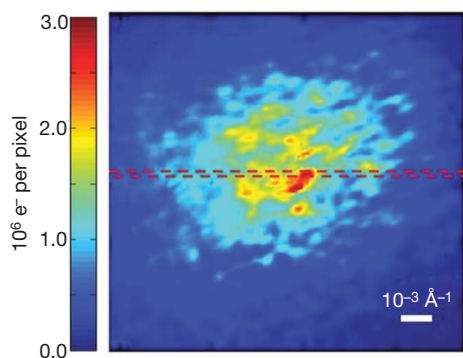


Figure 11. CCD image of the X-ray speckle observed for the chromium [200] lattice Bragg reflection (for more details, see Ref. [130]). Reprinted with permission from Macmillan Publishers Ltd: Nature 447, pp. 68-71, 2007, Copyright ©(2007) [130].

possible to study fluctuations of such fields [135, 136]. For example, SQUID probes were used to measure the nuclear spin noise as early as in 1985 [137]. An approach based on the STM tunneling spectroscopy was theoretically developed in [128].

A cantilever based detector was used in [124] to resolve mesoscopic nuclear spin noise in real time with submicron resolution. This experiment not only allowed studies of nuclear spin diffusion but also demonstrated the capability to manipulate the local nuclear spin distribution.

Considerable progress in the detection of nuclear spin noise has been achieved recently using nanomagnetometry based on NV-centers in diamonds [20, 21, 22]. Magnetic field fluctuations, as small as 10nT, from a single nuclear spin have been resolved with a nanometer precision [138]. Electronic spins in coupled GaAs quantum dots were also shown to work as a sensitive probe of the environmental field fluctuations [139].

Finally, although optical beams do not couple to the nuclear spin polarization directly, the noise power spectrum of nuclear spins has been recently observed by optical SNS [93]. In this experiment, the electronic spin noise in a silicon doped ultraclean GaAs semiconductor was studied. Surprisingly, in addition to the expected noise power peaks of donor-bound electrons, relatively weak peaks have been observed in the low frequency (10-100kHz) range. Such peaks responded to the external magnetic field as expected from the nuclear spin noise of the host isotopes: ^{75}As , ^{69}Ga and ^{71}Ga . This finding allowed the authors of [93] to explore the nuclear spin noise at very low magnetic field values and observe effects consistent with presence of quadrupole couplings. Apparently, this feature in the optically probed noise power spectrum follows from fluctuations of local Overhauser fields that nuclear spin fluctuations induce on observable electronic spins [140], [93](supplementary). It is possible, e.g., that a

precessing nuclear spin polarization creates an effective ac-like Overhauser field that can produce a noise power peak of electronic spins at the precession frequency as a 2nd order effect in the field amplitude [49].

4. Spin Correlators in Quantum Weak Measurement Theory

In the case of a quantum evolution, the measurements influence the system's state. For example, if projective measurements are performed at a high rate, the spin may not be able to precess due to the quantum Zeno effect [141]. Moreover, quantum mechanical spin correlators depend on products of operators at different moments of time. Spin operators, generally, do not commute. Hence, their product can be non-Hermitian and its trace with the equilibrium density matrix can be a complex number. There are different combinations of spin operator products that, after being traced with the density matrix, produce real but different results. The important questions then emerge about which combination is the quantum mechanically justified expression for the measured spin correlator in a particular experiment and how to perform minimally invasive measurements.

4.0.1. Weak Measurements. Being based on the idea of weak-measurement [142, 143], SNS can perform measurements at a high rate without producing strong disturbances. In optical SNS, the measurement beam does not make “hard” projective measurements of the total spin of a mesoscopic spin system. Instead, the spins are allowed to entangle weakly with the linearly polarized beam. One can describe such interaction by the effective Hamiltonian

$$\hat{H}_{\text{int}} = -i\lambda_{\text{SO}}\hat{S}_z\frac{\partial}{\partial\phi}, \quad (29)$$

where $-i\partial/\partial\phi$ is the operator inducing rotation of the linear polarization axis of the probe beam, \hat{S}_z is the quantum mechanical operator of the total spin polarization in the observation volume along z-axis, and λ is the coupling strength. Consider a photon wave packet that is allowed to interact with our spin system during a time interval δt . The wave packet is made of states with different polarization angles ϕ :

$$|\Psi_0\rangle = \int d\phi w(\phi)|\phi\rangle,$$

where $w(\phi)$ is a Gaussian function peaked near $\phi = 0$ and normalized so that $\int w^2(\phi)d\phi = 1$. Initially, the spin system is disentangled from this wave packet, i.e. the entire wave function is a product $|\psi_s\rangle|\Psi_0\rangle$, where $|\psi_s\rangle$ is the state vector of a spin system. The interaction is described by the evolution operator $\hat{U} =$

$\exp(-i\hat{H}_{\text{int}}\delta t)$. For example, if the initial density matrix of the spin system is given by a superposition of different projections of \hat{S}_z , i.e.

$$\hat{\rho}_s = \sum_{i,j} \rho_{ij} |s_z^i\rangle \langle s_z^j|, \quad (30)$$

then, after the interaction taking the time δt of the passage of the wave packet through the sample, the state of the total density matrix (the spin-photons state) is an entangled state:

$$\hat{\rho} = \iint d\phi_1 d\phi_2 w(\phi_1)w(\phi_2) \times \sum_{i,j} \rho_{ij} |\phi_1 - \bar{\lambda}s_z^i\rangle |s_z^i\rangle \langle s_z^j| \langle \phi_2 - \bar{\lambda}s_z^j|,$$

where $\bar{\lambda} = \lambda\delta t$.

The detector then performs the projective measurement of the rotation angle. The magnetization S_z is inferred from the observed polarization rotation, ϕ_0 , as $S_z = \phi_0/\bar{\lambda}$. Note that such an S_z is not the exact value of the magnetization but rather it is its most likely estimate. The probability to obtain an estimate S_z as a measurement result is

$$P(S_z) = \text{Tr} \left[\hat{\rho} \delta(\hat{\phi} - \phi_0) \right] = \sum_i \rho_{ii} w^2(\phi_0 - \bar{\lambda}s_z^i). \quad (31)$$

In principle, any measurement disturbs the system. In the case of the weak measurement, such disturbances are small. In order to evaluate the spin density matrix right after the measurement, we project the density matrix $\hat{\rho}$ into the measured polarization state ϕ_0 using the projection operator $|\phi_0\rangle \langle \phi_0|$. Up to a normalization constant, the result is

$$\hat{\rho}'_s \sim \sum_{i,j} \rho_{ij} w(\bar{\lambda}(S_z - s_z^i)) w(\bar{\lambda}(S_z - s_z^j)) |s_z^i\rangle \langle s_z^j|. \quad (32)$$

Note the changes compared to the initial spin density matrix (30).

4.0.2. Formulation Based on Kraus Operators. Generally, one can reformulate (31) and (32) by introducing the *Kraus operators*:

$$\hat{K}(S_z) = (2\bar{\lambda}/\pi)^{1/4} e^{-\bar{\lambda}(S_z - \hat{s}_z)^2}, \quad (33)$$

so that the probability of measuring the outcome S_z is given by [144]

$$P(S_z) = \text{Tr} [\hat{\rho}_1(S_z)], \quad \hat{\rho}_1(S_z) = \hat{K}(S_z) \hat{\rho}_s \hat{K}^\dagger(S_z). \quad (34)$$

It is now easy to extend this analysis to find the probability of observing an arbitrary trajectory $S_z(t)$. First, we note that a single wave packet passage through a sample can be considered extremely fast in

comparison with dynamics of the spin system. Because of this reason, the spin Hamiltonian does not appear in Eqs. (34). However, on a longer time scale, in the Heisenberg picture, the measurement operator evolves with time:

$$\hat{S}_z(t) = e^{i\hat{H}t} \hat{S}_z e^{-i\hat{H}t},$$

where \hat{H} is the Hamiltonian of the spin system.

One can then introduce a Kraus operator in the Heisenberg picture that corresponds to the observed trajectory $S_z(t)$ as [144]

$$\hat{K}[S_z(t)] = C \hat{T} e^{-\int \lambda(S_z(t) - \hat{S}_z(t))^2 dt},$$

where C is a normalization factor and \hat{T} is time-ordering operator (later times on the left). Finally, the probability of a trajectory (the functional probability) is given by [144]

$$P[S_z(t)] = \text{Tr} \left[\hat{K}^\dagger \hat{K} \hat{\rho}_s \right]. \quad (35)$$

By definition, $S_z(t)$ is a real-valued trajectory of the detector output. Having obtained probabilities of such trajectories, one can calculate arbitrary correlators by standard means. This task is straightforward but somewhat lengthy to be explained here. We refer the reader to Ref. [144] for the detailed discussion and summarize here only some results. It turns out that, within this model, the measurement of correlators corresponds to finding traces of the following operator products with the initial density matrix:

$$\langle S_z(t_1) S_z(t_2) \rangle = \text{Tr} \left[\check{S}_z \hat{U}(t_2, t_1) \check{S}_z \hat{U}(t_1, 0) \hat{\rho}_s \right], \quad (36)$$

$$\langle S_z(t_1) \dots S_z(t_n) \rangle =$$

$$\text{Tr} \left[\check{S}_z \hat{U}(t_n, t_{n-1}) \dots \check{S}_z \hat{U}(t_1, 0) \hat{\rho}_s \right],$$

where

$$\check{S}_z \hat{X} \equiv \frac{1}{2} \{ \hat{S}_z, \hat{X} \} \quad (37)$$

is normalized anticommutator of \hat{S}_z with the matrix on the right of it, and $\hat{U}(t_a, t_{a-1})$ is the evolution operator of the density matrix from time t_{a-1} to time t_a .

According to [144], the effect of measurement on the system has the following two consequences: First, the measured Faraday rotation is not strictly proportional to the spin polarization but has an uncorrelated background noise component: $\phi(t) = \bar{\lambda} S_z(t) + \zeta(t)$, with $\langle \zeta(t) S_z(t) \rangle = 0$, where $S_z(t)$ is the true instantaneous spin polarization. In fact, such a background noise can be measured separately and subtracted if one considers cumulants of the spin variables. Second, due to the system-detector coupling, the evolution of the system's density matrix has to be described by a *Lindblad*-type equation

$$\frac{d\hat{\rho}_s}{dt} = \hat{L}\hat{\rho}_s \equiv -\frac{i}{\hbar} \left[\hat{H}, \hat{\rho}_s \right] - \frac{\lambda}{2} [\hat{S}_z, [\hat{S}_z, \hat{\rho}_s]], \quad (38)$$

so that the evolution operator is defined as $\hat{U}(t_a, t_{a-1}) = \hat{T} \exp \int_{t_{a-1}}^{t_a} \hat{L} dt$.

An important consequence of Eq. (38) is that one can minimize the feedback effect of a detector by reducing the coupling constant λ . In the limit $\lambda \rightarrow 0$, the correlators (36) become a trace of the initial system density matrix with anticommutators of spin operators at different moments of time. One can calculate these correlators quantum mechanically without explicitly assuming the presence of a detector. There is a price to be paid for allowing the coupling to a detector to be small: a decrease in coupling implies an increase in the background noise $\zeta(t)$ and, hence, a longer time to filter it out experimentally.

Equations (36)-(38) were derived within a specific model of a detector. In the literature on SNS, one can encounter other detector models that correspond to a different choice of the Kraus operator [142]. In the limit of weak coupling to the detector, they produce the same prediction for the 2nd order correlator. However, higher order spin correlators, as well as the behavior of all correlators beyond the limit of the weak coupling to detector, can depend on the choice of the detector model.

Finally, as it is discussed in [145], different models of the weak measurement generally lead to different definitions of the operator \check{S}_z . For example, we may find that instead of (37) one should rather use

$$\check{S}_z \hat{X} = \frac{1}{2} \{ \hat{S}_z, \hat{X} \} - i\beta [\hat{S}_z, \hat{X}], \quad (39)$$

with some real constant β . The latter becomes non-zero, e.g., when the detector interferes by absorbing energy. Interestingly, in such a case one cannot guarantee the positivity of the noise power spectrum [145]. This fact may look impossible considering the definition (5), which is the average of squares of measured real numbers. This controversy is removed by noticing that the measured signal is actually the physical noise plus the background noise. Only this sum is constrained to have a positive noise power spectrum. However, when the power spectrum of the background noise is measured separately and then subtracted, one can discover that the physical spin noise power spectrum can be negative in a certain range of frequencies. The case $\beta = 0$, which we discussed in this section, however, does not allow this effect, as it follows from the following property.

The weak positivity property: The physical part of the noise power spectrum of the correlator (36) with $\check{S}_z \hat{X} = \frac{1}{2} \{ \hat{S}_z, \hat{X} \}$ is always positive definite. Indeed, using the fact that $2\langle S_z^2(t) \rangle \geq \langle \{ \hat{S}_z(t), \hat{S}_z(0) \} \rangle$, we find that the expression $\langle S_z(t) S_z(0) \rangle$ (as it is defined in (36)) is maximized at $t = 0$. The Fourier transform of such a real function of time is positive definite

(according to the Bochner's theorem [146]), which proves the statement.

It was shown that some properties of higher than 2nd order correlators are incompatible with classical physics even at $\beta = 0$ in Eq. (39). For example, the 3rd order correlator, measured at the thermodynamic equilibrium, may violate the 3rd order Onsager relations [145], and the 4th order correlator may break classical positivity constraints [144]. It should be kept in mind that experimental observations of such effects by SNS are yet to be achieved. In our opinion, such observations are highly desirable to demonstrate fundamental quantum mechanical phenomena at mesoscopic scale.

5. Faraday Rotation

The optical methods used for SNS do not always provide a pure spin noise signal. Faraday rotation fluctuations can be sensitive to other sources of physical fluctuations in a material, such as fluctuations of the background charge in quantum dots and valley polarization fluctuations in Dirac semiconductors. This section explains some fundamental effects that justify the optical SNS.

5.1. Faraday Effect

In the optical SNS, a linearly polarized beam passes through a volume of a material or a slab with atomic vapor. Polarization of the outgoing beam is rotated by an angle θ_F . In magnetic materials, this angle is typically proportional to the magnetization of the illuminated region. On the other hand, in paramagnetic systems, this angle would be zero on average. Nevertheless, due to the thermally induced spin fluctuations, the total magnetization of the illuminated region fluctuates as $\delta S_z(t) \sim \sqrt{N}$ where N is the number of spins in the observation volume. By analogy with the Faraday effect in ferromagnetic systems, one can expect that there is a linear dependence between the measured Faraday rotation signal and the instantaneous spin polarization:

$$\theta_F(t) = \alpha S_z(t), \quad (40)$$

where α is a non-universal coefficient that depends on material and setup characteristics. The time correlators of the signal $\theta_F(t)$ can then be interpreted as correlators of spin polarization times a setup specific constant.

Let $k_{\pm} = \bar{k} \pm \Delta k/2$ be wave vectors in the material for left and right circularly polarized waves, respectively,

$$\mathbf{E}_{\pm} = E_0(\hat{\mathbf{x}} \pm i\hat{\mathbf{y}})e^{-i(\omega t - k_{\pm}z)}. \quad (41)$$

Note that directions of propagation and frequencies of the circular polarized components are the same in Eq. (41). Suppose now that the incident wave is linearly polarized along x-axis: $\mathbf{E}_{\text{in}} = \mathbf{E}_+ + \mathbf{E}_-$ and passes through a slab of a material of width d . The outgoing wave then is given by

$$\mathbf{E}_{\text{out}} = E_0 e^{-i\omega t} \left[\hat{\mathbf{x}} (e^{ik_+d} + e^{ik_-d}) + i\hat{\mathbf{y}} (e^{ik_+d} - e^{ik_-d}) \right]. \quad (42)$$

Leaving only terms linear in small $\Delta kd \ll 1$, where $\Delta k \equiv (k_+ - k_-)$, we find:

$$\mathbf{E}_{\text{out}} = E_0 e^{-i\omega t + i\bar{k}d} (2\hat{\mathbf{x}} - \Delta kd\hat{\mathbf{y}}), \quad (43)$$

i.e. the out-going beam polarization is rotated by a small angle

$$\theta_F = \Delta kd/2 = (\omega d/2c)(n_+ - n_-), \quad (44)$$

where we used the fact that $k_{\pm} = \omega n_{\pm}/c$. Here c is the speed of light, and n_{\pm} are refraction coefficients for, respectively, clockwise (+) and counterclockwise (-) polarized beams.

For microscopic calculations, it is important to relate the difference $n_+ - n_-$ to the elements of polarization tensor of the medium. Consider, for simplicity, the case of a uniaxial optical anisotropy, such that the measurement z -axis coincides with the direction of the magnetization and the main optical axis of the system. The electromagnetic wave passing the sample induces the electric polarization

$$\mathbf{P}(\omega) = 4\pi\kappa(\omega)\mathbf{E}(\omega). \quad (45)$$

The polarizability tensor κ generally has off-diagonal components, e.g., an electric field along the x -axis induces the polarization along the y -axis. Disregarding dissipation, weak magnetic effects are described by such imaginary off-diagonal components in

$$\kappa = \begin{pmatrix} \kappa_{xx} & i\eta_{xy} & 0 \\ -i\eta_{xy} & \kappa_{yy} & 0 \\ 0 & 0 & \kappa_{zz} \end{pmatrix}, \quad (46)$$

where, in the case of uniaxial anisotropy considered here, $\kappa_{yy} = \kappa_{xx}$. More generally, the diagonal and off-diagonal components of the tensor (46) have both real and imaginary parts. We refer to Ref. [147] for a more detailed discussion. The tensor (46) is diagonalized in the rotating basis, i.e.,

$$\mathbf{P}_{\pm} = 4\pi(\kappa_{xx} \mp \eta_{xy})\mathbf{E}_{\pm}, \quad (47)$$

where E_{\pm} are defined in (43) and $\mathbf{P}_{\pm} \sim (\hat{\mathbf{x}} \pm i\hat{\mathbf{y}})$. The electric susceptibility can be defined then separately for each circular polarization: $\varepsilon_{\pm} = 1 + 4\pi(\kappa_{xx} \mp \eta_{xy})$. Using $n_{\pm} = \sqrt{\mu_0\varepsilon_{\pm}}$, we find $n_+ - n_- \approx -4\pi\eta_{xy}/\bar{n}$,

where $\bar{n} = (n_+ + n_-)/2$. Substituting the above into Eq. (44), we obtain

$$\theta_F \approx -2\pi\eta_{xy}(\omega)\frac{\omega d}{c\bar{n}}. \quad (48)$$

The off-diagonal component η_{xy} of the polarization tensor can be calculated microscopically by considering linear response of the charge polarization to the external electric field. There are differences in such calculations for conduction electrons and dielectric media.

5.2. Faraday Rotation Fluctuations due to Conduction Electrons

In the case of conduction electrons, one can associate the charge polarization with the current in the region: $\dot{P}_{\alpha}(t) = J_{\alpha}(t) = \int^t \sigma_{\alpha\beta}(t-t')E_{\beta}(t')dt'$, where $\sigma_{\alpha\beta}$ are the elements of the conductivity tensor. Taking the Fourier transform we find $\eta_{xy}(\omega) = \sigma_{xy}(\omega)/\omega$ and, hence,

$$\theta_F = -2\pi\sigma_{xy}(\omega)\frac{d}{c\bar{n}}. \quad (49)$$

Equation (49) is an approximation valid in the linear order in magnetization and in the limit of weak beam absorption, which is usually the case for weak spin fluctuations near the thermodynamic equilibrium and when the beam is sufficiently detuned from resonant optical transitions. Absorption effects would lead to corrections to (49) that depend on σ_{xx} .

In paramagnetic materials, at zero external magnetic field, the off-diagonal conductivity is zero, i.e. $\sigma_{xy} = 0$, which follows from the time reversal symmetry of the Hamiltonian. On the other hand, in all conduction materials, conduction electrons experience the spin-orbit coupling. This coupling leads to the intrinsic AC spin Hall effect [148], namely, electrons with spins $s_z = \pm 1/2$ deflect in transverse to the electric field direction, i.e. one can introduce spin-dependent conductivities σ_{xy}^{\uparrow} and σ_{xy}^{\downarrow} for up and down electronic spins, separately. The time-reversal invariance guarantees that $\sigma_{xy}^{\uparrow} = -\sigma_{xy}^{\downarrow}$ in a paramagnetic system on average. However, a local spin fluctuation creates an imbalance of spins up and down. Consequently, the total charge Hall conductivity $\sigma_{xy} = \sigma_{xy}^{\uparrow} + \sigma_{xy}^{\downarrow}$ does not vanish, and for a weak spin fluctuation it is proportional to the instantaneous spin polarization: $\sigma_{xy} \sim S_z(t)$.

This mechanism is responsible for observation of Faraday rotation fluctuations in conventional semiconductors, such as GaAs. However, the spin orbit coupling is not always responsible for a nonzero Hall conductivity. A notable example is the class of novel materials - transition metal dichalcogenides (TMD)s [149], in which, in addition to spins, conduction

electrons possess the “valley” discrete degree of freedom.

Consider, e.g., the 2D semiconductor MoS₂ – a prototypical group-VI dichalcogenide [150]. A monolayer MoS₂ is a direct gap semiconductor with a band gap of approximately 1.8 eV. Its band structure is characterized by the conduction and valence-band edges located at the corners (K and K' points) of the 2D hexagonal Brillouin zone. A strong spin-orbit coupling due to the d orbitals of the heavy metal atoms results in a significant spin-splitting of the valence band. In the vicinity of K -points the Hamiltonian can be written as

$$\hat{H} = at(\tau k_x \hat{\sigma}_x + k_y \hat{\sigma}_y) + \frac{\Delta}{2} \hat{\sigma}_z - \lambda \tau \frac{\hat{\sigma}_z - 1}{2} \hat{s}_z, \quad (50)$$

where a is the lattice constant, t is the effective hopping integral, $\tau = \pm$ denotes the valley degrees of freedom K and K' ; $\hat{\sigma}$ are the Pauli matrices describing the sublattice degrees of freedom, Δ is the bandgap, $2\lambda_{\text{SO}}$ is the spin splitting at the valence band caused by the spin-orbit coupling, and \hat{s}_z is the Pauli matrix for spins.

Note that the spin is conserved by the Hamiltonian (50). The energy dispersion of the Bloch bands for the same spin near each of the K -points corresponds to a massive 2D Dirac band, as shown in Fig. 12. Each of the electronic bands has a nonzero Hall conductivity [151]. However, the signs of such Hall conductivities depend on the valley index rather than spins. One can show that for the Hamiltonian (50), we have

$$\sigma_{xy}^{K\uparrow} \approx \sigma_{xy}^{K\downarrow}, \quad \sigma_{xy}^{K\uparrow} = -\sigma_{xy}^{K'\downarrow}, \quad \sigma_{xy}^{K\downarrow} = -\sigma_{xy}^{K'\uparrow}, \quad (51)$$

where, e.g., $\sigma_{xy}^{K\uparrow}$ is the Hall conductivity of electrons in the K valley having spins up [149].

At the thermodynamic equilibrium, the number of electrons in K and K' valleys is, on average, the same so the total Hall conductivity of the material is, on average, zero. However, intervalley scatterings and spin flips lead to the fluctuating imbalance of electrons in different bands, and hence to the Faraday rotation. The valley-dependent optical selection rules for interband transitions at K and K' points are shown schematically in Fig. 12. The frequency of the probe beam can be strongly detuned from the lower valence bands, while being almost in resonance between conduction electrons and the upper valence band. Optical transitions are spin conserving, so only electronic spins up in the K -valley and spins down in the K' valley become optically sensitive for such a light frequency.

As different valleys have different signs of the Hall conductivities, the corresponding Faraday rotation angle can be expressed as [149, 152]

$$\theta_F \sim N_{K\uparrow} - N_{K'\downarrow}, \quad (52)$$

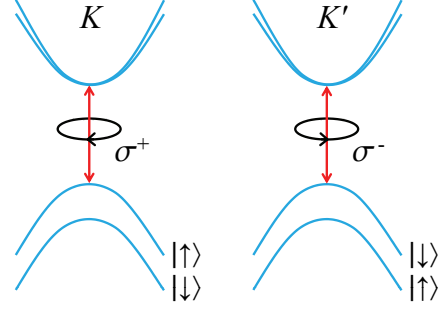


Figure 12. Schematics of valley and spin optical transition selection rules for a circularly polarized light with a close to band-gap photon energy.

where $N_{K\uparrow}$ is the excess number of electrons in the observation region with spins up in the K valley, and $N_{K'\downarrow}$ is the excess number of electrons with spins down in the K' valley. It is now convenient to introduce the valley polarization, $\delta N_v = (N_{K\uparrow} + N_{K\downarrow} - N_{K'\uparrow} - N_{K'\downarrow})/2$, and the spin polarization, $\delta S_z = (N_{K\uparrow} - N_{K\downarrow} + N_{K'\uparrow} - N_{K'\downarrow})/2$, in terms of which the Faraday rotation angle is expressed as

$$\theta_F(t) \sim \delta N_v(t) + \delta S_z(t). \quad (53)$$

Since both N_v and S_z experience fluctuations, Eq. (53) shows explicitly that the Faraday rotation noise may not always be proportional to the pure spin noise, as it was suggested in Eq. (40). The optically measured noise power spectrum contains additional information here that corresponds to the dynamics of N_v . Fortunately, the contributions of spin and valley polarizations should be easy to distinguish because they differently respond to application of an external magnetic field. Thus both types of fluctuations can potentially be explored by optical SNS [149].

5.3. Faraday Rotation from Spins in Quantum Dots

If a single electron is confined in a self-assembled semiconductor quantum dot, its wave function can be in an arbitrary superposition of two states:

$$|1/2\rangle = |E\rangle|\uparrow\rangle, \quad |-1/2\rangle = |E\rangle|\downarrow\rangle, \quad (54)$$

where $|E\rangle$ is the spatial component of the wave function.

For hole-doped quantum dots, in GaAs, the wave function is more complex. It can be represented as a superposition of states of the valence band with the

total angular momentum equal to $3/2$ [153]:

$$|3/2, 3/2\rangle = \frac{|X + iY\rangle}{\sqrt{2}} |\uparrow\rangle, \quad (55)$$

$$|3/2, 1/2\rangle = \frac{|X + iY\rangle |\downarrow\rangle - 2|Z\rangle |\uparrow\rangle}{\sqrt{6}}, \quad (56)$$

$$|3/2, -1/2\rangle = \frac{|X - iY\rangle |\uparrow\rangle + 2|Z\rangle |\downarrow\rangle}{\sqrt{6}}, \quad (57)$$

$$|3/2, -3/2\rangle = \frac{|X - iY\rangle}{\sqrt{2}} |\downarrow\rangle, \quad (58)$$

where $|X\rangle$, $|Y\rangle$ and $|Z\rangle$ are orbital functions with symmetries of, respectively, x , y and z .

The electronic states form a Kramer's doublet and, hence, are degenerate. In contrast, hole states in epitaxial InAs or InGaAs quantum dots are split into the heavy hole (hh) and light hole (lh) doublets. So, one can speak about two characteristic splittings between hole and electronic states: Δ_{hh} and Δ_{lh} for, respectively, heavy and light hole states. The frequency of the measurement beam can be tuned close to the resonance with the hh-states so that lh-states can be considered optically inactive and irrelevant.

Heavy holes are predominantly made of states $|3/2, \pm 3/2\rangle$. The time reversal invariance constrains them to be in a superposition of the following two vectors:

$$|\psi_1\rangle = \alpha(|3/2; 3/2\rangle + \beta|3/2; -1/2\rangle + \gamma|3/2; 1/2\rangle), \quad (59)$$

$$|\psi_2\rangle = \alpha(|3/2; -3/2\rangle + \beta^*|3/2; 1/2\rangle - \gamma^*|3/2; -1/2\rangle),$$

where $\alpha = 1/\sqrt{1 + |\beta|^2 + |\gamma|^2}$ ensures a proper normalization. Nonzero values of parameters β and γ originate from mechanical strains. The parameter β is nonzero due to nonzero components ε_{xy} and $\varepsilon_{xx} - \varepsilon_{yy}$ of the strain tensor (Ref. [153]), and the strain with $\varepsilon_{zx} - \varepsilon_{yz} \neq 0$ corresponds to the parameter $\gamma \neq 0$. The relative sizes of these two types of strains are usually strongly different. In the bulk of 3-dimensional GaAs samples, $\varepsilon_{xx} - \varepsilon_{yy}$ is typically substantial, while nonzero $\varepsilon_{zx} - \varepsilon_{yz}$ can be induced in samples grown along an unusual crystal direction. Hence, the parameter γ is typically assumed to be vanishingly small in the bulk of GaAs, while usually $|\beta|^2 \sim 0.1$ (Ref. [153]).

In the basis (59), the operator of the spin projection on the measurement axis has the following matrix form:

$$\hat{s}'_z = \frac{\alpha^2}{2} \begin{pmatrix} 1 + \frac{|\gamma|^2 - |\beta|^2}{3} & \frac{\gamma^* \beta^*}{3} \\ \frac{\gamma \beta}{3} & -1 - \frac{|\gamma|^2 - |\beta|^2}{3} \end{pmatrix}. \quad (60)$$

This operator, in the natural basis of states (59), is not proportional to the Pauli $\hat{\sigma}_z$ -matrix. Hence, the linear

relation between the average spin and the Faraday rotation angle is not *a priori* obvious.

The optical beam field couples states of a single hole to the exciton states that consist of one electron and two holes with opposite spins. We will assume that such an exciton state can be described similarly to the electronic state (54) with a different meaning of the spatial part of the wave function. Since all states inside the quantum dot are localized, the matrix elements of the coordinate operators are well defined, e.g.,

$$\langle E|\hat{x}|X\rangle = \langle E|\hat{y}|Y\rangle \equiv q \neq 0, \quad (61)$$

$$\langle E|\hat{x}|Y\rangle = \langle E|\hat{y}|X\rangle = \langle E|\hat{x}|Z\rangle = \langle E|\hat{y}|Z\rangle = 0, \quad (62)$$

where q is some constant parameter that characterizes the quantum dot.

Let us assume that the energy difference between the electron in the valence band and the exciton state is Δ_{hh} . Consider now the charge polarization induced by an ac-field $\mathbf{E}(t) = \mathbf{y}E_y e^{i\omega t}$. The system is then described by the Hamiltonian

$$\hat{H} = \hat{H}_0 + eE_y e^{i\omega t} \hat{y}, \quad (63)$$

where \hat{H}_0 is the unperturbed Hamiltonian of the quantum dot and \hat{y} is the y -coordinate operator. The charge polarization of a quantum dot in a state $|\Psi\rangle$, along the transverse to the electric field direction, is given by $P_x = e\langle\Psi|\hat{x}|\Psi\rangle$. Using the linear perturbation theory, we find that the linear order in the electric field contribution to P_x oscillates with the same frequency as the electric field:

$$P_x \approx \frac{-ie^2 E_y e^{i\omega t}}{\hbar} \sum_{s=\pm 1/2} \Im \left[\frac{\langle\Psi|\hat{y}|s\rangle\langle s|\hat{x}|\Psi\rangle}{\Delta_{hh} - \omega + i\Gamma} \right], \quad (64)$$

where s runs over localized exciton eigenstates (54) of the Hamiltonian and Γ is a phenomenological parameter describing broadening of the optical resonance. In derivation of (64) we used the assumption that $\Delta_{hh} - \omega \ll \Delta_{hh}$, which has always been the case in the optical SNS applications.

Using the relation (48) between the off-diagonal elements of the polarization tensor and the Faraday rotation angle, we find

$$\theta_F \sim \chi_1(\omega) \sum_{s=\pm 1/2} \Im [\langle\Psi|\hat{x}|s\rangle\langle s|\hat{y}|\Psi\rangle], \quad (65)$$

where

$$\chi_1(\omega) = \frac{\Delta_{hh} - \omega}{(\Delta_{hh} - \omega)^2 + \Gamma^2}, \quad (66)$$

and where we disregarded dissipative effects that are proportional to a Lorentzian-like broadening at a single resonant transition:

$$\chi_2(\omega) = \frac{\Gamma}{(\Delta_{hh} - \omega)^2 + \Gamma^2}, \quad (67)$$

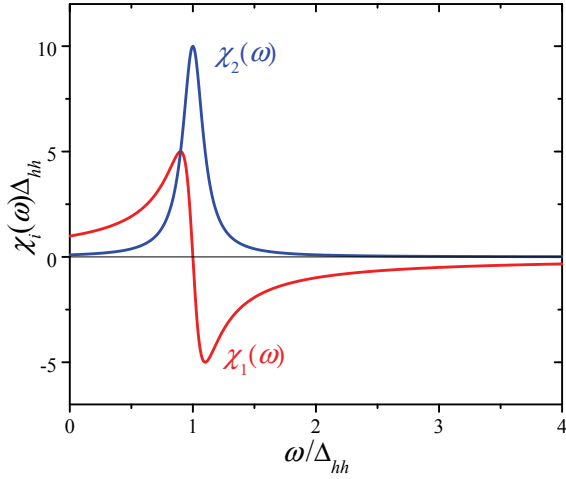


Figure 13. Functions $\chi_1(\omega)$ and $\chi_2(\omega)$ (Eqs. (66), (67)) at $\Gamma/\Delta_{hh} = 0.1$. Far from the resonance ($|\omega - \Delta_{hh}| \gg \Gamma$), the real part $\chi_1(\omega)$ is much larger in absolute value than the imaginary part $\chi_2(\omega)$.

which decays as $\chi_2 \sim 1/(\Delta_{hh} - \omega)^2$ at large detuning, i.e. much faster than $\chi_1(\omega)$.

Consider now the wave function in a superposition of pseudo-spin states (59):

$$|\Psi\rangle = a|\psi_1\rangle + b|\psi_2\rangle,$$

with some coefficients a and b . One can verify now that

$$\sum_{s=\pm 1/2} \Im \{ \langle \Psi | \hat{x} | s \rangle \langle s | \hat{y} | \Psi \rangle \} = q^2 \langle \Psi | \hat{s}'_z | \Psi \rangle,$$

where parameter q was defined in (61). Consequently, the contribution of the given quantum dot and its spin state to the Faraday rotation angle is given by

$$\theta_F = Q\chi_1(\omega) \langle \Psi | \hat{s}'_z | \Psi \rangle, \quad (68)$$

where Q is a constant that depends on the dipole matrix elements between electronic and heavy hole states of the quantum dot. Different dots contribute additively to the total observed Faraday rotation angle. This calculation verifies that the Faraday rotation is proportional to the spin polarization of the dots.

The beam frequency dependence of this effect is described by the function $\chi_1(\omega)$ in (66), which we show in Fig. 13. Generally, $\chi_1(\omega)$ has a more complex form due to strong Coulomb interaction in an electron-hole excitation, however, it is a rather general property that $\chi_1(\omega)$ decays as $\sim 1/(\Delta_{hh} - \omega)$ at large detuning from the resonance [154]. This is in contrast with dissipative absorption processes that are usually described by Gaussian or Lorentzian functions that decay much faster. Hence, the fact that the Faraday rotation decays slowly with detuning from the resonance allows

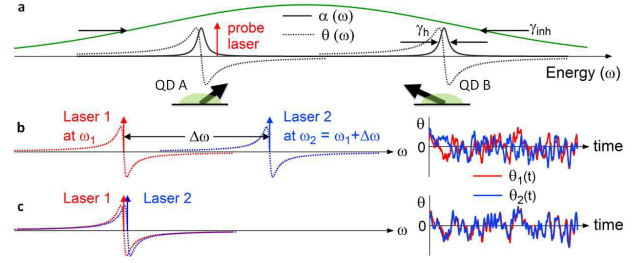


Figure 14. Two-color spin noise spectroscopy of a quantum dot ensemble [156]. (a) Gaussian inhomogeneous broadening of the absorption resonance in an ensemble of quantum dots (green) compared with homogeneous broadening of absorption and Faraday Rotation of single dots (QD A and QD B) probed by beams with different frequencies (respectively, solid and dotted black curves). (b-c) Comparison of the Faraday rotation fluctuations in beams detuned from each other by a large frequency difference $\Delta\omega$ and two beams without detuning (see Ref. [156] for more details). Reprinted with permission from Macmillan Publishers Ltd: Nature Communications 5, 4949, 2014, Copyright ©(2014) [156].

the probe beam frequency choice at which absorption of energy from the beam is tuned below a desired level.

The results of this subsection demonstrate that SNS is justified by the sensitivity of the Faraday rotation to the spin state in a quantum dot. Interestingly, a similar line of arguments was used to design another measurement technique [139, 155] that, instead of spins, probes charge fluctuations in the vicinity of a quantum dot. Such fluctuations occur relatively slowly (below 1MHz frequencies) and usually do not interfere with spin noise. This technique employs the fact that electrostatic time-dependent potential produced by such fluctuations modulates the size of the optical gap Δ_{hh} .

5.4. Spin Noise as a Probe of a Homogeneous Line-Width of an Optical Transition

Spin noise can be used not only to study spin interactions. It was shown in [156] that it can also be used as an alternative probe of optical characteristics of electronic systems, which previously could be studied only by much more invasive nonlinear optical methods.

In the previous subsection, we discussed that the Faraday rotation of a beam with a frequency ω has resonant character. The interaction of a spin system with an optical beam is described by the response function $\chi(\omega) = \chi_1(\omega) + i\chi_2(\omega)$. The imaginary part, $\chi_2(\omega)$, is responsible for an absorption peak, similar to the Lorentzian in Eq. (67), and the Faraday rotation is proportional to the real part $\chi_1(\omega)$, such as in Eq. (66). Imaginary and real parts of $\chi(\omega)$ are not independent. They can be expressed in terms of each other via the Kramers-Kronig relations [154].

A single quantum dot has a relatively sharp

resonance, described by the absorption curve $\chi_2(\omega)$ with a characteristic width γ_h , however, due to the disorder in shapes of quantum dots, there is a wide range of optical frequencies of the probe beam at which spin noise can be detected, as illustrated in Fig. 14(a). In [55], such a strong inhomogeneous broadening of the resonant frequency was observed in an ensemble of InGaAs quantum dots.

One can ask a question whether it is possible to determine the homogeneous broadening of a single dot when we can probe only many quantum dots simultaneously within the domain of linear optics. It was shown in [156] that this question can be resolved positively if one can detect fluctuations of the optical signal that are induced by spin fluctuations.

To illustrate the idea of Ref. [156], let us formalize the problem. Consider an abstract elementary system, such as a molecule or a quantum dot, which presence can be detected by a probe beam with the frequency ω . The system can be detected by changes in some characteristic X , which can be a detector voltage signal proportional to some characteristic of the optical beam, e.g., the rotation of the beam polarization. If interaction with the beam is weak, then X is generally proportional to the intensity of the probe beam. We assume that the elementary system, e.g., a single quantum dot, couples noticeably to the beam at frequencies around some resonant value ω_0 so that we can write a linear relation:

$$X(\omega) = f(\omega_0 - \omega)I(\omega), \quad (69)$$

where the function $f(y)$ is peaked at $y = 0$ and decays at a characteristic frequency γ_h . The latter is called the *homogeneous broadening*.

If there is only one quantum dot in the observation region, then γ_h can be determined simply by scanning the response to different probe beam frequencies ω . However, if we deal with a large ensemble of similar dots characterized by a distribution of ω_0 , then the linear response changes to

$$X(\omega) = \int d\omega_0 \rho(\omega_0) f(\omega_0 - \omega) I(\omega), \quad (70)$$

where $\rho(\omega_0)$ is the density, per unit frequency, of elementary systems with a resonant frequency ω_0 . Quite often, it happens that the homogeneous broadening γ_h is much smaller than the characteristic width of the *inhomogeneous* distribution $\rho(\omega_0)$. In such a case, one can approximately evaluate (70) as

$$X(\omega) = g\rho(\omega)I(\omega), \quad (71)$$

where $g = \int dy f(y)$ is a constant that, alone, does not contain enough information to determine γ_h . Equation (71) shows that, for a large inhomogeneous

broadening, the linear response characteristics cannot provide information about γ_h . Neither this information can be obtained if the ensemble of systems is probed by more than one beam at different frequencies, e.g., if we probe the system by two beams at frequencies ω_1 and ω_2 then

$$X = g[\rho(\omega_1)I(\omega_1) + \rho(\omega_2)I(\omega_2)], \quad (72)$$

which again is not giving information about γ_h .

Now, imagine that X is again the sum of responses from two beams at frequencies ω_1 and ω_2 but the function $f(\omega_0 - \omega)$ is no longer time-independent but rather experiences random fluctuations with time. For example, we know that in the case of quantum dots spin fluctuations induce fluctuations of the Faraday rotation. In such a case, the probed characteristic X will also be fluctuating. Let us assume that such fluctuations are independent for different quantum dots in the ensemble.

Curiously, even when the linear laws (69) and (72) are valid, by measuring fluctuations of X we can actually obtain the information about γ_h . When the ensemble is probed by two beams, the time averaged signal $\langle X \rangle$ is merely obtained from (72) with $g \rightarrow \langle g \rangle$. However, the variance of X appears to be nonlinear in probe beam intensities and contains a cross-correlation contribution:

$$\text{var}(X) \equiv \langle [X(t)]^2 \rangle - \langle X(t) \rangle^2 \approx g_{11}\rho I^2(\omega_1) + g_{22}\rho I^2(\omega_2) + g_{12}(\omega_1 - \omega_2)\rho I(\omega_2)I(\omega_1), \quad (73)$$

where dependence of coefficients g_{11} and g_{22} on frequencies of the probe beams, as well as the difference between $\rho(\omega_1)$ and $\rho(\omega_2)$, can be disregarded if $\delta\omega \sim \gamma_h$, where $\delta\omega \equiv \omega_1 - \omega_2$. The function $g_{12}(y)$ generally decays at $y \sim \gamma_h$, so it is sensitive to the difference between beam frequencies.

For example, the measured Faraday rotation in [156] could be described by $f(\omega) = \alpha\chi_1(\omega_0 - \omega)$, where $\chi_1(\omega)$ was the real part of the response function and α was the fluctuating spin noise signal with some $\langle \alpha \rangle$ and $\text{var}(\alpha)$. Using the fact that the variance of the sum of signals from independent quantum dots is the sum of variances from individual dots (which is a good assumption for well separated quantum dots) one can find that

$$g_{11} = g_{22} = \text{var}(\alpha) \int dy \chi_1^2(y), \quad (74)$$

$$g_{12} = 2\text{var}(\alpha) \int dy \chi_1(y)\chi_1(y - \delta\omega). \quad (75)$$

Eq. (75) shows that g_{12} is suppressed when $\delta\omega > \gamma_h$. The above expression for g_{12} is written in terms of the real component of $\chi(\omega)$. Using the Kramers-Kronig relation

$$\chi_1(y) = \frac{1}{\pi} \mathcal{P} \int \frac{\chi_2(z)}{y - z} dz, \quad (76)$$

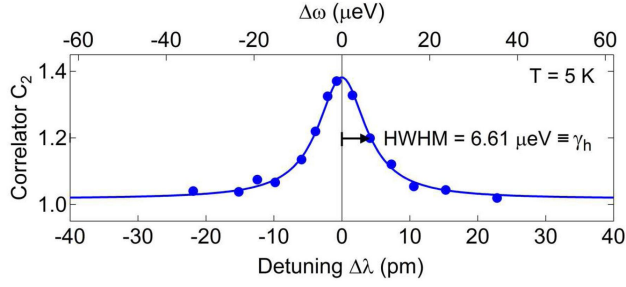


Figure 15. Two-color spin noise correlator as a function of the detuning between the probe lasers [156]. The solid line is a Lorentzian fit. Reprinted with permission from Macmillan Publishers Ltd: Nature Communications 5, 4949, 2014, Copyright ©(2014) [156].

and the identity [37]

$$\mathcal{P} \int \frac{dy}{(y-z_1)(y-z_2)} = \pi^2 \delta(z_1 - z_2), \quad (77)$$

we find that $\int dy \chi_1(y)\chi_1(y - \delta\omega) = \int dy \chi_2(y)\chi_2(y - \delta\omega)$, so

$$g_{12} \sim \int dy \chi_2(y)\chi_2(y - \delta\omega), \quad (78)$$

i.e. even though the experiment measures the Faraday rotation, the correlator g_{12} can be expressed via the dissipative part $\chi_2(\omega)$ of the optical response function.

Consider the Lorentzian broadening

$$\chi_2(\omega) = \frac{\gamma_h}{(\omega - \omega_0)^2 + \gamma_h^2}. \quad (79)$$

Substituting (79) into (78) one can find that g_{12} is of the Lorentzian form [156]

$$g_{12}(\delta\omega) \sim \frac{2\pi\gamma_h}{(\delta\omega)^2 + 4\gamma_h^2}. \quad (80)$$

As another example, consider that individual quantum dots have a Gaussian absorption due to, e.g., substantial fluctuations of the resonance frequency ω_0 caused by charge fluctuations in the vicinity of the dots. Then,

$$\chi_2(\omega) = \frac{\gamma_h}{\pi} e^{-\gamma_h^2(\omega - \omega_0)^2}, \quad (81)$$

and

$$g_{12}(\delta\omega) \sim \frac{\gamma_h}{\sqrt{2\pi}} e^{-\frac{\gamma_h^2(\delta\omega)^2}{2}}, \quad (82)$$

i.e. we find the Gaussian form of g_{12} . In the experiment [156], a Lorentzian shape of $g_{12}(\delta\omega)$ was observed (Fig. 15), which was also used to determine the homogeneous broadening γ_h in hole-doped InGaAs quantum dots.

6. Thermodynamic Constraints

The statistics of spontaneous fluctuations at the thermodynamic equilibrium should be in agreement with the laws of thermodynamics. One of such laws is the existence of the thermodynamic equilibrium, which is described by the Boltzmann distribution of microstate probabilities at a given temperature. In this section, we discuss some notable consequences of such constraints on spin noise correlators that can be observed experimentally.

6.1. Sum Rules for Integrated Noise Power

Consider the total area $A_{\alpha\beta}$ under a curve representing the noise power spectrum for any two spin variables:

$$A_{\alpha\beta} \equiv \int_{-\infty}^{\infty} P_{\alpha\beta}(\omega) d\omega, \quad (83)$$

where

$$P_{\alpha\beta}(\omega) = \int_{-\infty}^{\infty} e^{i\omega t} \langle S_\alpha(t) S_\beta(0) \rangle dt. \quad (84)$$

Here, the indices $\alpha, \beta = x, y, z$ can be either the same or different. Moreover, the spin variables in Eq. (84) can even correspond to spin components of different electrons or atoms. Substituting Eq. (84) into Eq. (83), the integral over ω results in the time delta function removed by the integration over t . The result is

$$A_{\alpha\beta} = 2\pi \langle S_\alpha(0) S_\beta(0) \rangle. \quad (85)$$

Thus, we have found that the area under the noise power spectrum does not depend on the dynamics of spin fluctuations in the sense that it depends only on the equal time correlator of spin polarization components. This correlator is a thermodynamic characteristic. Its value at the thermodynamic equilibrium can be found from the knowledge of the free energy of the system as a function of the static external magnetic field.

SNS experiments are often performed in relatively weak magnetic fields (below 0.1T). At typical temperatures of spintronics experiments (above 3K), the corresponding Zeeman splitting energy is then about two orders of magnitude smaller than $k_B T$. Therefore, while the spin dynamics can be very sensitive to such fields, the probabilities of microstates do not change substantially, and, consequently, such external fields do not affect the equal time correlators, such as the one given by Eq. (85). This observation leads to the following approximate but valuable sum rule:

Area Conservation Rule: *The area under the noise power spectrum curve remains unchanged after*

the application of an external magnetic field or any other static perturbation if the corresponding coupling energy, such as Zeeman level splitting, is much smaller than $k_B T$.

This rule is quite handy, e.g., it helps making a quick check of a result of lengthy theoretical calculations or to interpret experimental data. We note again that the application of a weak magnetic field can change the spectrum $P_{\alpha\beta}(\omega)$ considerably, e.g. by shifting the peaks of the noise power to new Larmor frequencies. At the same time, such changes do not significantly affect the area under the spectral curve.

In hot atomic gases, the temperature energy scale is much larger than energies of characteristic spin interactions. In such situations, all relevant spin microstates can be considered as equally probable and statistically independent. Moreover, for any state with a spin polarization S_α , there is an equally probable state with spin polarization $-S_\alpha$. This leads to the following rule:

No-Go Rule: *At the thermodynamic equilibrium and in the limit of large temperature, the integrated noise power spectrum of cross-correlators ($\alpha \neq \beta$ in Eq. (84)), is zero.*

This rule restricts our ability to use the total area of the noise power spectrum for studying cross-correlations when the temperature exceeds characteristic energy scales of spin dynamics. In other words, in cross-correlators, the useful information is contained only in the functional form of $P_{\alpha\beta}(\omega)$. The corrections to the area conservation and no-go rules are of the order of $gB/k_B T$, where B is the magnetic field strength and g is the corresponding g -factor. In the case of warm alkali vapors, where $T \sim 400\text{K}$ but Zeeman and hyperfine energies are $\lesssim 1\text{K}$ in the temperature scale, the no-go sum rule holds with a high accuracy.

6.2. Fluctuation-Dissipation Theorem

The fluctuation-dissipation theorem is another important result that is frequently used in theoretical calculations. It relates the noise power spectrum to linear response characteristics [37, 36]. In what follows, this connection is explicitly demonstrated.

The quantum-mechanically justified expression for the noise power spectrum is given by

$$P(\omega) = \int_{-\infty}^{\infty} d\tau e^{i\omega\tau} \text{Tr} \left(\hat{\rho} \frac{1}{2} \{ \hat{S}_z(\tau), \hat{S}_z(0) \} \right), \quad (86)$$

where $\{ \dots, \dots \}$ is the anti-commutator, and $\hat{\rho}$ is the density matrix at the thermodynamic equilibrium. The probability w_m of a microstate m can be written as

$$w_m = e^{\frac{F - E_m}{k_B T}}. \quad (87)$$

Here, F is the free energy and E_m is the energy of the microstate. One can now rewrite Eq. (86) as

$$P(\omega) = \frac{1}{2} \int_{-\infty}^{\infty} d\tau \sum_{mn} w_m (S_{mn}(\tau) S_{nm}(0) + S_{mn}(0) S_{nm}(\tau)) e^{i\omega\tau}, \quad (88)$$

where, in terms of eigenstates of the unperturbed Hamiltonian,

$$S_{mn}(\tau) \equiv \langle u_m | \hat{S}_z(\tau) | u_n \rangle.$$

Note that since $\hat{S}_z(\tau) = e^{i\hat{H}_0\tau/\hbar} \hat{S}_z(0) e^{-i\hat{H}_0\tau/\hbar}$,

$$S_{mn}(\tau) = e^{-i\omega_{nm}\tau} S_{mn} \quad \text{with} \quad \omega_{nm} = \frac{E_n - E_m}{\hbar}.$$

Here we also highlight that in this subsection we do not use the convention $\hbar = 1$ adopted in the most other parts of the review. This is related to the fact that the quantum and classical versions of the fluctuation-dissipation theorem look differently. The classical version is obtained from the quantum one in the limit $\hbar\omega \ll k_B T$, in which the Plank constant cancels out, as it will be clear from the final result.

Substituting the above relations into Eq. (88), and performing the integration over τ we find

$$\begin{aligned} P(\omega) &= \pi \sum_{mn} w_m |S_{mn}|^2 (\delta(\omega - \omega_{nm}) + \delta(\omega + \omega_{nm})) = \\ &= \pi \sum_{mn} (w_m + w_n) |S_{mn}|^2 \delta(\omega - \omega_{nm}). \end{aligned}$$

Finally, using $w_n = e^{-\hbar\omega_{nm}/(k_B T)} w_m$, the following expression for the noise power spectrum can be obtained

$$P(\omega) = \pi \sum_{mn} w_m \left(1 + e^{-\frac{\hbar\omega_{nm}}{k_B T}} \right) |S_{mn}|^2 \delta(\omega - \omega_{nm}), \quad (89)$$

which, taking into account the time delta function, can be rewritten in the equivalent form

$$P(\omega) = \pi \left(1 + e^{-\frac{\hbar\omega}{k_B T}} \right) \sum_{mn} w_m |S_{mn}|^2 \delta(\omega - \omega_{nm}). \quad (90)$$

Consider now the following expression:

$$C(\omega) \equiv \frac{1}{2\hbar} \int_{-\infty}^{\infty} d\tau e^{i\omega\tau} \langle [\hat{S}_z(\tau), \hat{S}_z(0)] \rangle, \quad (91)$$

where the square brackets are the standard commutator of operators. Going through the same steps, we find

$$\begin{aligned} C(\omega) &= \frac{1}{2\hbar} \int_{-\infty}^{\infty} d\tau e^{i\omega\tau} \sum_{mn} w_m (e^{-i\omega_{nm}\tau} - e^{i\omega_{nm}\tau}) = \\ &= \frac{\pi}{\hbar} \left(1 - e^{-\frac{\hbar\omega}{k_B T}} \right) \sum_{mn} w_m |S_{mn}|^2 \delta(\omega - \omega_{nm}). \end{aligned} \quad (92)$$

Comparing (90) and (92), we obtain

$$P(\omega) = \hbar \coth\left(\frac{\hbar\omega}{2k_B T}\right) C(\omega). \quad (93)$$

Let us now provide the physical interpretation of $C(\omega)$. Consider the linear response of the spin system to a time-dependent magnetic field $h_z(t)$ applied along the z -axis. The Hamiltonian term describing this interaction is $\hat{H}_h(t) = -h_z(t)\hat{S}_z$. Up to the linear order in $h(t)$, we have

$$\begin{aligned} \langle \hat{S}_z(t) \rangle &= \\ &= \langle e^{(i/\hbar) \int_{-\infty}^t \hat{H}_h(t') dt'} \hat{S}_z(t) e^{-(i/\hbar) \int_{-\infty}^t \hat{H}_h(t') dt'} \rangle \approx \\ &\approx \frac{i}{\hbar} \int_{-\infty}^t dt' h_z(t') \langle [\hat{S}_z(t), \hat{S}_z(t')] \rangle. \end{aligned} \quad (94)$$

Let us now introduce the *linear response function* $A_{zz}(t)$, such that

$$A_{zz}(t) = 0 \quad \text{for } t < 0,$$

and

$$\langle \hat{S}_z(t) \rangle = \int_{-\infty}^t dt' A_{zz}(t-t') h_z(t'). \quad (95)$$

Comparing (94) and (95) we find

$$A_{zz}(\tau) = \frac{i}{\hbar} \theta(\tau) \langle [\hat{S}_z(\tau), \hat{S}_z(0)] \rangle. \quad (96)$$

Hence,

$$\int_0^{\infty} d\tau e^{i\omega\tau} \langle [\hat{S}_z(\tau), \hat{S}_z(0)] \rangle = -i\hbar A_{zz}(\omega). \quad (97)$$

Note also that

$$\begin{aligned} \int_{-\infty}^0 d\tau e^{i\omega\tau} \langle [\hat{S}_z(\tau), \hat{S}_z(0)] \rangle &= \\ &= - \int_0^{\infty} d\tau e^{-i\omega\tau} \langle [\hat{S}_z(\tau), \hat{S}_z(0)] \rangle = \\ &= i\hbar A_{zz}(-\omega) = -i\hbar A_{zz}^*(\omega), \end{aligned} \quad (98)$$

where we used the fact that, due to the translation in time invariance of the equilibrium correlator, $\langle [\hat{S}_z(\tau), \hat{S}_z(0)] \rangle = -\langle [\hat{S}_z(-\tau), \hat{S}_z(0)] \rangle$, and that $A_{zz}(t)$ is real valued. Substituting (97) and (98) into (91) and then (93), we find:

$$\begin{aligned} P(\omega) &= -\frac{i}{2} \hbar (A_{zz}(\omega) - A_{zz}^*(\omega)) \coth\left(\frac{\hbar\omega}{2k_B T}\right) = \\ &= \hbar \Im [A_{zz}(\omega)] \coth\left(\frac{\hbar\omega}{2k_B T}\right). \end{aligned} \quad (99)$$

Equation (99) is the famous fluctuation-dissipation theorem stating that the equilibrium noise power spectrum is related to the imaginary part of the response function.

6.3. Higher Order Fluctuation Relations

Higher order spin correlators also satisfy their own fluctuation relations that connect these correlators to nonlinear response characteristics and lower order cumulants at nonequilibrium conditions. Such relations encountered, for example, in the theory of spin glass dynamics [157].

Nonlinear and nonequilibrium thermodynamics is currently a highly active field of research because profound symmetries were identified at the level of the full counting statistics that became known as *Fluctuation Relations*. These are exact formulas that hold true even in systems that are driven arbitrarily far away from the thermodynamic equilibrium [158, 159, 160, 161, 162, 163]. In particular, fluctuation relations for spin currents were considered in [163]. The experimental verification of fluctuation relations can provide information about system parameters that cannot be easily extracted by standard approaches [164].

Numerous relations between higher order cumulants and nonlinear response characteristics have been reviewed in [165, 166]. Specifically, the simplest of the known fluctuation relations, beyond the standard fluctuation-dissipation theorem, relate the response of the spin correlator to a time-dependent perturbation with the nonlinear response of the average spin polarization. Since SNS beyond the thermodynamic equilibrium and linear response has already been successfully demonstrated in [49], it is likely that some of the predictions of nonlinear thermodynamics will be tested in the near future. Below, we discuss two examples that are valid in the domain of classical overdamped stochastic dynamics.

6.3.1. Higher Order Onsager Relations. Onsager relations are equalities between different cross-correlators of variables at the thermodynamic equilibrium [165].

Consider a mesoscopic classical interacting spin system with Markovian stochastic evolution among N discrete states. Let $\mathbf{p}(t)$ be the vector of probabilities of all possible microstates of the spin system. Each classical microstate $|i\rangle$ is characterized by the energy E_i and eigenvalue of the spin polarization operator \hat{s}_α , where $\alpha = x, y$ or z , or other spin indexes in the case of a multicomponent spin system. Note that projections of the classical spin commute with each other.

The Markovian evolution is described by the master operator \hat{H} according to

$$\frac{d}{dt} \mathbf{p} = \hat{H} \mathbf{p}. \quad (100)$$

Section 4 of Ref. [166] explains the derivation of the master equation from microscopic Hamiltonian equations of motion. At the thermodynamic

equilibrium, kinetic rates satisfy the detailed balance condition that can be included by writing the elements of the Liouville operator matrix in the Arrhenius parametrization [167, 168]: $H_{ij} = ke^{\beta(E_j - W_{ij})}$, $H_{jj} = -\sum_{i \neq j} H_{ij}$, where $W_{ij} = W_{ji}$ are real parameters describing the ‘‘barriers’’ between the states, k is a constant real parameter, and $\beta = 1/(k_B T)$. This parametrization guarantees that the evolution converges to the Boltzmann distribution $[\mathbf{P}_{eq}]_i = Ce^{-\beta E_i}$, where $C = \left(\sum_{i=1}^N e^{-\beta E_i}\right)^{-1}$ is the normalization constant. Obviously, the operator \hat{H} satisfies the condition

$$\hat{H}^\dagger = e^{\beta \hat{E}} \hat{H} e^{-\beta \hat{E}}, \quad (101)$$

where $\hat{E} = \text{diag}\{E_1, \dots, E_N\}$.

The spin correlator $C_{\alpha_n \dots \alpha_1} \equiv \langle s_{\alpha_n}(t_n) \dots s_{\alpha_1}(0) \rangle$ is then given by

$$C_{\alpha_n \dots \alpha_1} = \langle \hat{\mathbf{1}} | \hat{s}_{\alpha_n} e^{\hat{H}(t_n - t_{n-1})} \dots \hat{s}_{\alpha_2} e^{\hat{H}t_1} \hat{s}_{\alpha_1} | \mathbf{P}_{eq} \rangle, \quad (102)$$

where $\langle \hat{\mathbf{1}} | = (1, \dots, 1)$ is the vector with all unit entries. Since the correlator (102) is a real function, it coincides with its complex conjugated expression:

$$C_{\alpha_n \dots \alpha_1} = \langle \mathbf{P}_{eq} | \hat{s}_{\alpha_1} e^{\hat{H}^\dagger t_1} \hat{s}_{\alpha_2} \dots e^{\hat{H}^\dagger(t_n - t_{n-1})} s_{\alpha_n} | \hat{\mathbf{1}} \rangle, \quad (103)$$

Using Eq. (101) and the relation $|\hat{\mathbf{1}}\rangle = (e^{\beta \hat{E}}/C)|\mathbf{P}_{eq}\rangle$, Eq. (103) leads to a higher order Onsager relation [165, 157]:

$$\langle s_{\alpha_n}(t_n) \dots s_{\alpha_1}(0) \rangle = \langle s_{\alpha_1}(t_n) s_{\alpha_2}(t_n - t_2) \dots s_{\alpha_{n-1}}(t_n - t_{n-1}) s_{\alpha_n}(0) \rangle \quad (104)$$

Here, $n = 2$ corresponds to the standard Onsager reciprocity relation $\langle s_{\alpha_2}(t) s_{\alpha_1}(0) \rangle = \langle s_{\alpha_1}(t) s_{\alpha_2}(0) \rangle$, while $n = 3$ corresponds to a higher order relation

$$\langle s_{\alpha_3}(t_2) s_{\alpha_2}(t_1) s_{\alpha_1}(0) \rangle = \langle s_{\alpha_1}(t_2) s_{\alpha_2}(t_2 - t_1) s_{\alpha_3}(0) \rangle. \quad (105)$$

6.3.2. Bochkov-Kuzovlev Type of Fluctuation Relations. Other classical higher order relations are most easily derived from the Bochkov-Kuzovlev formulas [158] (see also chapter 1 in [166] for a textbook introduction). Let $U(\mathbf{s})$ and $S(\mathbf{s})$ be the energy and entropy of a spin system with a known spin fluctuation size \mathbf{s} , assuming that all other degrees of freedom quickly equilibrate at a given temperature, and let us define a spin-dependent conditional free energy: $F(\mathbf{s}) = U(\mathbf{s}) - k_B T S(\mathbf{s})$. The application of a constant external magnetic field \mathbf{h} leads to a change of the free energy $F(\mathbf{s})$: $F(\mathbf{s}) = f(\mathbf{s}) - \mathbf{h} \cdot \mathbf{s}$, where $f(\mathbf{s})$ is the independent of \mathbf{h} part, and where the Bohr magneton and g -factor are included into the definition of \mathbf{h} . A

system at a constant \mathbf{h} always relaxes to the thermodynamic equilibrium with the probability distribution (see, e.g., Sec. 2.2.7 of Ref. [165] for details):

$$p_{eq}(\mathbf{s}) = \frac{e^{-\beta F(\mathbf{s})}}{Z}, \quad (106)$$

where $Z = Z(\mathbf{h})$ is the partition function. In order to guarantee such a relaxation, kinetic rates must satisfy the detailed balance constraints, so that probabilities of processes that connect microstates with spin polarizations \mathbf{s} and \mathbf{s}' are connected by

$$\frac{p_{\mathbf{s} \rightarrow \mathbf{s}'}}{p_{\mathbf{s}' \rightarrow \mathbf{s}}} = e^{\beta(F(\mathbf{s}) - F(\mathbf{s}'))}. \quad (107)$$

Consider now the case when the system is initially at the thermodynamic equilibrium with $\mathbf{h} = 0$ but then the field is suddenly switched on to a constant value. We are interested in the ratio of probabilities of observing transitions from the state \mathbf{s} to \mathbf{s}' and backwards. This ratio is influenced by the initial state probabilities:

$$\frac{p_{eq}(\mathbf{s}) p_{\mathbf{s} \rightarrow \mathbf{s}'}}{p_{eq}(\mathbf{s}') p_{\mathbf{s}' \rightarrow \mathbf{s}}} = e^{\beta \mathbf{h} \cdot (\mathbf{s}' - \mathbf{s})}. \quad (108)$$

Note that equilibrium distribution prefactors in (108) completely cancelled the dependence of the rhs on $f(\mathbf{s})$.

Bochkov and Kuzovlev showed that Eq. (108) can be extended to an arbitrary driving protocol $\mathbf{h}(t)$. Let the external field be zero up to time $-T_m/2$, and assume that it changes with time during the measurement interval $t \in (-T_m/2, T_m/2)$, returning to zero value at the end: $\mathbf{h}(T_m/2) = \mathbf{h}(-T_m/2) = 0$. One of the Bochkov-Kuzovlev formulas relates the probability $P(\mathbf{s}(t)|\mathbf{h}(t))$ of observation of a trajectory of the spin system $\mathbf{s}(t)$ under the driving protocol $\mathbf{h}(t)$ with the probability $P(\mathbf{s}^R(t)|\mathbf{h}^R(t))$ of observation of the reversed in time trajectory $\mathbf{s}^R(t) = \mathbf{s}(-t)$ under the action of the reversed in time driving protocol $\mathbf{h}^R(t) = \mathbf{h}(-t)$ [Eq. (2.11) in Ref. [158]]:

$$\frac{P(\mathbf{s}(-t)|\mathbf{h}(-t))}{P(\mathbf{s}(t)|\mathbf{h}(t))} = e^{-\beta W}, \quad (109)$$

where

$$W = \int_{-T_m/2}^{T_m/2} dt \mathbf{h}(t) \cdot \dot{\mathbf{s}}(t) \quad (110)$$

is the work done by the time-dependent field on the spin system. To derive (109) we should split the time interval in infinitesimal steps (t_i, t_{i+1}) , $i = 0, \dots, N$ with $N \gg 1$. At each step, the field $\mathbf{h}(t_i)$ can be considered constant. Hence, Eq. (107) can be applied at given $\mathbf{h}(t_i)$ during this interval. Using this constraint and the definition $P(\mathbf{s}(t)|\mathbf{h}(t)) = p_{eq}(\mathbf{s}_0) \prod_i p_{\mathbf{s}_i \rightarrow \mathbf{s}_{i+1}}$,

and $P(\mathbf{s}(-t)|\mathbf{h}(-t)) = p_{\text{eq}}(\mathbf{s}_N) \prod_i p_{\mathbf{s}_{i+1} \rightarrow \mathbf{s}_i}$, one can verify the validity of Eq. (109).

The next observation made by Bochkov and Kuzovlev was that the expression for the probability functionals (109) can be used to generate numerous relations between higher and lower order correlators at the thermodynamic equilibrium. For example, following [157], we move the denominator in (109) to the right-hand side, multiply both sides of equation by $s_j(t_1)$ and sum over all possible trajectories. Then, in the sum over all trajectories, each $\mathbf{s}(t)$ encounters with the time-reversed one, $\mathbf{s}(-t)$. Hence,

$$\sum_{\mathbf{s}(t)} P(\mathbf{s}(-t)|\mathbf{h}(-t))s_j(t_1) = \sum_{\mathbf{s}(t)} P(\mathbf{s}(t)|\mathbf{h}(-t))s_j(-t_1).$$

This finally gives us

$$\langle s_j(-t_1) \rangle_{\mathbf{h}^R} = \langle s_j(t_1) e^{-W} \rangle_{\mathbf{h}}, \quad (111)$$

where the index \mathbf{h} means that the average is taken under the action of the protocol $\mathbf{h}(t)$. By equating the linear in $\mathbf{h}(t)$ terms in (111) we find

$$\beta \frac{\partial}{\partial t_2} \langle s_j(t_1) s_k(t_2) \rangle = \frac{\delta \langle s_j(t_1) \rangle}{\delta h_k(t_2)} - \frac{\delta \langle s_j(-t_1) \rangle}{\delta h_k(-t_2)}, \quad (112)$$

where the averages are already over the equilibrium probability distribution of microstates of the system. The causality requires $\delta \langle s_j(-t_1) \rangle / \delta h_k(-t_2) = 0$ at $t_1 > t_2$. Therefore,

$$\beta \frac{\partial}{\partial t_2} \langle s_j(t_1) s_k(t_2) \rangle = \frac{\delta \langle s_j(t_1) \rangle}{\delta h_k(t_2)}, \quad t_1 > t_2. \quad (113)$$

In the frequency domain, Eq (113) reproduces the fluctuation-dissipation relation (99) in the ‘‘classical’’ limit $\omega \ll k_B T$. To show this, consider $k = j = z$ and identify $\frac{\delta \langle s_j(t_1) \rangle}{\delta h_k(t_2)}$ with $A_{zz}(t_1 - t_2)$ in (99), and note that due to the time translation invariance, $\frac{\partial}{\partial t_2} \langle s_z(t_1) s_z(t_2) \rangle = -\frac{\partial}{\partial t_1} \langle s_z(t_1) s_z(t_2) \rangle$. Afterwards we multiply both sides of Eq. (113) by $2 \sin(\omega \tau)$, with $\tau = t_1 - t_2$, and integrate over τ from zero to infinity. We then obtain an equation

$$-2 \int_0^\infty d\tau \sin(\omega \tau) \partial_\tau \langle s_z(\tau) s_z(0) \rangle = \int d\tau A_{zz}(\tau) \sin(\omega \tau).$$

On the left-hand side of this equation, we perform integration by parts and use the Wiener-Khinchine theorem in Eq. (7). For the right-hand side, we note that $\int d\tau A_{zz}(\tau) \sin(\omega \tau) = 2\Im[A_{zz}(\omega)]$. The final result is

$$P(\omega) = \frac{2k_B T}{\omega} \Im[A_{zz}(\omega)], \quad (114)$$

which coincides with (99) in the limit $\omega \ll k_B T$.

Similarly, we can derive relations between higher order correlators. Multiplying both sides of (109) by $s_j(t_1) s_l(t_2)$ and repeating the same steps for $-t_2 > t_1 > 0 > t_2$, we find a higher order fluctuation relation:

$$\beta \frac{\partial}{\partial t_2} \langle s_j(-t_2) s_k(t_1) s_l(t_2) \rangle = \frac{\delta \langle s_j(-t_2) s_l(t_2) \rangle}{\delta h_k(t_1)} - \frac{\delta \langle s_l(-t_2) s_j(t_2) \rangle}{\delta h_k(-t_1)}. \quad (115)$$

It relates the 3rd order correlator at the equilibrium to a linear response of the 2nd order correlators.

Quantum theory predicts that higher order relations, like (105) and (115), are not generally satisfied [145]. At the same time, some other extensions of higher order fluctuation relations to the quantum domain are known [165]. Their implications for spin fluctuations remain to be understood.

As a side note, we point that the modern research on higher order fluctuation relations has shifted from relations between correlators to studies of global properties of statistics of work and information flow [159, 162, 169]. Therefore, the article [158] by Bochkov and Kuzovlev is often associated with a special consequence of Eq. (109), which is obtained by moving $P(\mathbf{s}(t)|\mathbf{h}(t))$ from the denominator to the right-hand side of this equation and averaging over all possible trajectories:

$$\langle e^{-\beta W} \rangle_{\mathbf{h}} = 1. \quad (116)$$

For example, Eq. (116) is often mentioned as the first but only one of many other similar relations, the most widely known of which is the Jarzynski equality [159]

$$\langle e^{-\beta W_J} \rangle_{\mathbf{h}} = e^{-\beta \Delta F}, \quad (117)$$

where ΔF is the change of the equilibrium free energy between the initial and final values of the time-dependent parameter $\mathbf{h}(t)$, and W_J is the work defined differently from W , namely, $W_J = \int \mathbf{s}(t) \cdot (d\mathbf{h}/dt) dt$, in our notation.

Jarzynski equality (117) generally carries a different meaning than Eq. (116), and it has appeared quite influential, e.g., for applications to nonequilibrium free-energy sampling. It seems, however, that Bochkov-Kuzovlev relations like (109), (111), and (116), with the definition of work (110), carry special importance because they provide the most straightforward way to derive higher order relations between various correlators at the equilibrium, such as Eq. (115).

7. Methods I: Spin Noise Phenomenology

The phenomenological approach and relaxation time approximation are justified by essentially the same arguments. In both cases, the spin dynamics is described

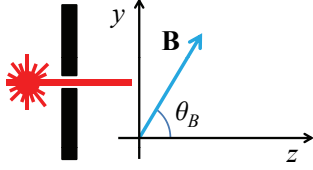


Figure 16. Schematics of the measurement geometry.

by equations with several phenomenological parameters. The microscopic derivation of these parameters is beyond the scope of the phenomenological approach. Its basic power is related to the fact that the phenomenological approach can be formulated without paying a close attention to specific system details. This makes its predictions particularly useful as a “first guess” in many situations. We note, however, that by no means the phenomenological approach is universally applicable. For example, it cannot be generally applied to explain $1/\omega^\alpha$ type of spectra that encounter in disordered strongly interacting spin systems.

7.1. Spin Fluctuation Dynamics

7.1.1. Bloch Equation. Let’s consider a spontaneous spin fluctuation \mathbf{S} emerged at $t = 0$ in the observation volume. The Bloch equation describes the dynamics of this fluctuation, namely, its precession in an external magnetic field \mathbf{B} and relaxation:

$$\frac{dS_\alpha}{dt} = g\varepsilon_{\alpha\beta\gamma}B_\beta S_\gamma - \frac{S_\alpha}{\tau_s^\alpha}, \quad (118)$$

where $\alpha, \beta = x, y, z$, g is the electron g -factor (the Bohr magneton is included in its definition), and we also set $\hbar = 1$. In semiconductors, the g -factor is usually a tensor due the atomic lattice anisotropy. For the sake of simplicity, we disregard this detail here. We assume that the measurement beam is directed along the z -axis and the magnetic field vector points in the yz -plane, making an angle θ_B with the z -axis (see Fig. 16).

The parameters τ_s^α are the relaxation times along different axes. In many semiconductors, the relaxation time is anisotropic, i.e. $\tau_s^x \neq \tau_s^y \neq \tau_s^z$. However, in frequently discussed SNS applications (the hot atomic vapors and bulk GaAs), the relaxation time can be considered as almost isotropic: $\tau_s \equiv \tau_x = \tau_y = \tau_z$. Instead of relaxation times, we will also often use *the relaxation rates* defined as the inverses of relaxation times, e.g.,

$$\Gamma_s = 1/\tau_s. \quad (119)$$

The solution of Eq. (118) for an isotropic relaxation rate shows that a spontaneous spin fluctuation $\mathbf{S} = \hat{z}S_{z0}$ initially emerged along the measurement axis precesses around the magnetic field

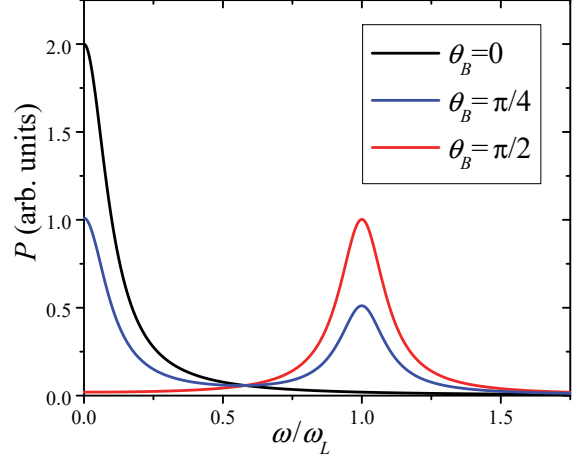


Figure 17. The noise power spectrum $P(\omega)$ (Eq. (121)) shown for several values of the angle θ_B between the external field and the measurement axis. Spin relaxation is isotropic with $\omega_L \tau_s = 10$.

and decays according to

$$S_z(t) = S_{z0} \cos^2(\theta_B) e^{-t/\tau_s} + S_{z0} \sin^2(\theta_B) e^{-t/\tau_s} \cos(\omega_L t), \quad (120)$$

where $\omega_L = g|B|$ is the Larmor frequency.

The Bloch equation (118) can also be solved for the case of an oscillating magnetic field. In SNS setup, the multiphoton absorption processes due to the oscillating field can be observed in spin noise [170].

7.1.2. Noise Power Spectrum in a Tilted Magnetic Field. The noise power spectrum is obtained as the Fourier transform of the spin-spin correlator:

$$P(\omega) = 2 \int_0^\infty dt \cos \omega t \langle S_z(t) S_z(0) \rangle = \langle S_{z0}^2 \rangle \left(\frac{2 \cos^2(\theta_B)/\tau_s}{\omega^2 + \frac{1}{\tau_s^2}} + \sum_{s=\pm 1} \frac{\sin^2(\theta_B)/\tau_s}{(\omega - s\omega_L)^2 + \frac{1}{\tau_s^2}} \right) \quad (121)$$

Here, $s = \pm 1$. Due to the symmetry of the spectrum under $\omega \rightarrow -\omega$ transformation, only the positive values of ω are informative. Figure 17 shows that, in a tilted magnetic field, the noise power spectrum typically consists of two Lorentzian peaks centered at zero and Larmor frequencies (see the blue curve in Fig. 17). In the limiting cases of $\theta = 0$ ($\pi/2$) only the zero (Larmor) frequency peak is present. These limiting cases are presented by the black (zero frequency peak) and red (Larmor frequency peak) curves in Fig. 17.

The relative areas of peaks are controlled by the angle θ_B that the external field makes with the measurement axis. An important property is independence of the total area under the spectrum on the direction and magnitude of the external field.

Moreover, the total area under the spectrum is a thermodynamic characteristic independent of kinetic rates. Indeed, due to the property

$$\int_{-\infty}^{\infty} d\omega \frac{\gamma}{\omega^2 + \gamma^2} = \pi, \quad (122)$$

the total area of the noise power spectrum is given by

$$\int_{-\infty}^{\infty} P(\omega) d\omega = 2\pi \langle S_{z0}^2 \rangle, \quad (123)$$

i.e. it depends only on statistical properties of the equal time correlator. The latter can be estimated from the knowledge of the equilibrium spin distribution.

7.1.3. Characteristic Sizes of Spin Fluctuations. The variance of a fluctuation size, $\langle S_{z0}^2 \rangle$, enters the expression for the noise power spectrum (121) as a parameter. In many situations, it can be easily estimated without resorting to complex microscopic techniques. Consider, for example, spin noise of noninteracting conduction electrons that form a Fermi sea. The Fermi-Dirac distribution

$$f_D(\epsilon) = \frac{1}{1 + e^{-\epsilon/k_B T}} \quad (124)$$

describes the occupancy of energy levels by electrons in the system. Each level is doubly degenerate due to the two possible spin orientations of electron. There is no contribution to $\langle S_{z0}^2 \rangle$ from either empty levels or levels populated by two electrons. Spin fluctuations originate only from the energy levels occupied by a single electron. Such electrons can be found in the up- or down-spin state with the same probability. The probability that a given energy level ϵ is populated by a single electron is given by $f_{\uparrow}(1 - f_{\downarrow}) + f_{\downarrow}(1 - f_{\uparrow}) = 2f_D(\epsilon)(1 - f_D(\epsilon))$, where $f_{\uparrow/\downarrow}$ are the probabilities that coincide with (124) at the thermodynamic equilibrium.

Spin fluctuations from independent singly occupied energy levels (orbitals) contribute additively to the variance of the total spin fluctuation. The average of the spin projection squared of a single electron is $\langle \hat{s}_z^2 \rangle = 1/4$. Taking into account that, at sufficiently low temperatures, the main contribution to spin noise comes from the conduction electrons near the Fermi surface, we find

$$\langle S_{z0}^2 \rangle = \frac{D}{4} \int d\epsilon 2f_D(\epsilon)(1 - f_D(\epsilon)) = \frac{1}{2} D k_B T, \quad (125)$$

where D is the density of states per spin direction. This example shows that in a sufficiently cold Fermi liquid ($k_B T \ll \epsilon_F$), the Pauli exclusion principle leads to a linear temperature dependence of the area under the spin noise power spectrum curve.

Another frequently encountered situation is when spin noise is created by $N \gg 1$ truly noninteracting electrons. This situation is found, e.g. in an insulating state when spin noise is produced by localized electrons that are well separated and do not interact with each other. In this case, each localized spin-degenerate state is always populated by a single electron, so that

$$\langle S_{z0}^2 \rangle = \frac{N}{4}, \quad (126)$$

i.e. each of N electrons provides the same contribution (1/4) to the variance. Moreover, a similar situation takes place at high temperatures $k_B T \gg \epsilon_F$, when one can disregard the Pauli exclusion principle and assume that all electrons are uncorrelated. Figure 7 shows that the experimentally obtained integrated noise power depends on temperature linearly, in agreement with (125), but has a finite offset value at $T = 0$ in agreement with (126).

7.1.4. Relaxation Time Anisotropy. A significant application area for SNS is the field of semiconductors, including novel 2D semiconducting materials [149]. In many of such systems, due to an intrinsic anisotropy, the spin relaxation rate depends on the direction of spin polarization. For example, the in-plane spin relaxation in MoS₂ was estimated to be about an order of magnitude faster than the out-of-plane spin relaxation [152]. Such anisotropy leads to the deviation of the behavior of the spin noise power spectrum from the one described by Eq. (121).

Let's consider only the most important case of a purely in-plane magnetic field. In the presence of anisotropy in relaxation rates, $\Gamma_s^{\perp} \neq \Gamma_s^z$, where Γ_s^{\perp} is the in-plane relaxation rate, the dynamics of spin polarization can be described by the equation

$$\frac{d\mathbf{S}}{dt} = gB_y \hat{y} \times \mathbf{S} - \Gamma_s^{\perp} (S_x \hat{x} + S_y \hat{y}) - \Gamma_s^z S_z \hat{z}. \quad (127)$$

The solution of Eq. (127) with the initial condition $\mathbf{S} = S_0 \hat{z}$ can be written explicitly. Depending on the strength of the magnetic field and anisotropy, the spin polarization exhibits either a monotonous decay or oscillating behavior.

I. First, assume the situation with $\Gamma_s^{\perp} > \Gamma_s^z$ and a relatively weak magnetic field $gB_y < (\Gamma_s^{\perp} - \Gamma_s^z)/2$. The spin polarization then relaxes monotonously:

$$S_z(t) = S_{z0} e^{-\frac{(\Gamma_s^z + \Gamma_s^{\perp})t}{2}} \times \left(\cosh(\Omega t) + \frac{(\Gamma_s^{\perp} - \Gamma_s^z) \sinh(\Omega t)}{2\Omega} \right), \quad (128)$$

where

$$\Omega = \frac{\sqrt{(\Gamma_s^{\perp} - \Gamma_s^z)^2 - 4(gB_y)^2}}{2}.$$

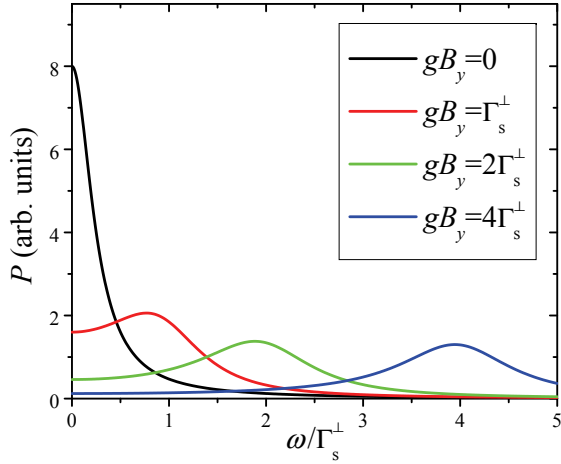


Figure 18. The noise power spectrum $P(\omega)$ (Eqs. (129), (131)) shown for several values of the external in-plane magnetic field at $\Gamma_s^z = 0.25\Gamma_s^\perp$. The peak at zero magnetic field is noticeably narrower than the peak at large field values.

The noise power spectrum consists of a single peak centered at zero frequency (Fig. 18, black curve). The shape of this peak is described by the sum of two Lorentzians with different amplitudes and half-widths:

$$P(\omega) = \langle S_{z0}^2 \rangle \left(\frac{A_+ \gamma_+}{\omega^2 + \gamma_+^2} + \frac{A_- \gamma_-}{\omega^2 + \gamma_-^2} \right), \quad (129)$$

where

$$A_\pm = 1 \pm \frac{\Gamma_s^z - \Gamma_s^\perp}{2\Omega}, \quad \gamma_\pm = \bar{\Gamma}_s \pm \Omega, \quad \bar{\Gamma}_s = \frac{\Gamma_s^z + \Gamma_s^\perp}{2}.$$

II. When $gB_y > (\Gamma_s^\perp - \Gamma_s^z)/2$ and $\Gamma_s^\perp > \Gamma_s^z$, the spin polarization shows an oscillatory behavior:

$$S_z(t) = S_{z0} e^{-\frac{(\Gamma_s^z + \Gamma_s^\perp)t}{2}} \times \left(\cos(\Omega t) + \frac{(\Gamma_s^\perp - \Gamma_s^z) \sin(\Omega t)}{2\Omega} \right), \quad (130)$$

where

$$\Omega = \frac{\sqrt{4(gB_y)^2 - (\Gamma_s^\perp - \Gamma_s^z)^2}}{2}.$$

The noise power spectrum consists of two nearly Lorentzian peaks centered at $\omega = \pm\Omega$ (Fig. 18, blue, green, and red curves), whose half-widths are determined by the average of two relaxation rates:

$$P(\omega) = \sum_{s=\pm} \frac{\langle S_{z0}^2 \rangle (\Gamma_s^\perp + s\beta\omega)}{(\omega + s\Omega)^2 + \bar{\Gamma}_s^2}, \quad \beta = \frac{\Gamma_s^\perp - \Gamma_s^z}{2\Omega}. \quad (131)$$

III. Finally, consider the regime of $\Gamma_s^\perp < \Gamma_s^z$, which takes place, for example, in the Rashba 2D electron system. This system is analyzed in more detail in Sec. 8. One can show that this regime is also characterized by the same equations as presented in the

paragraphs **I.-II.** above. However, now the transition from the monotonous relaxation to oscillatory behavior occurs at $gB_y = (\Gamma_s^z - \Gamma_s^\perp)/2$.

7.2. Langevin Equation and Fluctuation-Dissipation theorem

The approach based on the Bloch equation is not self-consistent. It uses the size of a typical spin fluctuation as an input parameter, and does not include the dynamics leading to the appearance of spin fluctuations. Such an approach is not easy to generalize, e.g., to include nonlinear interactions or calculate higher order correlators. A more rigorous approach is based on the Langevin equation that includes a noise term as a source of spin fluctuations:

$$\dot{\mathbf{S}} = -\hat{\mathbf{R}}\mathbf{S} + \boldsymbol{\xi}, \quad (132)$$

where $\hat{\mathbf{R}}$ is called the *relaxation matrix* (since its elements contain information about characteristic relaxation rates), and $\boldsymbol{\xi}$ is the noise term. The elements of $\hat{\mathbf{R}}$ can be read directly from the Bloch equation (118):

$$R_{\alpha\beta} = -g\varepsilon_{\alpha\gamma\beta} B_\gamma + \frac{\delta_{\alpha\beta}}{\tau_s^\alpha}. \quad (133)$$

In mesoscopic systems, unless higher order spin correlators are needed, the noise term can be usually well approximated by a Gaussian delta-correlated noise:

$$\langle \xi_\alpha(t) \xi_\beta(t') \rangle = G_{\alpha\beta} \delta(t - t'), \quad (134)$$

where $\alpha, \beta = x, y, z$ and $G_{\alpha\beta}$ are elements of the *correlation matrix* $\hat{\mathbf{G}}$. This approximation is justified by the fact that when the number of observed spins is large, $N \gg 1$, one can choose a time scale δt such that it is much smaller than the ensemble average spin relaxation time but sufficiently large for many random spin flips to happen. Since the time interval δt is much smaller than the spin relaxation time, the number of spins that experience spin flips during δt is much smaller than the total number of spins N . Hence, it is highly unlikely for any given spin to flip more than once in two consecutive time intervals of the size δt or influence the dynamics of other spins. In turn, this means that spin fluctuations in nearby time intervals can be considered as statistically independent. Therefore, on a much longer time scale of spin relaxation, one can assume that the spin fluctuations are produced by a delta-correlated white noise.

At the thermodynamic equilibrium, one can derive the correlation matrix $\hat{\mathbf{G}}$ from the knowledge of the relaxation matrix $\hat{\mathbf{R}}$ and the condition that the equilibrium distribution of electronic spins is described by the Fermi-Dirac statistics. The arguments run as follows:

First, one can prove the following formula (see also Eq. (4.4.51) in [171]), which is valid for any steady stochastic process described by the equation of the type (132):

$$\hat{\mathbf{R}}\hat{\sigma} + \hat{\sigma}\hat{\mathbf{R}}^\dagger = \hat{\mathbf{G}}, \quad (135)$$

where $\hat{\sigma}$ is the matrix of equal time spin correlators, with components

$$\sigma_{\alpha\beta} = \langle S_\alpha(t)S_\beta(t) \rangle. \quad (136)$$

Proof: A formal solution of Eq. (132) can be written as

$$\mathbf{S}(t) = \int_{-\infty}^t dt_1 e^{-\hat{\mathbf{R}}(t-t_1)} \boldsymbol{\xi}(t_1). \quad (137)$$

Substituting (137) and (136) into the left-hand side of Eq. (135), and then applying (134) we find:

$$\begin{aligned} \hat{\mathbf{R}}\hat{\sigma} + \hat{\sigma}\hat{\mathbf{R}}^\dagger &= \int_{-\infty}^t dt' \left[\hat{\mathbf{R}}e^{-\hat{\mathbf{R}}(t-t')} \hat{\mathbf{G}}e^{-\hat{\mathbf{R}}^\dagger(t-t')} + \right. \\ &\quad \left. + e^{-\hat{\mathbf{R}}(t-t')} \hat{\mathbf{G}}e^{-\hat{\mathbf{R}}^\dagger(t-t')} \hat{\mathbf{R}}^\dagger \right] = \\ &= \int_{-\infty}^t dt' \frac{d}{dt'} \left[e^{-\hat{\mathbf{R}}(t-t')} \hat{\mathbf{G}}e^{-\hat{\mathbf{R}}^\dagger(t-t')} \right] = \hat{\mathbf{G}}. \end{aligned}$$

This proves the formula (135).

Usually, Eq. (135) cannot be used to derive the correlation matrix because the matrix $\hat{\sigma}$, by itself, has to be found self-consistently by solving the Langevin equation. However, for a system at the thermodynamic equilibrium, the equal time correlator is directly related to the equilibrium Boltzmann-Gibbs distribution and can be derived whenever the free energy function of the system is known. Thus, for the equal time correlator of the Fermi gas, one can verify that the magnetic field dependent terms in the correlation matrix (133) do not contribute to the matrix $\hat{\mathbf{G}}$. Equation (125) then gives

$$G_{\alpha\beta} = \delta_{\alpha\beta} \frac{Dk_B T}{\tau_s}, \quad (138)$$

and for the system of N independent spins, Eq. (126) gives

$$G_{\alpha\beta} = \frac{N}{2\tau_s} \delta_{\alpha\beta}. \quad (139)$$

The experimentally measurable characteristic is the Fourier transform of the fluctuating spin polarization. For a large measurement time interval T , it is given by

$$S_\alpha(\omega) = \lim_{T \rightarrow \infty} \frac{1}{\sqrt{T}} \int_{-T/2}^{T/2} e^{i\omega t} S_\alpha(t) dt, \quad (140)$$

from which the spin correlators in the frequency domain are obtained as

$$P_{\alpha\beta} = \langle S_\alpha(\omega)S_\beta(-\omega) \rangle. \quad (141)$$

Taking the Fourier transform of Eq. (132) we find

$$\boldsymbol{\xi}(\omega) = (i\omega\hat{\mathbf{1}} + \hat{\mathbf{R}})\mathbf{S}(\omega), \quad (142)$$

and noting that $\langle \xi_\alpha(\omega)\xi_\beta(-\omega) \rangle = G_{\alpha\beta}$, the spin correlators can be written as

$$P_{\alpha\beta}(\omega) = \frac{1}{i\omega\hat{\mathbf{1}} + \hat{\mathbf{R}}} \hat{\mathbf{G}} \frac{1}{-i\omega\hat{\mathbf{1}} + \hat{\mathbf{R}}^\dagger}. \quad (143)$$

The noise power spectrum is an element of $\hat{\mathbf{P}}$: $P(\omega) \equiv P_{zz}(\omega)$. For example, for the Fermi gas electrons in a strong in-plane magnetic field along the y -axis and anisotropic spin relaxation, we find using this approach:

$$\begin{aligned} P(\omega) &= \sum_{s=\pm} \frac{k_B T D / (2\tau_s)}{(\omega - s\omega_L)^2 + (1/\tau_s)^2}, \\ \frac{1}{\tau_s} &= \frac{1}{2} \left(\frac{1}{\tau_s^z} + \frac{1}{\tau_s^x} \right). \end{aligned} \quad (144)$$

7.3. Cross-Correlation SNS and Multicomponent Spin Systems

7.3.1. Off-Diagonal Correlators. Consider the setup shown in Fig. 19 consisting of two measurement beams directed along different axes and probed separately by individual detectors. Signals from these detectors will be correlated because in the overlap region both beams interact with the same electrons/atoms. Let Detector 1 measure the spin polarization along the z -axis and convert it into the Fourier transform $S_z(\omega)$, as defined by Eq. (140). Respectively, Detector 2 obtains $S_x(\omega)$. Multiplying the two and averaging over repeated measurements during equal time intervals, one can obtain the cross-correlation spectrum, $P_{zx}(\omega) = \langle S_z(\omega)S_x(-\omega) \rangle$. As this expression is generally complex-valued, it is convenient to consider its real and imaginary parts separately:

$$P_{zx}^{Re}(\omega) \equiv \text{Re}\langle S_z(\omega)S_x(-\omega) \rangle,$$

$$P_{zx}^{Im}(\omega) \equiv \text{Im}\langle S_z(\omega)S_x(-\omega) \rangle.$$

For example, consider an atomic vapor of N atoms in the observation region subjected to a weak magnetic field along the y -axis at a high temperature. Then, the spin relaxation rate is almost isotropic, so that the relaxation and correlation matrices read:

$$R_{\alpha\beta} = -gB_y \varepsilon_{\alpha\gamma\beta} + \Gamma_s \delta_{\alpha\beta}, \quad G_{\alpha\beta} = \frac{N\Gamma_s \delta_{\alpha\beta}}{2}.$$

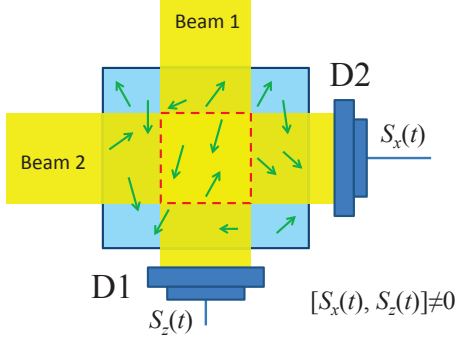


Figure 19. Two probe beams to study correlations between different spin polarization components. Here, D1 and D2 are detectors measuring Faraday rotation angles. The crossing region is denoted by the red dashed line.

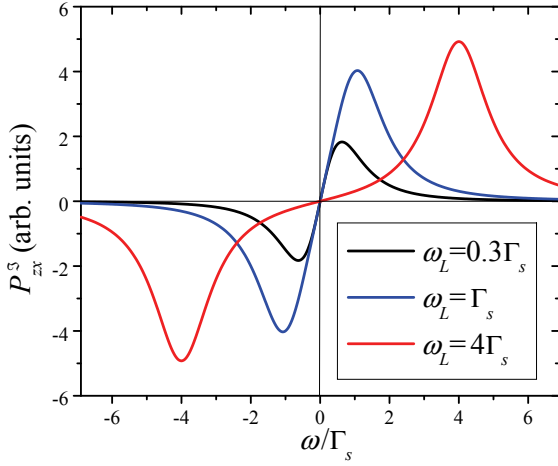


Figure 20. The cross-correlation spectrum $P(\omega)$ (Eq. (145)) shown for several values of the external in-plane magnetic field $gB_y \equiv \omega_L$.

Using the above expressions, one can find $P_{zx}^{Re}(\omega) = 0$ and

$$P_{zx}^S(\omega) = \frac{N\omega_L\omega}{2(\omega^2 + \omega_L^2 + \Gamma_s^2)} \sum_{s=\pm} \frac{\Gamma_s}{(\omega - s\omega_L)^2 + \Gamma_s^2}, \quad (145)$$

where $\omega_L = gB_y$. At zero magnetic field ($B_y = 0$) this correlator vanishes, while at large fields ($\omega_L \gg \Gamma_s$) its peak at $\omega > 0$ has a Lorentzian shape: $P_{zx}^S(\omega) \sim N\Gamma_s/[4[(\omega - \omega_L)^2 + \Gamma_s^2]]$. Behavior of $P_{zx}^S(\omega)$ at several different values of the external magnetic field is shown in Fig. 20.

7.3.2. 2D Dirac Materials. There are emerging applications of SNS requiring an extension of SNS theory (e.g., Eq. (132)) to include some additional discrete degrees of freedom. For example, in the family of new 2D materials called the transition metal decalcogenides, the spectrum of electrons contains two Dirac valleys, K and K' (Fig. 12). The Dirac

valleys are coupled as electrons can scatter between the valleys. Moreover, the spin dynamics is valley-dependent because of the spin-orbit coupling, which can be considered as an effective out-of-plane magnetic field leading to a Zeeman splitting with opposite signs of interaction in different valleys. In such a case, it is convenient to think that this system consists of spins of two different kinds, marked by additional index $\tau = 1(-1)$ for K (K'). Spins from different valleys can interact with each other and even transform into each other by short-range impurity scattering.

The generalization of the Bloch equation to such a situation was discussed in [149, 152]:

$$\frac{d\mathbf{S}^\tau}{dt} + \tau\mathbf{S}^\tau \times \boldsymbol{\Omega}_{\text{SO}} + \mathbf{S}^\tau \times \boldsymbol{\Omega}_L = -\Gamma_s\mathbf{S}^\tau + \frac{\mathbf{S}^{-\tau} - \mathbf{S}^\tau}{2T_v}, \quad (146)$$

where $\boldsymbol{\Omega}_{\text{SO}} = \boldsymbol{\Omega}_{\text{SO}}(k_F)\mathbf{z}$ is the effective out-of-plane magnetic field induced by the spin-orbit coupling, Γ_s is the spin relaxation rate, T_v the valley relaxation time, $\boldsymbol{\Omega}_L = g\mathbf{B}$, and, as an index in \mathbf{S}^τ , $\tau = K, K'$ and $-K = K'$.

The elements of the relaxation matrix $\hat{\mathbf{R}}$ now can be indexed by a complex index $\alpha\tau$, $\alpha = x, y, z$, $\tau = \pm$. One can read the elements of this matrix directly from Eq. (146). It is then straightforward to upgrade Eq. (146) to a Langevin equation by adding a Gaussian noise term, whose correlation matrix components can be obtained by application of the fluctuation-dissipation theorem:

$$G_{\alpha\tau, \beta\tau'} = 2Dk_B T \left[\frac{(\delta_{\tau\tau'} - \delta_{-\tau\tau'})\delta_{\alpha\beta}}{2T_v} + \Gamma_s\delta_{\tau\tau'}\delta_{\alpha\beta} \right]. \quad (147)$$

The detailed discussion of the Langevin equation based on (146) can be found in [149]. Here we note also that, in application to MoS₂, there is a strong experimental evidence that the valley relaxation is much faster than the spin relaxation [152]. In such a case, the fast valley degrees of freedom can be integrated out and an effective description can be obtained in terms of the standard Bloch equation (118) with a strong anisotropy of relaxation rates: $\Gamma_s^z \gg \Gamma_s^\perp$ that we have already discussed. The arguments go as follows.

Consider the total spin polarization $\mathbf{S} = \mathbf{S}^K + \mathbf{S}^{K'}$, which changes relatively slowly with time, and the quickly relaxing combination, $\mathbf{S}^- = \mathbf{S}^K - \mathbf{S}^{K'}$. In terms of these variables, Eq. (146) reads:

$$\frac{d\mathbf{S}}{dt} = gB_x\hat{x} \times \mathbf{S} + \boldsymbol{\Omega}_{\text{SO}}\hat{z} \times \mathbf{S}^- - \Gamma_s\mathbf{S}, \quad (148)$$

$$\frac{d\mathbf{S}^-}{dt} = gB_x\hat{x} \times \mathbf{S}^- + \boldsymbol{\Omega}_{\text{SO}}\hat{z} \times \mathbf{S} - \frac{\mathbf{S}^-}{T_v} - \Gamma_s\mathbf{S}^-. \quad (149)$$

Several approximations follow [152]: Due to the fast valley relaxation, it is safe to disregard the left-hand side in Eq. (149) and the last term on the right hand

side. Moreover, estimates show that Ω_{SO} is much larger than the typical external magnetic field, which can be also disregarded in (149). Hence,

$$\mathbf{S}^- = T_v \Omega_{\text{SO}} \hat{z} \times \mathbf{S}. \quad (150)$$

Let us now introduce a new relaxation rate

$$\Gamma_v = T_v \Omega_{\text{SO}}^2. \quad (151)$$

Substituting (150) into (149), we find the equation for the total spin polarization:

$$\frac{d\mathbf{S}}{dt} = gB_x \hat{x} \times \mathbf{S} - (\Gamma_v + \Gamma_s) (\hat{x} S_x + \hat{y} S_y) - \hat{z} \Gamma_s S_z, \quad (152)$$

which has the form of the Bloch equation with anisotropic relaxation rates.

7.3.3. Mixtures of Hot Atomic Vapors. Consider a mixture of two interacting hot atomic gases, A and B. After some approximations, the spin kinetics of this mixture is described by a set of coupled Bloch equations for spin polarizations of both atomic species [66, 84]:

$$\frac{d\mathbf{S}^A}{dt} = g_A \mathbf{S}^A \times \mathbf{B} - \gamma_A \mathbf{S}^A - \frac{\gamma_{AB}}{2} (N_B \mathbf{S}^A - N_A \mathbf{S}^B), \quad (153)$$

$$\frac{d\mathbf{S}^B}{dt} = g_B \mathbf{S}^B \times \mathbf{B} - \gamma_B \mathbf{S}^B - \frac{\gamma_{AB}}{2} (N_A \mathbf{S}^B - N_B \mathbf{S}^A),$$

where $A \equiv \text{Cs}$ and $B \equiv \text{Rb}$, and N_A, N_B are numbers of, respectively, Cs and Rb atoms in the observation region. The kinetic rate γ_{AB} describes the rate of random spin exchange interactions at scatterings of atoms of different kind. Note also that g -factors and individual relaxation rates for different atoms are generally different. The relaxation matrix elements can be read from Eq. (153):

$$R_{ij}^{\alpha\beta} = \delta_{ij} \left[\delta_{\alpha\beta} \gamma_\alpha + \frac{\gamma_{AB} (\delta_{\alpha\beta} N_\beta - \delta_{\alpha\bar{\beta}} N_\alpha)}{2} \right] - \delta_{\alpha\beta} g_\alpha B_x \varepsilon_{xij}, \quad (154)$$

where we defined a bar-operation as $\bar{A} = B$ and $\bar{B} = A$.

In recent experiments performed with hot atomic vapors [66, 84], the temperature was several orders of magnitude higher than the characteristic energy scale for spin dynamics. This condition fixes the form of the correlation matrix elements:

$$G_{ij}^{\alpha\beta} = \frac{\delta_{ij}}{2} \left[\delta_{\alpha\beta} \gamma_\alpha N_\alpha + \frac{\gamma_{AB} N_A N_B}{2} (\delta_{\alpha\beta} - \delta_{\alpha\bar{\beta}}) \right]. \quad (155)$$

In Ref. [66], the spin cross-correlator that corresponds to the Langevin equation with matrices (154) and (155) was investigated theoretically and compared with an experiment on the mixture of Cs and Rb. Experimental and theoretical results appeared to be

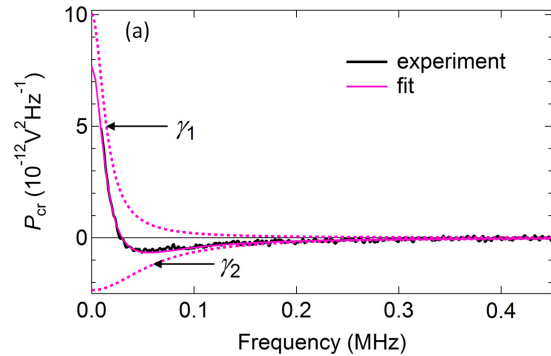


Figure 21. Cross-correlator of a mixture of Cs and Rb atomic vapors at zero magnetic field. Reprinted with permission from Macmillan Publishers Ltd: Scientific Reports 5, article number: 9573, 2015, Copyright ©(2015) [66].

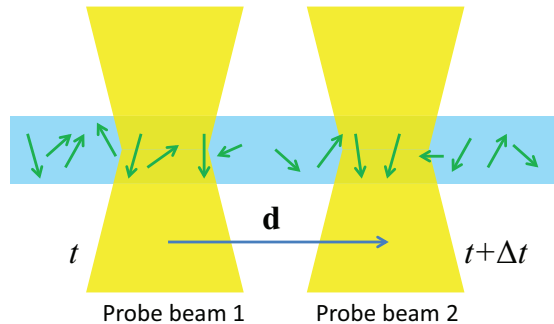


Figure 22. Two laser beams separated by a distance d measure correlations between time-shifted spin fluctuations at different space locations. Y. V. Pershin et al., Applied Physics Letters 102, p. 202405, 2013 [172]. Copyright (2013), American Institute of Physics.

in excellent agreement with each other. For example, Eq. (143) predicts that at zero magnetic field the cross correlator has a simple form

$$P_{\text{cr}}(\omega) = Q \left(\frac{\gamma_1}{\omega^2 + \gamma_1^2} - \frac{\gamma_2}{\omega^2 + \gamma_2^2} \right), \quad (156)$$

which is the difference of two equal-area Lorentzians with widths γ_1 and γ_2 . Here $Q = N_A N_B / (N_A + N_B)$, and the parameter γ_1 has the meaning of the effective total spin relaxation rate, while the difference $\gamma_2 - \gamma_1$ is the spin exchange rate. Note that even though the exchange interactions conserve the total spin polarization, the spin exchange rate can be extracted by means of the two-color SNS from measurements of the cross-correlator. Figure 21 shows perfect agreement of the theoretical prediction (Eq. (156)) with experimental results.

7.3.4. Spatial Correlations. Up to this point, we considered correlation and cross-correlation functions of spin fluctuations coming from the same spatial location. However, (cross-)correlation functions in

both time and space provide more information regarding a system compared to correlations in time alone. These correlators are particularly important for problems involving spin transport/diffusion when we want to know how a spin fluctuation propagates through a semiconductor material or a nanowire. Optical SNS allows investigation of the spin transport at equilibrium, namely, without any external excitation or bias voltage.

Ref. [172] presents a theory of two-beam SNS in semiconductor wires with Bychkov-Rashba spin-orbit interaction taking into account several possible spin relaxation channels and finite size of laser beams. A possible experiment geometry is shown in Fig. 22. This theory predicts a peak shift with respect to the Larmor frequency to higher or lower frequencies depending on the strength of spin orbit interaction and distance between the beams.

8. Methods II: Spin Noise of Conduction Electrons

The basic framework for theoretical studies of spin noise of itinerant electrons was developed in Ref. [173]. Here, we illustrate some of the theoretical methods applicable to conduction electrons. Our illustration is based on the model of the Rashba 2D electrons described by the Hamiltonian

$$\hat{H} = \frac{\hbar^2 \mathbf{k}^2}{2m_e} + \lambda_{\text{SO}}(k_y \hat{\sigma}_x - k_x \hat{\sigma}_y) + V(\mathbf{r}), \quad (157)$$

where \mathbf{k} is the electron momentum, m_e is the electron mass, λ_{SO} is the Rashba spin orbit coupling and $V(\mathbf{r})$ is a static disorder potential. In simplified model calculations, the disorder potential is often assumed to be Gaussian δ -correlated, i.e. $\langle V(\mathbf{r}) \rangle = 0$ and $\langle V(\mathbf{r})V(\mathbf{r}') \rangle = V_0^2 \delta(\mathbf{r} - \mathbf{r}')$, where V_0 is a constant. Due to the Rashba spin-orbit interaction, the electron spins experience an effective momentum-dependent in-plane magnetic field. The elastic impurity scattering leads to fast fluctuations of this field, which in turn are responsible for the relaxation and fluctuations of spins of electrons.

8.1. Drift-Diffusion Approach

The spin drift-diffusion (DD) approach stays in between more rigorous calculations based on quantum Boltzmann equation (or the Kubo formula) and the phenomenological theory. Instead of postulating the form of the Langevin equation with phenomenological parameters, DD equations are based on the microscopic Hamiltonian (157). These equations are derived using a semiclassical description of the electron spatial motion and quantum-mechanical description of the dynamics of electron spins.

DD approach is most useful to reveal the microscopic physics leading to spin noise and relaxation and to develop an intuition for systems with more complex interactions. However, it has to be used with extra caution because it lacks the mathematical rigor of more advanced calculation techniques.

8.1.1. Spin Diffusion Equations Following Ref. [174], we present a simple derivation of spin diffusion equations for the 2D non-degenerate electron gas. For the sake of simplicity, we assume the electrical neutrality and the absence of external electromagnetic field.

Within DD approach, 2D electrons are characterized by the momentum relaxation time τ and the mean free path ℓ , so that the average velocity of electrons is $v = \ell/\tau$. From elementary gas-kinetic considerations [175] we can write an equation for the change of electron spin polarization $\Delta \mathbf{S}(x, y, t)$ in a region of dimensions $2\ell \times 2\ell$ with the center at (x, y) during the time interval τ :

$$(2\ell)^2 \Delta \mathbf{S}(x, y, t) = \frac{1}{4} v \tau (2\ell) \{ \mathbf{S}'(x - 2\ell, y, t) + \mathbf{S}'(x + 2\ell, y, t) + \mathbf{S}'(x, y - 2\ell, t) + \mathbf{S}'(x, y + 2\ell, t) - 4\mathbf{S}(x, y, t) \}. \quad (158)$$

In the right hand side of Eq. (158), the first four terms are the spin polarization fluxes into the region from four sides with length 2ℓ , and the last term is the flux out of this region. The prime symbols in Eq. (158) denote a change of spin polarization because of SO interaction-induced spin precession by the angle $2\Omega\tau = 4\lambda_{\text{SO}}m_e\ell/\hbar = 2\eta\ell$, where $\eta = \Omega\tau/\ell$ is the spin precession angle per unit length. For example,

$$\mathbf{S}'(x - 2\ell, y, t) = \cos(2\eta\ell)\mathbf{S}(x - 2\ell, y, t) - \sin(2\eta\ell)\mathbf{y} \times \mathbf{S}(x - 2\ell, y, t) + 2\sin^2(\eta\ell)\mathbf{y} \cdot \mathbf{S}(x - 2\ell, y, t)\mathbf{y}, \quad (159)$$

where \mathbf{y} is the unit vector along y -axis.

In order to obtain spin diffusion equations, we substitute the expressions for \mathbf{S}' into Eq. (158), and expand trigonometrical functions up to quadric terms with respect to small $2\eta\ell$ and \mathbf{S}' terms up to quadric terms with respect to 2ℓ . The resulting system of diffusion equations for spin polarization has a form

$$\frac{\partial S_x}{\partial t} = D\Delta S_x + C\frac{\partial S_z}{\partial x} - 2\gamma S_x, \quad (160)$$

$$\frac{\partial S_y}{\partial t} = D\Delta S_y + C\frac{\partial S_z}{\partial y} - 2\gamma S_y, \quad (161)$$

$$\frac{\partial S_z}{\partial t} = D\Delta S_z - C\left(\frac{\partial S_x}{\partial x} + \frac{\partial S_y}{\partial y}\right) - 4\gamma S_z, \quad (162)$$

where

$$C = 2\eta D, \quad \gamma = \frac{1}{2}\eta^2 D, \quad (163)$$

and

$$D = \frac{\ell^2}{2\tau}. \quad (164)$$

Here D is the coefficient of diffusion, C describes spin rotations, and γ is the coefficient describing spin relaxation. The same spin diffusion equations (160-163) can be obtained for the model of 2D localized electrons on a lattice in the hopping regime with the only difference that $D = \ell^2/(4\tau)$, where τ is now the characteristic hopping time and ℓ is the distance between the lattice sites. We note that Eqs. (160-163) can be easily extended to account for a drift term.

8.1.2. Average Spin Relaxation. Next, we consider the relaxation of homogeneous spin polarization in the DD limit. In this case, different components of spin polarization are uncoupled (see Eqs. (160)-(162)) and the dynamics of their relaxation is characterized by the following spin relaxation times:

$$\frac{1}{\tau_s^z} = 4\gamma = \left(\frac{2\lambda_{\text{SO}} m_e v}{\hbar} \right)^2 \tau, \quad (165)$$

$$\tau_s^x = \tau_s^y = 2\tau_s^z. \quad (166)$$

According to Eqs. (165)-(166), the spin relaxation time for S_z is two times shorter than the spin relaxation times for S_x and S_y . The reason is that the effective in-plane spin-orbit field (causing the spin relaxation) is always perpendicular to S_z .

8.1.3. Spin Fluctuations. In order to find various correlation functions, one can assume [172] that at an arbitrary selected moment of time $t = 0$ the vector of spin polarization density is given by a vector of continuous random variables $\mathbf{S}(\mathbf{r}, 0) = \boldsymbol{\xi}(\mathbf{r})$ such that $\langle \xi_i(\mathbf{r}) \rangle = 0$ and $\langle \xi_i(\mathbf{r}) \xi_j(\mathbf{r}') \rangle = \lambda \delta(\mathbf{r} - \mathbf{r}') \delta_{ij}$, where $\langle \dots \rangle$ denotes averaging over different realizations, $i, j = x, y, z$, and λ is a parameter describing the strength of spin fluctuations. Using statistical considerations [175], one can show that $\lambda = n/4$, where n is the 2D electron density.

For a given realization of initial spin polarization density, the spin polarization at $t > 0$ can be written using a Green's function G_{ij} of the spin diffusion equations

$$S_i(\mathbf{r}, t) = \int_A G_{ij}(\mathbf{r}, t; \mathbf{r}', 0) S_j(\mathbf{r}', 0) d\mathbf{r}', \quad (167)$$

where A is the sample area, and $d\mathbf{r}' = dx' dy'$. Any new noise created in the system at $t > 0$ is uncorrelated with the initial noise and thus is not included into Eq. (167). Next, we note that a probe beam used in typical SNS setup averages the space distribution of the Faraday rotation angle $\theta(\mathbf{r}, t) = \kappa S_z(\mathbf{r}, t)$ according to

$$\bar{\theta}(t) = \frac{1}{P_0} \int_A I_m(\mathbf{r}) \theta(\mathbf{r}, t) d\mathbf{r} = \frac{\kappa}{P_0} \int_A I_m(\mathbf{r}) S_z(\mathbf{r}, t) d\mathbf{r}. \quad (168)$$

Here, κ is a constant that couples z -component of spin polarization density with a local value of Faraday rotation angle, P_0 is the integrated laser beam intensity (power), and $I_m(\mathbf{r})$ is the space distribution of beam intensity.

In SNS experiments, the most typical determined correlation function is

$$R(t) = \langle \bar{\theta}(0) \bar{\theta}(t) \rangle. \quad (169)$$

Using Eqs. (167)-(169), and the expression $\langle \xi_i(\mathbf{r}) \xi_j(\mathbf{r}') \rangle = \lambda \delta(\mathbf{r} - \mathbf{r}') \delta_{ij}$ (introduced above Eq. (167)), we find the general equation determining the second order spin noise correlation function:

$$R(t) = \frac{\lambda \kappa^2}{P_0^2} \int_A \int_A I(\mathbf{r}) I(\mathbf{r}') G_{zz}(\mathbf{r}, t; \mathbf{r}', 0) d\mathbf{r} d\mathbf{r}'. \quad (170)$$

The Fourier transform of $R(t)$ with respect to t is the noise power spectrum

$$S(\omega) = 2 \int_0^\infty R(t) \cos(\omega t) dt. \quad (171)$$

We emphasize that although Eq. (170) contains only zz component of the Green function, the latter (as a solution of a system of spin diffusion equations) incorporates both transverse and longitudinal dynamics of spin polarization.

As a practical example of this approach, let us consider spin noise in quantum wires subjected to an in-plane magnetic field. Assuming a Gaussian distribution of the incident laser beam intensities along the x -direction, namely, $I(x) \propto \exp(-x^2/(2R_0^2))$, where R_0 is the beam radius, and using the Green's function of one-dimensional spin diffusion equation,

$$G_{zz}(x, t; x', 0) = \frac{1}{\sqrt{4\pi Dt}} e^{-\frac{(x-x')^2}{4Dt}} \cos(\eta(x-x') - \omega_L t), \quad (172)$$

where ω_L is the Larmor frequency, we find (with a help of Eq. (170)) the noise correlation function

$$R(t) \propto \frac{\cos(\omega_L t)}{\sqrt{Dt + R_0^2}} e^{-\frac{R_0^2 \eta^2 Dt}{Dt + R_0^2}}. \quad (173)$$

Assuming that the short times provide the main contribution to the Fourier transform of Eq. (173) [172], one can obtain

$$S(\omega) \propto \frac{\tau_{DP}}{1 + \tau_{DP}^2 (\omega_L - \omega)^2}, \quad (174)$$

where $\tau_{DP} = (\eta^2 D)^{-1}$ is the D'yakonov-Perel' spin relaxation time [176, 177]. According to Eq. (174), the spin noise spectrum shows a Lorentzian peak centered

at ω_L . The peak width is determined by the spin relaxation time.

In addition to the regular Rashba (Eq. (157)) and/or Dresselhaus [178] spin-orbit coupling, any semiconductor structure has a random contribution to the strengths of spin-orbit interactions due to various types of disorders (such as interface fluctuations, random doping, etc.). A theory of SNS in quantum wires with randomness in the spin-orbit coupling was developed in [179]. This work analyzes various transport regimes and demonstrates that the spin relaxation can be very slow, and the resulting noise power spectrum can increase algebraically as the frequency goes to zero [179].

8.2. Kubo Formula

The most rigorous way to calculate the spin noise power spectrum at the thermodynamic equilibrium is based on the Kubo formula. The application of this approach to SNS was demonstrated in Ref. [180], which explores the effects of spatial diffusion of electrons. Here we provide a simplified example that rederives results of some phenomenological calculations from previous sections.

First we note that, via the fluctuation-dissipation theorem, the 2nd order symmetrized spin correlator can be expressed through the linear response function as

$$\chi_{zz}(t-t') = i\theta(t-t')\langle[\hat{s}_z(t), \hat{s}_z(t')]\rangle. \quad (175)$$

The diagrammatic technique to calculate the linear response function in terms of a power series expansion in the disorder potential can be justified after switching to the imaginary time (Matsubara) representation [181]. Importantly, one does not have to perform all calculations at the finite temperature before returning to the real time. Instead, one can consider first the formal expression for (175) in the imaginary time, then take the low temperature limit and transform the expression back to the real time. The result is the Kubo-type expression for the susceptibility [182]:

$$\chi_{zz}(\Omega) = -i\Omega R(\epsilon_F - i\delta, \epsilon_F + \Omega + i\delta), \quad (176)$$

where

$$R(\epsilon_F - i\delta, \epsilon_F + \Omega + i\delta) = \frac{1}{4} \text{Tr} \left[\hat{\sigma}_z \langle \hat{G}(\epsilon_F - i\delta) \hat{\sigma}_z \hat{G}(\epsilon_F + \Omega + i\delta) \rangle_{dis} \right] \quad (177)$$

Here, $\hat{G}(\epsilon_F)$ is the single electron Green function taken at the Fermi energy. We note that in (177) and henceforth, the hats mark objects that are matrices in spin states, and $\langle \dots \rangle_{dis}$ denotes averaging over disorder. The trace in (177) corresponds to the summation over all occupied single electron states,

including the summation over the spin indexes. We also note that Eq. (176) appears different from the analogous expression, e.g., in [182], since we define the Fourier transform $\chi_{zz}(\Omega)$ of $\chi_{zz}(t)$ without a 2π denominator and the factor $1/4$ accounts for transition from spin-1/2 operators \hat{s}_z to Pauli matrices $\hat{\sigma}_z$.

The eigenstates of the disorder free part of the Rashba Hamiltonian (157)

$$|u_{\mathbf{k}}^{\pm}\rangle = \frac{1}{\sqrt{2}} \begin{pmatrix} 1 \\ \pm ie^{i\phi} \end{pmatrix} \quad (178)$$

correspond to the eigenvalues

$$\epsilon_{\mathbf{k}}^{\pm} = \frac{k^2}{2m} \mp \lambda_{SO} k, \quad (179)$$

where $k_x + ik_y \equiv ke^{i\phi}$. The disorder free Green function is given by

$$\hat{G}_0(\omega \pm i\delta, \mathbf{k}) = \frac{|u_{\mathbf{k}}^+\rangle\langle u_{\mathbf{k}}^+|}{\omega - \epsilon_{\mathbf{k}}^+ \pm i\delta} + \frac{|u_{\mathbf{k}}^-\rangle\langle u_{\mathbf{k}}^-|}{\omega - \epsilon_{\mathbf{k}}^- \pm i\delta}. \quad (180)$$

The averaging over disorder in Eq. (177) can be performed in two steps. First, one should obtain the average of a single Green function. In the self-consistent Born approximation, this leads to the appearance of a finite self-energy. According to [183], for a Gaussian weak white-noise type of disorder, this effect for the Rashba system reduces to a simple renormalization of the parameter δ

$$\delta \rightarrow \Gamma,$$

where

$$\Gamma = n_i V_0^2 \frac{\nu_+ + \nu_-}{4}. \quad (181)$$

Here n_i is the impurity concentration, V_0^2 is the average square of the impurity potential $V_i(\mathbf{r}) = V_0\delta(\mathbf{r} - \mathbf{r}_i)$, and

$$\nu_{\pm} = k_F^{\pm} \left| \frac{\partial \epsilon_{\mathbf{k}}^{\pm}}{\partial k} \right|^{-1}$$

are the Fermi surface densities of states of the two bands of the Rashba Hamiltonian.

The second effect of disorder averaging, in the self-consistent Born approximation, is the renormalization of the vertex in between two Green functions:

$$\hat{\sigma}_z \rightarrow \hat{\Theta}_z \equiv a\hat{\sigma}_z, \quad (182)$$

where

$$\hat{\Theta}_z = \hat{\sigma}_z + n_i V^2 \iint \frac{d^2\mathbf{k}}{(2\pi)^2} \hat{G}_0(\epsilon_F - i\Gamma) \hat{\Theta}_z \hat{G}_0(\epsilon_F + \Omega + i\Gamma). \quad (183)$$

To calculate this effect, it is useful to note that

$$\langle u_{\mathbf{k}}^{\pm} | \hat{\sigma}_z | u_{\mathbf{k}}^{\pm} \rangle = 0, \quad \langle u_{\mathbf{k}}^{\pm} | \hat{\sigma}_z | u_{\mathbf{k}}^{\mp} \rangle = 1.$$

Next, in Eq. (183) we switch to polar coordinates in the momentum space. Up to the off-diagonal terms that integrate to zero, the integration over the polar angle simplifies some expressions, e.g.,

$$|u_{\mathbf{k}}^{\pm}\rangle\langle u_{\mathbf{k}}^{\mp}| \rightarrow \frac{\hat{\sigma}_z}{2}.$$

In the intermediate calculations, defining $\Delta \equiv \epsilon_{\mathbf{k}}^- - \epsilon_{\mathbf{k}}^+ \approx 2\lambda_{\text{SO}}k_F$, we use the identity

$$\frac{1}{(\epsilon_F - \epsilon_{\mathbf{k}}^+ - i\Gamma)(\epsilon_F - \epsilon_{\mathbf{k}}^- + \Omega + i\Gamma)} \approx \frac{1}{\Omega - \Delta + 2i\Gamma} \times \left(\frac{1}{\epsilon_F - \epsilon_{\mathbf{k}}^+ - i\Gamma} - \frac{1}{\epsilon_F - \epsilon_{\mathbf{k}}^- + \Omega + i\Gamma} \right).$$

The expression in parentheses is simplified using the fact that only its imaginary parts are substantial in the physical limit

$$\epsilon_F \gg \Gamma \gg \lambda_{\text{SO}}k_F \gg \Omega \sim \frac{(\lambda_{\text{SO}}k_F)^2}{\Gamma}. \quad (184)$$

There are many other simplifications in this case, for example,

$$\nu_+ + \nu_- \approx 2m_e, \quad \nu_+ - \nu_- \approx -m_e(\lambda_{\text{SO}}k_F)/\epsilon_F.$$

Hence we can replace, e.g.,

$$\frac{1}{\epsilon_F - \epsilon_{\mathbf{k}}^+ - i\Gamma} \approx i\pi\delta(\epsilon_F - \epsilon_{\mathbf{k}}^+),$$

and then use

$$i\pi \iint \frac{d^2\mathbf{k}}{(2\pi)^2} \delta(\epsilon_F - \epsilon_{\mathbf{k}}^+) = i\frac{\nu_+}{2}.$$

After these manipulations, we obtain an equation that determines the parameter a :

$$a = 1 + \frac{2ia\Gamma}{\nu_+ + \nu_-} \left(\frac{\nu_+}{\Omega - \Delta + 2i\Gamma} + \frac{\nu_-}{\Omega + \Delta + 2i\Gamma} \right). \quad (185)$$

Using Eq. (181) and all the relations (184), we find

$$a \approx \frac{2i\Gamma}{\Omega + 2i(\lambda_{\text{SO}}k_F)^2/\Gamma}. \quad (186)$$

Note that at this point the spin relaxation time appears in the calculations:

$$1/\tau_s \equiv 2(\lambda_{\text{SO}}k_F)^2/\Gamma = (2\lambda_{\text{SO}}k_F)^2\tau_{\text{tr}}, \quad (187)$$

where τ_{tr} is the transport lifetime of conduction electrons [183], defined as $\tau_{\text{tr}} = 1/(2\Gamma)$.

Substituting Eqs. (182), (185), into Eq. (177) we get

$$\chi_{zz}(\Omega) = \frac{i\Omega}{4} \text{tr} \iint \frac{d^2\mathbf{k}}{(2\pi)^2} \hat{G}_0(\epsilon_F - i\Gamma) \hat{\Theta}_z \hat{G}_0(\epsilon_F + \Omega + i\Gamma), \quad (188)$$

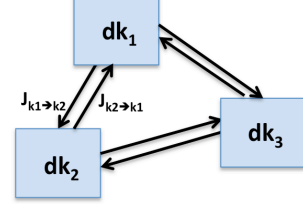


Figure 23. Spin fluctuations originate from the shot noise of spin currents between mesoscopic phase space volumes.

where “tr” means here merely the trace over the spin indexes. In the limits (184) we obtain

$$\chi_{zz}(\Omega) = \frac{i\Omega a}{4} \frac{\nu_+ + \nu_-}{2\Gamma} = -\frac{\Omega}{4} \frac{\nu_+ + \nu_-}{\Omega + i/\tau_s}.$$

Finally, we can apply the fluctuation-dissipation theorem (99) to calculate the noise power spectrum. Before making further calculations we emphasize that the majority of experiments are performed at relatively high temperatures, $k_B T \gg \hbar\Omega$. In this limit, $\coth\left(\frac{\hbar\Omega}{2k_B T}\right) \approx 2k_B T/(\hbar\Omega)$ and

$$P(\Omega) = \frac{k_B T(\nu_+ + \nu_-)}{2} \frac{1/\tau_s}{\Omega^2 + (1/\tau_s)^2}, \quad (189)$$

Since $(\nu_+ + \nu_-)/2$ corresponds to the density of states per spin parameter D in Eq. (125), the result (189) coincides with Eq. (121) at $\omega_L = 0$, which was derived previously with the phenomenological approach.

8.3. Quantum Boltzmann Equation

An alternative calculation tool for conduction electrons is the upgraded quantum Boltzmann equation approach introduced in [74], which was applied to a 2D electron system with Rashba and Dresselhaus spin orbit coupling.

The quantum Boltzmann equation is similar to the standard kinetic equation. It describes the evolution of the single particle density matrix $\hat{\rho}$, which includes both charge and spin degrees of freedom, changing due to “hydrodynamic” evolution in external fields and random scatterings:

$$\partial_t \hat{\rho} - i[\hat{\rho}, \hat{H}] = \hat{I}_{\text{col}} + \hat{\zeta}(\hat{\rho}, \hat{H}), \quad (190)$$

where \hat{H} is the part of the Hamiltonian without random interactions, and I_{col} is the collision integral describing for scatterings. All but the last term in (190) can be derived by previously developed diagrammatic and semiclassical methods [184, 183, 185, 186, 187]. The last term in Eq. (190), $\hat{\zeta}(\hat{\rho}, \hat{H})$, is the main addition that describes the local spin-charge *fluctuations* due to random scattering events of all kinds. This term becomes important only when

small ($\sim \sqrt{N}$) fluctuations are considered, which is the case of our interest now. Solving Eq. (190), one can derive various correlators, such as $\langle \rho_\alpha(t, r') \rho_\beta(0, r) \rangle$, e.t.c, where $\rho_\alpha(t, r')$ are variables parametrizing the density matrix $\hat{\rho}$; index α can run, e.g., over x,y,z coefficients that define spin-1/2 density matrix in the Pauli matrix basis. For this purpose, the correlation properties of ζ_α , such as $\langle \zeta_\alpha(t, r') \zeta_\beta(0, r) \rangle$, should be priorly obtained quantum-mechanically with scattering theory methods.

An approach to derive the statistical properties of the noise term was suggested in [74]. It starts from the observation that scattering processes in the momentum space happen much faster than the local spin relaxation in different phase space volumes that comprise mesoscopic numbers of electrons. Therefore, on the time scale of the transport lifetime, one can assume that different phase space volumes are described by approximately constant values of the spin density, while such volumes exchange quickly fluctuating spin currents with each other, as shown in Fig. 23. The spin current from a phase space volume with a characteristic momentum \mathbf{k}_1 to the volume with a characteristic momentum \mathbf{k}_2 is denoted by $\mathbf{J}_{\mathbf{k}_1 \rightarrow \mathbf{k}_2}$, where different elements of the spin current vector are $J_{\mathbf{k}_1 \rightarrow \mathbf{k}_2}^\alpha$, and $\alpha = x, y, z$ are spin projection components.

The problem of finding properties of the noise term in (190) thus reduces to the problem of finding statistical properties of spin currents between large ‘‘reservoirs’’ of electrons with different single particle density matrices $\hat{\rho}_{\mathbf{k}_i}$ and $\hat{\rho}_{\mathbf{k}_j}$. This type of problems has been studied within the theory of electronic counting statistics [188]. This theory predicts that if one chooses a time scale δt such that the number of scattered electrons during δt is large but δt is still much smaller than the spin relaxation time, then cumulants of the transferred spin $\delta \mathbf{s}_{\mathbf{k}_i \rightarrow \mathbf{k}_j} \equiv \int_0^{\delta t} dt \mathbf{J}_{\mathbf{k}_i \rightarrow \mathbf{k}_j}$ become linear in δt . Following Ref. [74], one can show that in the leading order in deviation from the equilibrium,

$$\langle \delta s_{\mathbf{k}_i \rightarrow \mathbf{k}_j}^\alpha \rangle = \omega_{\mathbf{k}_i \mathbf{k}_j} (\mathbf{s}_{\mathbf{k}_i} - \mathbf{s}_{\mathbf{k}_j})^\alpha \delta t, \quad (191)$$

$$\text{var} \left(\delta s_{\mathbf{k}_i \rightarrow \mathbf{k}_j}^\alpha \right) = \omega_{\mathbf{k}_i \mathbf{k}_j} f_D(\epsilon) (1 - f_D(\epsilon)) \frac{\delta t}{2}, \quad (192)$$

where $\omega_{\mathbf{k}_i \mathbf{k}_j}$ is the scattering rate between phase space volumes i and j , and $f_D(\epsilon)$ is the Fermi-Dirac distribution function at the energy of scattered electrons. The scattering rate can be estimated quantum mechanically, e.g., by applying the golden rule, as discussed in [185]. Equation (191) can be used to estimate the standard collision term, \hat{I}_{col} , in (190), while Eq. (192) can be used to obtain Gaussian correlators of the noise term. Afterwards, the quantum Boltzmann equation acquires the form of a Langevin equation in the phase space, which can be studied using

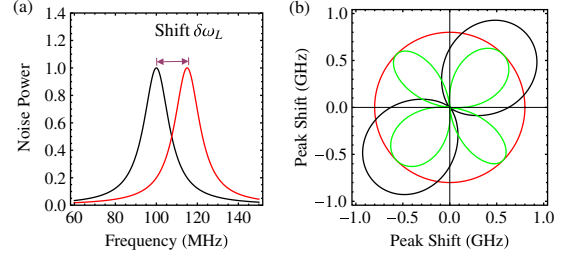


Figure 24. (a) Noise power peak shift in electric field and (b) its magnitude vs angle of electric field direction for several different ratios of Rashba and Dresselhaus spin orbit couplings. Reprinted figure with permission from F. Li et al., Physical Review Letters 111, p. 067201, 2013 [74]. Copyright ©(2013) by the American Physical Society.

standard techniques that we discussed in the previous section. We refer the reader to Ref. [74] for further details.

Here we note that fluctuations of the spin currents between the phase space volumes appear even when the scattering conserves spins. It is rather a shot noise type of fluctuations that arise from discreteness of electrons. Such fluctuating spin currents conserve the total spin. However, in presence of the spin orbit coupling, they become responsible for fluctuations of the spin precession in the spin-orbit field, and, therefore, lead to fluctuations of the total spin in the system at a longer time scale $\sim 1/(\lambda_{SO} k_F)$. It is the strength of the quantum Boltzmann equation, in comparison to the Kubo formula, that such a physical interpretation can be developed starting from microscopic physical processes and finishing with the slowest dynamics of the total spin relaxation.

8.4. Conduction Electrons Beyond Thermodynamic Equilibrium

Several nonequilibrium effects that can be revealed by SNS of conduction electrons have been discussed in [74, 75, 76] within the kinetic equation approach. The application of an electric field induces charge currents that influence the spin noise power spectrum via the spin-orbit coupling [74]. Thus, the electric field E acts on conducting electron spins like an in-plane magnetic Zeeman field $\sim \lambda_{SO} e E \tau_{tr}$, where λ_{SO} is the strength of the Rashba spin-orbit coupling, τ_{tr} is the transport lifetime. This effect can be observed in the spin noise power spectrum as a shift of the Larmor peak of conduction (but not localized) electrons (Fig. 24a) and can be used, e.g. to determine anisotropy of spin-orbit coupling (Fig. 24b) and separate contributions of localized and conducting electrons [74]. This effect was suggested as a tool to measure the spin orbit coupling anisotropy.

Another interesting research direction is to explore

the regime of a strong electric field (above 10 Vcm^{-1}) in GaAs. At such conditions, electrons dissipate energy by exciting localized electrons from the donor band [189, 190], creating considerable correlations and avalanches of electrons in the conduction band. Spin noise in this regime is hard to predict at present, e.g., because the effect of dynamics of recombination processes on spin relaxation is unclear. Kinetic equation is particularly suitable to study such a strongly nonequilibrium regime theoretically because it provides self-consistent description even in the cases when only phenomenological justification exists. An example of such theoretical studies of spin fluctuations in the streaming regime of ballistic electrons can be found in [76]. Finally, we point to the recently developed kinetic equation approach based on the Keldysh technique that was applied to nonequilibrium effects in SNS [191].

8.5. Higher Order SNS and Stochastic Path Integral

The noise term in Eq. (190) is generally non-Gaussian and depends nontrivially on the size of a spin fluctuation, e.g., in the case of many-body exchange interactions. Calculations of higher order spin correlators from the quantum Boltzmann equation would require the knowledge of the higher order correlations of the noise term, such as $\langle \zeta_\alpha(t_3, \mathbf{r}_3) \zeta_\beta(t_2, \mathbf{r}_2) \zeta_\gamma(t_1, \mathbf{r}_1) \rangle$. Higher order statistics of microscopic currents has been the subject of research in the context of the electronic shot noise. One powerful method to obtain statistics of fluctuating *charge* currents is the Levitov-Lezovik formula [192, 193, 194, 195, 196]. However, in our situation the statistics of spin currents is harder to define since the derivation of the Levitov-Lesovik formula assumes a charge measurement, i.e. the measurement operator should commute with the density matrix before and after the evolution. Hence, extension of the theory of full counting statistics to spin currents currently remains poorly developed. One possible way around this problem was suggested in [197], where universality of some shapes of higher order cumulants was found that was justified by the law of large numbers and the fluctuation theorem.

The derivation of the stochastic Boltzmann equation as well as finding its solution in the case of non-Gaussian noise terms require a special approach. A possible way is to combine Eq. (190) with the method of the *stochastic path integral*, which has been previously applied to nonlinear stochastic equations [198, 199, 200]. Pedagogical introduction to the path integrals with applications to the higher order SNS can be found in [41, 201].

The idea is to introduce a generating function that is the sum over all possible stochastic trajectories τ of the single particle density matrix $\hat{\rho}$, weighted by a

counting field χ_c , e.g.

$$Z(\chi_c) = \sum_{\tau} P_{\tau} e^{\chi_c f_{\tau}}, \quad (193)$$

where P_{τ} is the probability of a trajectory τ and f_{τ} is the counted variable, e.g. the change of the magnetization in the observation region produced by a trajectory. Knowing $Z(\chi_c)$ one can calculate an arbitrary correlator of f_{τ} by taking derivatives of $Z(\chi_c)$ at $\chi_c = 0$. For a mesoscopic number of observable electrons, $Z(\chi_c)$ can be written in the form of a familiar path integral over system variables [198, 197]:

$$Z(\chi_c, T) = \int d\boldsymbol{\rho}(t) \int d\boldsymbol{\chi}(t) e^{\int_0^T dt \{i\dot{\boldsymbol{\rho}}\boldsymbol{\chi} + H(\boldsymbol{\rho}, \boldsymbol{\chi}, \chi_c)\}}, \quad (194)$$

where $\boldsymbol{\rho}$ is the vector that parametrizes elements of the density matrix $\hat{\rho}$ in (190) and $\boldsymbol{\chi}$ is a conjugated variable. The function H plays a similar role to a Hamiltonian, which is very different from the physical Hamiltonian \hat{H} in Eq. (190). The form of Eq. (194) is the starting point for various well justified approximations, for example, the limit of a large number of spins corresponds to the semiclassical limit in the path integral. This technique can be used to integrate over fast degrees of freedom and obtain an effective significantly simplified description of relatively slow processes without the loss of information about their fluctuations, including higher order correlations [200]. Such a time-scale separation happens typically in applications of Eq. (190). Indeed, usually spin relaxation is orders of magnitude slower than the electron scattering times. There is generally a hierarchy of such different time-scales in interacting electron systems, with fast processes eventually influencing the slow spin dynamics. This situation is ideal for application of the technique [200]. Finally, we note that the path integral technique can incorporate purely quantum effects within the weak measurement framework, as it is discussed in [202, 203].

9. Methods III: Discrete Spin Models

In this section, we review spin noise characteristics of several specific discrete spin models. These models have attracted the attention from SNS community for their applicability to experimental systems that can be studied by SNS techniques at frequencies below 1 THz.

9.1. Symmetric Central Spin Model

The central spin models describe interactions of a single spin, which is usually the electron spin-1/2, with bath spins, which are usually the nuclear spins (Fig. 25). Recently, new realizations of the central



Figure 25. The central spin model describes a single spin interacting with a bath of N nuclear spins.

spin model were obtained experimentally based on magnetically doped semiconductor quantum dots that can, potentially, also be probed by SNS [204].

In the simplest model of this type, it is assumed that interactions between the central and nuclear bath spins are isotropic and of the same strength. In this case, the model Hamiltonian is given by

$$\hat{H}_{cs} = g \sum_{i=1}^N \hat{\mathbf{S}} \cdot \hat{\mathbf{s}}^i, \quad (195)$$

where $\hat{\mathbf{S}}$ is the central spin operator and $\hat{\mathbf{s}}^i$ is the spin operator of the i -th nuclear spin, N is the number of nuclear spins, and g is the coupling constant. Usually the goal is to find the correlator for the central spin projection along the z -axis, $\langle \hat{S}_z(t) \hat{S}_z(0) \rangle$, because nuclear spins are optically inactive.

Equation (195) model can be solved exactly [205, 206]. Introducing the spin operator of the nuclear spin bath, $\hat{\mathbf{I}}_N = \sum_{i=1}^N \hat{\mathbf{s}}_i$, and the operator of the total spin, $\hat{\mathbf{I}} \equiv \hat{\mathbf{S}} + \hat{\mathbf{I}}_N$, one can rewrite the Hamiltonian (195) as

$$\hat{H}_{cs} = \frac{g}{2} \left(\hat{\mathbf{I}}^2 - \hat{\mathbf{I}}_N^2 - \hat{\mathbf{S}}^2 \right). \quad (196)$$

Taking into account that $\hat{\mathbf{S}}^2 = 3/4$ for the central spin-1/2, and that the operator $\hat{\mathbf{I}}_N^2$ commutes both with $\hat{\mathbf{I}}^2$ and the projection operator of the total spin along the z -axis, \hat{I}_z , the Hamiltonian (195) can be diagonalized in the basis of eigenstates of $\hat{\mathbf{I}}^2$ and \hat{I}_z . The construction of these eigenstates in terms of eigenstates of $\hat{\mathbf{S}}$ and $\hat{\mathbf{s}}_i$ is described in textbooks on quantum mechanics [207]. Details for the model (196) can be found in [206].

Typically, the number of nuclear spins is very large ($N \sim 10^4 - 10^6$). In the limit of $N \rightarrow \infty$, it was found that the quantum-mechanical exact result for the 2nd order spin correlator (found within Eq. (195) model) coincides with the prediction of a mean field approach that treats the effect of the nuclear spin bath on the central spin in terms of a constant magnetic field with a magnitude taken from the Gaussian distribution [100]. According to the full quantum-mechanical solution for $N \gg 1$, at high temperatures, the central spin noise power spectrum has the form shown in Fig. 10 [206]. This solution does not explain discrepancies

between experimental observations and results of the semiclassical theory [103].

The major difference between the full quantum-mechanical solution and the semiclassical solution is the quantum echo effect. The semiclassical theory predicts that after the averaging over all possible initial states of the bath spins, the central spin polarization relaxes (on average) to 1/3 of its initial value. The quantum-mechanical model makes the same prediction, however, for a finite N , there is a time $\tau \sim 1/g$ when the central spin returns to the fully polarized state. Such a behavior, however, has never been observed experimentally, which is one more proof that Eq. (195) model is too simplistic to describe realistic central spin systems.

The exact solution becomes more useful either in the low temperature regime ($k_B T < g$) or when the nuclear spin bath is strongly polarized. In such cases, quantum correlations within the ground state become substantial and the semiclassical solution may become insufficient. The partition function of Eq. (195) model [205] shows, for example, that this model does not have a phase transition at any finite temperature. In the low temperature regime, spin noise in the central spin model was discussed in [208]. The exact solution also results in some nontrivial features when higher than 2nd order spin correlators are considered [206].

9.2. Disordered Central Spin Problem

In order to explain the experimentally observable spin relaxation of localized electronic spins, the central spin model was generalized to include random coupling effects as follows [100]:

$$\hat{H}_{cs} = \sum_{i=1}^N g_i \hat{\mathbf{S}} \cdot \hat{\mathbf{s}}^i, \quad (197)$$

where parameters g_i are taken from some distribution. It turns out that the model (197) is solvable by the Gaudin ansatz [102, 209], which reduces the complexity to that of a system of nonlinear algebraic equations. Unfortunately, the time to solve such equations numerically becomes too long when the number of nuclear spins is $N \gtrsim 40$. However, it suffices to observe the trends of this model. Alternatively, the model (197) was explored numerically by simulating the quantum-mechanical evolution directly. However, exact numerical algorithms can treat no more than 20-30 spins [206, 210, 211, 102].

Fortunately, it was discovered in [101] that a semiclassical approach that is based on an enforced factorization of the density matrix produces indistinguishable results for spin relaxation calculations from the results of exact algorithms when the spin bath is not

polarized and the number of spins $N > 20$. This allowed studies of the central spin relaxation with parameters that are close to realistic, e.g., simulations of $N = 50000$ nuclear spins were performed in [107].

Numerical simulations have demonstrated that the effect of randomness of hyperfine couplings on the central spin relaxation is unexpectedly weak, especially in presence of an out-of-plane anisotropy, which is typical for hole-doped quantum dots [103, 210]. This fact can be attributed to the integrability of the model (197), as discussed in [211]. Hence, there is a considerable experimental evidence that the model (197) is still insufficient to describe the spin relaxation in semiconductor quantum dots. A relatively strong quadrupole interaction (see Eq. (28)) should be taken into account to explain some experimental results [62, 103, 107, 106].

9.3. Spin Cluster Model

This model describes a system of mutually interacting spins subjected to the external magnetic field applied along the z -axis. The system Hamiltonian is given by [212, 213]

$$\hat{H} = g \sum_{i>j=1}^N \hat{\mathbf{s}}^i \hat{\mathbf{s}}^j + \boldsymbol{\Omega} \sum_{i=1}^N \hat{\mathbf{s}}^i, \quad (198)$$

where g is the coupling constant, and $\boldsymbol{\Omega}$ is the external magnetic field. The eigenstates and eigenvalues of this model (and hence the spin correlators) can be found similarly to these in the symmetric central spin model, since the Hamiltonian (198) involves only the commuting operators I^2 and I_z , where $\hat{\mathbf{I}} \equiv \sum_{i=1}^N \hat{\mathbf{s}}^i$.

Let us consider an insulating semiconductor in the vicinity of transition to the conduction regime. Imagine that there are isolated islands constructed of well connected states. In this case, the electrons can hop between connected states of the same island and, hence, interact with each other. In Ref. [214], Eq. (198) model was used to mimic effects of the exchange interaction among electrons inside such an island.

Similarly to the symmetric central spin model, Eq. (198) model shows somewhat trivial behavior in the case of $N \gg 1$ and high temperatures [212, 213]. The spin noise power spectrum is the same as in a classical model in which spins rotate around an effective static field produced by a static spin fluctuation of the order of \sqrt{N} . Hence, the spectrum of Eq. (198) model strongly resembles the spectrum of the central spin model shown in Fig. 10(b).

9.4. Central Spin Problem at Higher Temperatures

The Langevin equation can be used to describe the relaxation of a spin localized in a quantum dot [215,

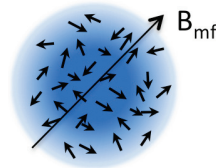


Figure 26. The spin cluster model describes the interaction of N identical spins. Each spin couples equally to all other spins. At $N \gg 1$, the mean field description in which each spin precesses around an effective magnetic field $B_{mf} \sim g\sqrt{N}$ reproduces the exact spin noise power spectrum.

216]. In this approach, the nuclear spin effects can be taken into account by a term describing the coupling of the central spin to the nuclear Overhauser field, which is defined in Eq. (25). Then, the Langevin equation is written as

$$\dot{\mathbf{S}} = (\boldsymbol{\Omega} + \boldsymbol{\Omega}_O) \times \mathbf{S} - \Gamma \mathbf{S} + \boldsymbol{\xi}(t), \quad (199)$$

where $\boldsymbol{\Omega}$ corresponds to the external magnetic field, $\boldsymbol{\Omega}_O$ corresponds to the time-independent component of the Overhauser field, and Γ is the relaxation rate. It is assumed that $\boldsymbol{\Omega}_O$ is taken from the Gaussian distribution with parameters discussed in [100].

The authors of [215] have shown that the noise term $\boldsymbol{\xi}(t)$ introduces a Lorentzian broadening of the zero frequency peak such as the one shown in Fig. 10(b). By increasing the strength of this noise, they observed the disappearance of the Gaussian peak and transformation of the noise power spectrum into a single Lorentzian peak centered at zero frequency.

Originally, Eq. (199) was proposed to describe the effect of nuclear spin bath dynamics [215]. Such an approach seems, however, to be an oversimplification for such a complex many-body problem as the central spin interacting with nuclear spins. While the Overhauser field does have its own dynamics, this dynamics is not independent of the dynamics of the central spin, what is typically the case in electron-doped quantum dots. Moreover, even when the feedback from the central spin can be disregarded, as, e.g., in hole-doped quantum dots [103], the Overhauser field fluctuations have a finite amplitude and correlation time. The form of this field correlator is also nontrivial. Such details, however, are needed, e.g., to explain the quick suppression of central spin relaxation by an out-of-plane magnetic field [62].

Instead, it is expected that Eq. (199) approach is applicable to the electron-doped quantum dots at relatively high temperatures ($T > 10\text{K}$). In this situation, the phonon-related mechanisms dominate in spin relaxation. Therefore, the relaxation and noise terms in Eq. (199) are no longer related to the spin bath physics. At the same time, the effect of the Overhauser field on the coherent precession of the

central spin cannot be disregarded. As measurements of spin correlators in electron doped quantum dots have become available [106, 107], an opportunity appears to test predictions of this Langevin equation approach.

9.5. Spin Hopping Models

It was shown theoretically that the electron hopping between quantum dots influences the spin noise properties [217]. In this work, the evolution of electron spin density \mathbf{S}_i at the site i was described by an equation including a hopping term and a term of interaction with the local nuclear Overhauser field, $\boldsymbol{\Omega}_O^i$, [217]:

$$\frac{d\mathbf{S}_i}{dt} = \boldsymbol{\Omega}_O^i \times \mathbf{S}_i + \sum_j [W_{ij}\mathbf{S}_j - W_{ji}\mathbf{S}_i], \quad (200)$$

where W_{ij} is the hopping rate between sites j and i . In addition to electronic spin dynamics [218], such models have been extensively studied, e.g., in the field of molecular spintronics [219], so spin relaxation in such models is well understood.

When the hopping rate is small compared to $|\boldsymbol{\Omega}_O|$, the electron spin makes many rotations around the local field before the electron jumps to a different dot. In this case, the spectrum is an average of single quantum dot spectra with a Gaussian distribution of $\boldsymbol{\Omega}_O^i$, as shown in Fig. 10(b). On the other hand, in the large hopping rate limit, electron spins experience quickly fluctuating Overhauser fields. As in the case of the Dyakonov-Perel spin relaxation, a randomly fluctuating nuclear field causes an exponential electron spin relaxation [218]. Therefore, the noise power spectrum is Lorentzian in this limit. The width of the Lorentzian peak is inversely proportional to the hopping rate, i.e. faster transitions lead to a longer spin life-time (the motional narrowing). The transition between these two regimes and implications for the spin noise power spectrum are discussed in more detail in [217].

We also note that quantum effects at coherent hopping of electrons between two singly and doubly charged coupled quantum dots (a quantum dot molecule) were discussed in [220]. The Coulomb coupling and hopping are manifested then in specific noise power spectrum peaks. The authors of [220] pointed to an interesting fact: Since different quantum dots have different optical properties, the hopping between different quantum dots, even without any spin relaxation, will produce measurable fluctuations of the Faraday rotation angle. This effect can be used to characterize many parameters, which may not be directly related to spin relaxation in nanostructures.

9.6. Spin Diffusion in Disordered Spin Lattices

The application of SQUID- and cantilever-based magnetometry to disordered interacting spin systems has raised a theoretical interest to spin noise in systems with a model Hamiltonian of the type [122]

$$\hat{H} = \sum_{ij} J_{ij} \mathbf{S}_i \cdot \mathbf{S}_j, \quad (201)$$

where J_{ij} are coupling constants for spins i and j . These constants are often selected randomly based on a distribution $P(J_{ij})$, which mimics the complex RKKY oscillatory-type interaction among randomly positioned spins.

A cantilever or SQUID measures spin polarization in a small region. Although the Hamiltonian (201) conserves the total spin polarization, spin diffusion between the observation and outside regions leads to observable fluctuations. Usually, Eq. (201)-type models displays a power law ($1/\omega^\alpha$) dependence in the spin noise power spectrum defined by a non-universal parameter α . It's a non-trivial task to express α through model parameters.

In two recent theoretical papers [221, 222], successful approaches to predict the spin noise power spectrum for Eq. (201)-type models were developed. The paper by Sykes *et al.* [221] presents a type of mean field approach based on the Bloch-Redfield theory. The authors of [221] assume that the dynamics of any spin is influenced by an effective field from all other environmental spins. An important addition to the standard mean-field approach is the assumption that the environmental field has a noisy component with a correlator that can be determined self-consistently.

The second successful method is a numerical renormalization group approach [222]. This method starts with identifying a pair of spins with the strongest effective coupling. Assuming a static environment, the fast dynamics of this pair of spins is found analytically including its contribution to the noise power spectrum. After that, the selected pair of spins is replaced by an effective single spin with some updated couplings to other spins. This process is repeated over and over again so that at each step a new pair of spins with the strongest coupling is selected. It was shown in [222] that for a disordered 1D chain with random couplings J_{ij} , the numerical renormalization group approach finds the noise power spectra, which are almost indistinguishable from these calculated using the exact diagonalization.

The mean field and numerical renormalization group approaches complement each other. The former is expected to work better for long-range interactions, while the latter is best suited for short-range couplings.

10. Perspectives

In this Review, we have examined a variety of different applications of SNS ranging from conduction electrons to atomic spin systems and quantum dots. Potentially, SNS can be applied to any system that demonstrates measurable Faraday or Kerr rotation effects in the states with finite spin polarization, including cuprates and unconventional superconductors. However, for some potential applications, the required sensitivity and extension of the frequency bandwidth to the terahertz range are yet to be demonstrated.

Continuous instrumentation and methodological improvements of SNS that we have been observing during the last decade give confidence that many new applications of SNS will be developed. Along this path, SNS should not be perceived as merely an alternative way to determine basic linear response characteristics. Instead, SNS enables an essentially new methodology in materials science. Large streams of information – gigabytes per second – can now be processed to extract useful spin correlators. The complexity of higher-order spin correlators, which are multidimensional in the frequency space, creates new challenges of interpreting large amounts of information. Such new information could be most suitable for simultaneous multiparameter fits, e.g., to infer the full spin Hamiltonian with all parameters “at once” by advanced statistical methods [223] and signal processing [224].

Below, we review several currently challenging research directions that could be possibly addressed by SNS within the foreseeable future.

10.1. Full Counting Statistics

There is a strong interest in advanced statistical methods to explore some highly unusual characteristics including the ones that have never been detected in the condensed matter systems. For example, SNS has a potential to investigate the *global properties* of the generating function containing the information about all order spin correlators. Indeed, since the optical SNS directly measures the phase shift acquired by the polarized beam, $e^{i\theta_F(t)}$, where $\theta_F(t)$ is the Faraday rotation angle, sufficiently long experimental data sets can be used to find the average of any power of this exponent, $\langle [e^{i\theta_F(t)}]^\lambda \rangle$. Since $\theta_F(t) \sim S_z(t)$, SNS thus allows experimental determination of the following generating function:

$$Z(\lambda, t) = \langle e^{i\lambda \hat{S}_z(t)} e^{-i\lambda \hat{S}_z(0)} \rangle \equiv \langle e^{i\lambda \delta S_z(t)} \rangle, \quad (202)$$

where \hat{S}_z is the operator of the total spin polarization along the z -axis and λ is the *counting parameter*.

10.1.1. Phase Transitions in Rare Event Statistics. The possibility to observe phase transitions in statistics of rare events attracts a lot of theoretical attention [225, 226, 227, 228, 229, 230]. However, these critical phenomena, which provide unique opportunities to understand strongly correlated systems, remain practically unstudied experimentally. Usually, phase transitions at the fluctuation level occur when a system is not at the critical state but close to it in some parameter space.

In 1952, Lee and Yang [231, 232] showed that, in a large class of interacting spin systems, the partition function becomes zero at certain points on the complex plane of fugacity or a magnetic field. In the case of a general Ising ferromagnet, all the Lee-Yang zeros are located on the unit circle in the complex fugacity plane. When the number of interacting spins is large, such zeros merge and create a branch cut (Fig. 27). A nice approach to test the Lee-Yang zeros was proposed in [229] showing that a probe spin coherence demonstrates sudden death and birth at the critical times corresponding to the Yang-Lee singularities. $Z(\lambda, t)$ given by Eq. (202) could be considered as a probe in analogy to the probe spin coherence discussed in [229].

Relation to phase transitions at fluctuation level can be established when the number of interacting spins is large. Lee-Yang zeros then merge and create a branch cut (Fig. 27). When $q \equiv e^{i\lambda}$ enters the values at this cut, generating functions, such as in Eq. (202), may experience a sharp change of behavior [229]. Critical exponents in the vicinity of this transition can be derived similarly to how it is done in applications of Lee-Yang zeros to the theory of classical phase transitions.

In a recent experiment performed by analogy with liquid NMR quantum computing, Lee-Yang zeros of the partition function with a complex fugacity were observed in molecular nuclear spins [233]. In other recent inspiring papers [234, 235], it was demonstrated theoretically that in order to explore the phase transitions at the fluctuation level, unusual rare events do not need to be detected. Namely, it was shown that phase transitions at the fluctuation level lead to time-dependent oscillations of potentially measurable lowest cumulants. By tracing such oscillations, it is possible to explore the discontinuities of $Z(\lambda, t)$ [234, 235]. Additionally, it was shown in Ref. [236] that the well known disappearance of the quantum coherent oscillations due to strong coupling to a detector, near the onset of the quantum Zeno effect [141, 237, 238, 239, 240], can be manifestation of such a discontinuity of the generating function of the spin noise statistics. This proves that, in some sense, phase transitions at the fluctuation level have been already observed

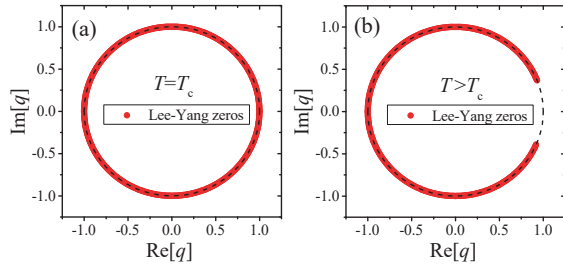


Figure 27. Positions of Lee-Yang zeros on the unit circle (a) at the critical temperature, and (b) for a paramagnetic phase of Ising model.

experimentally, in particular, in solid state qubits [241]. The authors of Ref. [236] also argue that the quantum Zeno effect can be further explored by SNS.

10.1.2. Quantum Entanglement Entropy and Entanglement Witness. It was shown theoretically that the counting statistics of spin fluctuations can be used to reconstruct the quantum entanglement entropy (QEE) of spins with their environment [242]. This work was done in analogy with the demonstration by Klich and Levitov [11] that the generating function of counting statistics of charge currents is directly related to QEE between the leads. The knowledge of QEE can be used to determine topological characteristics of correlated electrons and to detect quantum phase transitions [243, 244, 245, 246, 247, 248, 249, 250, 251, 252, 253].

QEE has not been experimentally measured by SNS techniques yet but there is encouraging experimental progress towards this goal. Thus, spin noise measurements in atomic vapors have been already used to unveil quantum many-body correlations [80, 81, 82, 83]. Moreover, the recently demonstrated two-color SNS [66, 156] now allows experimental studies of cross-correlations between different spin subsystems, that are of interest in the context of QEE. These experiments gave birth to hopes that SNS might eventually be used to study QEE [254].

While experimental studies of QEE require considerable advances of the higher order SNS, the quantum entanglement can already be studied by SNS techniques that probe 2nd order spin correlators. For example, the spin susceptibility can be used to test the boundaries of the entanglement witness [255, 256, 257] (if these boundaries are broken then the quantum state of a spin system cannot be represented as a product of different spin states). It was already shown that the off-resonant optical pulses could be useful both to create macroscopic entanglement and to detect it by exploring quantum spin fluctuations [83].

Here, we would like to point out that almost all previous studies of QEE and susceptibility as an entanglement witness have been focused on static

characteristics related to the equal time correlators of variables. The strength of SNS measurement techniques is rather in resolving *temporal* correlations. Hence, the convergence of SNS with the physics of quantum entanglement will strongly depend on the future theoretical work clarifying the entanglement information encoded in time-correlators of spin variables. Steps in this direction have recently been taken [258].

10.2. Strongly Correlated Spin Systems

SNS can be particularly useful to study strongly correlated systems because the noise power spectrum can reveal correlations in a wide range of energy scales. It is likely that some new applications of SNS in this important research area will emerge in the very near future. Here we briefly discuss possible research directions.

Magnetic Semiconductors. A dilute magnetic semiconductor can be created if a few percent of atoms in a paramagnetic semiconductor are replaced with magnetic ions. Such materials would be especially well-suited for future spintronic devices if the mechanisms behind their ferromagnetism were better understood. Spin noise studies of such materials have recently become possible [109]. Consider, e.g., the magnetic semiconductor $\text{Ga}_{1-x}\text{Mn}_x\text{As}$. In the ferromagnetic phase, it shows a strong Faraday effect due to the steady spin polarization of holes [259]. In the paramagnetic phase, spins of holes have relatively fast dynamics but close to the phase transition, when the mean spin polarization is zero on average, spin fluctuations are expected to be considerable, possibly with a strongly non-Lorentzian shape of the noise power spectrum due to the critical slow-down of the dynamics and disorder. One can expect, for example, that there are regions with accidentally large concentration of Mn ions with relatively strong ferromagnetic interactions. Such regions may behave as “quasiparticles with large spins”, whose sizes can be obtained by measuring high order correlations [201].

Luttinger Liquid, Kondo Effect, etc. Recently, a renormalization group study of spin noise in a Luttinger liquid with spin-orbit coupling was performed by Sun and Pokrovsky [260]. They have demonstrated the sensitivity of spin correlators to phase transitions and optical resonances in the Luttinger liquid [261]. Numerical renormalization group methods were also used in [262] to demonstrate that signatures of the Kondo effect can be observed in SNS experiments. The two-beam SNS was also proposed to detect a dynamic localization of quasiparticles in spin chains [263]. As SNS sensitivity has reached the single spin limit [104], one can realistically expect the spin noise detection in thin

References

- [1] J. B. Johnson. Thermal agitation of electricity in conductors. *Phys. Rev.*, 32:97–109, 1928.
- [2] H. Nyquist. Thermal agitation of electric charge in conductors. *Phys. Rev.*, 32:110–113, 1928.
- [3] R Kubo. The fluctuation-dissipation theorem. *Rep. Prog. Phys.*, 29:255, 1966.
- [4] D R White, R Galleano, A Actis, H Brixy, M De Groot, J Dubbeldam, A L Reesink, F Edler, H Sakurai, R L Shepard, and J C Gallop. The status of johnson noise thermometry. *Metrologia*, 33:325, 1996.
- [5] Y M Blanter and M Buttiker. Shot noise in mesoscopic conductors. *Physics Reports*, 336:1 – 166, 2000.
- [6] Y V Nazarov. *Quantum Noise in Mesoscopic Physics*. Springer, 2003.
- [7] L S Levitov, H W Lee, and G B Lesovik. Electron counting statistics and coherent states of electric current. *J. Math. Phys.*, 37:4845, 1996.
- [8] R de Picciotto, M Reznikov, M Heiblum, V Umansky, G Bunin, and D Mahalu. Direct observation of a fractional charge. *Nature*, 389:162, 1997.
- [9] C L Kane and M P A Fisher. Nonequilibrium noise and fractional charge in the quantum Hall effect. *Phys. Rev. Lett.*, 72:724, 1994.
- [10] D A Ivanov and A G Abanov. Phase transitions in full counting statistics for periodic pumping. *Europhys. Lett.*, 92:37008, 2010.
- [11] I Klich and L Levitov. Quantum noise as an entanglement meter. *Phys. Rev. Lett.*, 102:100502, 2009.
- [12] A H Myerson, D J Szwer, S C Webster, D T C Allcock, M J Curtis, G Imreh, J A Sherman, D N Stacey, A M Steane, and D M Lucas. High-fidelity readout of trapped-ion qubits. *Phys. Rev. Lett.*, 100:200502, 2008.
- [13] D B Gutman, Y Gefen, and A D Mirlin. Full counting statistics of a Luttinger liquid conductor. *Phys. Rev. Lett.*, 105:256802, 2010.
- [14] Y V Nazarov. Full counting statistics and field theory. *Ann. Phys.*, 16:720, 2007.
- [15] E B Aleksandrov and V S Zapasskii. Magnetic resonance in the Faraday rotation noise spectrum. *Zh. Eksp. Teor. Fiz.*, 81:132, 1981.
- [16] S A Crooker, D G Rickel, A V Balatsky, and D L Smith. Spectroscopy of spontaneous spin noise as a probe of spin dynamics and magnetic resonance. *Nature*, 431:49, 2004.
- [17] M Oestreich, M Römer, R J Haug, and D Hägele. Spin noise spectroscopy in GaAs. *Phys. Rev. Lett.*, 95:216603, 2005.
- [18] S A Crooker, J Brandt, C Sandfort, A Greulich, D R Yakovlev, D Reuter, A D Wieck, and M Bayer. Spin noise of electrons and holes in self-assembled quantum dots. *Phys. Rev. Lett.*, 104:036601, 2010.
- [19] R Budakian, H J Mamin, B W Chui, and D Rugar. Creating order from random fluctuations in small spin ensembles. *Science*, 307:408, 2005.
- [20] G Balasubramanian, I Y Chan, R Kolesov, M Al-Hmoud, J Tisler, C Shin, C Kim, A Wojcik, P R Hemmer, A Krueger, T Hanke, A Leitenstorfer, R Bratschitsch, Fedor Jelezko, and J Wrachtrup. Nanoscale imaging magnetometry with diamond spins under ambient conditions. *Nature*, 455:648, 2008.
- [21] J R Maze, P L Stanwix, J S Hodges, S Hong, J M Taylor, P Cappellaro, L Jiang, M V Gurudev Dutt, E Togan, A S Zibrov, A Yacoby, R L Walsworth, and M D Lukin. Nanoscale magnetic sensing with an individual electronic spin in diamond. *Nature*, 455:644, 2008.
- [22] H J Mamin, M H Sherwood, and D Rugar. Detecting external electron spins using nitrogen-vacancy centers. *Phys. Rev. B*, 86:195422, 2012.
- [23] F Berski, H Kuhn, J G Lonnemann, J Hübner, and M Oestreich. Ultrahigh bandwidth spin noise spectroscopy: Detection of large g -factor fluctuations in highly- n -doped GaAs. *Phys. Rev. Lett.*, 111:186602, 2013.
- [24] S Starosielec and D Hägele. Ultrafast spin noise spectroscopy. *App. Phys. Lett.*, 93:051116, 2008.
- [25] G M Müller, M Römer, J Hübner, and M Oestreich. Gigahertz spin noise spectroscopy in n -doped bulk gallium arsenide. *Phys. Rev. B*, 81:121202(R), 2010.
- [26] J Hübner, J G Lonnemann, P Zell, H Kuhn, F Berski, and M Oestreich. Rapid scanning of spin noise with two free running ultrafast oscillators. *Opt. Express*, 21:5872, 2013.
- [27] G M Müller, M Römer, J Hübner, and M Oestreich. Efficient data averaging for spin noise spectroscopy in semiconductors. *Appl. Phys. Lett.*, 97:192109, 2010.
- [28] M Römer M, J Hübner, and M Oestreich. Spin noise spectroscopy in semiconductors. *Rev. Sci. Instrum.*, 78:103903, 2007.
- [29] E B Aleksandrov and V S Zapasskii. Spin noise spectroscopy. *J. Physics Conference Series*, 324:012002, 2011.
- [30] V S Zapasskii. Spin-noise spectroscopy: from proof of principle to applications. *Adv. in Optics and Photonics*, 5:131, 2013.
- [31] G M Müller, M Georg, M Oestreich, M Römer, and J Hübner. Semiconductor spin noise spectroscopy: Fundamentals, accomplishments, and challenges. *Physica E*, 43:569, 2010.
- [32] J Hübner, F Berski, R Dahbashi, and M Oestreich. The rise of spin noise spectroscopy in semiconductors: From acoustic to GHz frequencies. *Phys. Status Solidi B*, 251:1824, 2014.
- [33] J Hübner, R Dahbashi, F Berski, J Wiegand, H Kuhn, and M Oestreich. Spin noise spectroscopy in semiconductors: from a billion down to single spins. *SPIE Proceedings*, 9167:91672R, 2014.
- [34] M M Glazov and V S Zapasskii. Linear optics, Raman scattering, and spin noise spectroscopy. *Optics Express*, 23:11713, 2015.
- [35] B. C. Pursley, X. Song, and V. Sih. Resonant and time-resolved spin noise spectroscopy. *Appl. Phys. Lett.*, 107:182102, 2015.
- [36] S Kogan. *Electronic noise and fluctuations in solids*. Cambridge University Press, Cambridge, UK, 1996.
- [37] H L Pécseli. *Fluctuations in physical systems*. Cambridge University Press, Cambridge, UK, 2000.
- [38] Steven T Cundiff and Shaul Mukamel. Optical multidimensional coherent spectroscopy. *Physics Today*, 66:44–49, 2013.
- [39] S Starosielec, R Fainblat, J Rudolph, and D Hägele. Two-dimensional higher order noise spectroscopy up to radio frequencies. *Rev. Sci. Instr.*, 75:125101, 2010.
- [40] A Bechtold, F Li, K Müller, T Simmet, P Ardel, J J Finley, and N A Sinitsyn. Quantum fingerprints in higher order correlators of a spin qubit. *arXiv/1511.03684*, 2015.
- [41] F Li, S A Crooker, and N A Sinitsyn. Higher order spin noise spectroscopy of atomic spins in fluctuating external fields. *Phys. Rev. A*, 2016.
- [42] P Schad, B N Narozhny, G Schön, and A Shnirman. Nonequilibrium spin noise and noise of susceptibility. *Phys. Rev. B*, 90:205419, 2014.
- [43] P Schad, Y Makhlin, B N Narozhny, G Schön, and A Shnirman. Majorana representation for dissipative spin systems. *Ann. Phys.*, 361:401, 2015.
- [44] D Budker and D F J Kimball. *Optical magnetometry*. Cambridge University Press, New York, 2013.
- [45] P A Bokhan, V V Buchanov, N V Fateev, M M Kalugin,

- M A Kazaryan, A M Prokhorov, and D E Zakrevskii. Laser isotope separation in atomic vapor. *Wiley-VCH*, 2006.
- [46] N Behbood, G Colangelo, F Martin Ciurana, M Napolitano, R J Sewell, and M W Mitchell. Feedback cooling of an atomic spin ensemble. *Phys. Rev. Lett.*, 111:103601, 2013.
- [47] R Inoue, S-I-R Tanaka, R Namiki, T Sagawa, and Y Takahashi. Unconditional quantum-noise suppression via measurement-based quantum feedback. *Phys. Rev. Lett.*, 110:163602, 2013.
- [48] G E Katsoprinakis, M Polis, A Tavernarakis, A T Dellis, and I K Kominis. Quantum random number generator based on spin noise. *Phys. Rev. A*, 77:054101, 2008.
- [49] P Glasenapp, N A Sinitsyn, L Yang, D G Ricket, D Roy, A Greilich, M Bayer, and S A Crooker. Spin noise spectroscopy beyond thermal equilibrium and linear response. *Phys. Rev. Lett.*, 113:156601, 2014.
- [50] B Mihaila, S A Crooker, K B Blagoev, D G Ricket, P B Littlewood, and D L Smith. Spin noise spectroscopy to probe quantum states of ultracold fermionic atom gases. *Phys. Rev. A*, 74:063608, 2006.
- [51] B Mihaila, S A Crooker, D G Ricket, K B Blagoev, P B Littlewood, and D L Smith. Quantitative study of spin noise spectroscopy in a classical gas of ^{41}K atoms. *Phys. Rev. A*, 74:043819, 2006.
- [52] G E Katsoprinakis, A T Dellis, and I K Kominis. Measurement of transverse spin-relaxation rates in a rubidium vapor by use of spin-noise spectroscopy. *Phys. Rev. A*, 75:042502, 2007.
- [53] H Horn, G M Müller, E M Rasel, L Santos, J Hübner, and M Oestreich. Spin-noise spectroscopy under resonant optical probing conditions: Coherent and nonlinear effects. *Phys. Rev. A*, 84:043851, 2011.
- [54] V Shah, G Vasilakis, and M V Romalis. High bandwidth atomic magnetometry with continuous quantum nondemolition measurements. *Phys. Rev. Lett.*, 104:013601, 2010.
- [55] V S Zapasskii, A Greilich, S A Crooker, Y Li, G G Kozlov, D R Yakovlev, D Reuter, A D Wieck, and M Bayer. Optical spectroscopy of spin noise. *Phys. Rev. Lett.*, 110:176601, 2013.
- [56] C H H Schulte, G M Müller, H Horn, J Hübner, and M Oestreich. Analyzing atomic noise with a consumer sound card. *Am. J. Phys.*, 80:240, 2012.
- [57] G R Stewart. Heavy fermion systems. *Rev. Mod. Phys.*, 56:755, 1984.
- [58] P Aynajian, E H da Silva Neto, A Gyenis, R E Baumbach, J D Thompson, Z Fisk, E D Bauer, and A Yazdani. Visualizing heavy fermions emerging in a quantum critical Kondo lattice. *Nature*, 486:201, 2012.
- [59] A V Khaetskii, D Loss, and L Glazman. Electron spin decoherence in quantum dots due to interaction with nuclei. *Phys. Rev. Lett.*, 88:186802, 2002.
- [60] L Cywiński, W M Witzel, and S Das Sarma. Electron spin dephasing due to hyperfine interactions with a nuclear spin bath. *Phys. Rev. Lett.*, 102:057601, 2009.
- [61] H Bluhm, S Foletti, I Neder, M Rudner, D Mahalu, V Umansky, and A Yacoby. Dephasing time of GaAs electron-spin qubits coupled to a nuclear bath exceeding 200 μs . *Nature Physics*, 7:109, 2011.
- [62] Y Li, N Sinitsyn, L D Smith, D Reuter, A D Wieck, D R Yakovlev, M Bayer, and S A Crooker. Intrinsic spin fluctuations reveal the dynamical response function of holes coupled to nuclear spin baths in (In,Ga)As quantum dots. *Phys. Rev. Lett.*, 108:186603, 2012.
- [63] T Jungwirth, J Sinova, J Mašek, J Kučera, and A H MacDonald. Theory of ferromagnetic (III,Mn)V semiconductors. *Rev. Mod. Phys.*, 78:809, 2006.
- [64] T Dietl. A ten-year perspective on dilute magnetic semiconductors and oxides. *Nature Materials*, 9:965, 2010.
- [65] T G Walker and W Happer. Spin-exchange optical pumping of noble-gas nuclei. *Rev. Mod. Phys.*, 69:629, 1997.
- [66] D Roy, L Yang, S A Crooker, and N A Sinitsyn. Cross-correlation spin noise spectroscopy of heterogeneous interacting spin systems. *Scientific Reports*, 5:9573, 2015.
- [67] D K Young, J A Gupta, E Johnston-Halperin, R Epstein, Y Kato, and D D Awschalom. Optical, electrical and magnetic manipulation of spins in semiconductors. *Sem. Sci. Techn.*, 17:275, 2002.
- [68] M Kryvohuz and S Mukamel. Multidimensional characterization of stochastic dynamical systems based on multiple perturbations and measurements. *J. Chem. Phys.*, 142:212430, 2015.
- [69] B R Mollow. Power spectrum of light scattered by two-level systems. *Phys. Rev.*, 188:1969–1975, 1969.
- [70] S H Autler and C H Townes. Stark effect in rapidly varying fields. *Phys. Rev.*, 100:703–722, 1955.
- [71] D Budker, D F Kimball, and D P DeMille. *Atomic Physics*. Oxford, New York, 2004.
- [72] C Cohen-Tannoudji, J Dupont-Roc, and G Grynberg. *Atom-Photon Interactions-Basic Processes and Applications*. Wiley-VCH, New York, 1998.
- [73] Z Yue and M E Raikh. Evolution of inhomogeneously broadened spin-noise spectrum with ac drive. *Phys. Rev. B*, 91:155301, 2015.
- [74] F Li, Y V Pershin, V A Slipko, and N A Sinitsyn. Nonequilibrium spin noise spectroscopy. *Phys. Rev. Lett.*, 111:067201, 2013.
- [75] V A Slipko, N A Sinitsyn, and Y V Pershin. Hybrid spin noise spectroscopy and the spin Hall effect. *Phys. Rev. B*, 88:201102(R), 2013.
- [76] D S Smirnov and L E Golub. Spin dynamics and fluctuations in the streaming regime. *Phys. Rev. B*, 92:035437, 2015.
- [77] D S Smirnov and M M Glazov. Exciton spin noise in quantum wells. *Phys. Rev. B*, 90:085303, 2014.
- [78] D J Wineland, J J Bollinger, W M Itano, and D J Heinzen. Squeezed atomic states and projection noise in spectroscopy. *Phys. Rev. A*, 50:67, 1994.
- [79] J L Sorensen, J Hald, and E S Polzik. Quantum noise of an atomic spin polarization measurement. *Phys. Rev. Lett.*, 80:3487, 1998.
- [80] B Dubost, M Koschorreck, M Napolitano, N Behbood, R J Sewell, and M W Mitchell. Efficient quantification of non-gaussian spin distributions. *Phys. Rev. Lett.*, 108:183602, 2012.
- [81] F Wolfgramm, A Cerè, F A Beduini, A Predojević, M Koschorreck, and M W Mitchell. Squeezed-light optical magnetometry. *Phys. Rev. Lett.*, 105:053601, 2010.
- [82] F Wolfgramm, Y A de Icaza Astiz, F A Beduini, A Cerè, and M W Mitchell. Atom-resonant heralded single photons by interaction-free measurement. *Phys. Rev. Lett.*, 106:053602, 2011.
- [83] B Julsgaard, A Kozhekin, and E S Polzik. Experimental long-lived entanglement of two macroscopic objects. *Nature*, 413:400, 2001.
- [84] A T Dellis, M Loulakis, and I K Kominis. Spin-noise correlations and spin-noise exchange driven by low-field spin-exchange collisions. *Phys. Rev. A*, 90:032705, 2014.
- [85] J Meineke, J-P Brantut, D Stadler, T Müller, H Moritz, and T Esslinger. Interferometric measurement of local spin fluctuations in a quantum gas. *Nature Physics*, 8:454, 2012.
- [86] S A Crooker, L Cheng, and D L Smith. Spin noise of

- conduction electrons in n -type bulk gallium arsenide. *Phys. Rev. B*, 79:035208, 2009.
- [87] S. Starosielec and D. Hägele. Ultrafast spin noise spectroscopy. *Appl. Phys. Lett.*, 93:051116, 2008.
- [88] M Römer, H Bernien, G Müller, D Schuh, J Hübner, and M Oestreich. Electron-spin relaxation in bulk GaAs for doping densities close to the metal-to-insulator transition. *Phys. Rev. B*, 81:075216, 2010.
- [89] M Römer, J Hübner, and M Oestreich. Spatially resolved doping concentration measurement in semiconductors via spin noise spectroscopy. *Appl. Phys. Lett.*, 94:112105, 2009.
- [90] Q Huang and D S Steel. Optical excitation effects on spin-noise spectroscopy in semiconductors. *Phys. Rev. B*, 83:155204, 2011.
- [91] P S Pershan, J P van der Ziel, and L D Malmstrom. Theoretical discussion of the inverse Faraday effect, Raman scattering, and related phenomena. *Phys. Rev.*, 143:574, 1966.
- [92] I I Ryzhov, G G Kozlov, D S Smirnov, M M Glazov, Y P Efimov, S A Eliseev, V A Lovtcius, V V Petrov, K V Kavokin, A V Kavokin, and V S Zapasskii. Spin noise explores local magnetic fields in a semiconductor. *Scientific Reports*, 6:21062, 2016.
- [93] Berski, J Hübner, M Oestreich, A Ludwig, A D Wieck, and M Glazov. Interplay of electron and nuclear spin noise in n -type GaAs. *Phys. Rev. Lett.*, 115:176601, 2015.
- [94] S V Poltavtsev, I I Ryzhov, M M Glazov, G G Kozlov, V S Zapasskii, A V Kavokin, P G Lagoudakis, D S Smirnov, and E L Ivchenko. Spin noise spectroscopy of a single quantum well microcavity. *Phys. Rev. B*, 89:081304(R), 2014.
- [95] P Glasenapp, A Greulich, I I Ryzhov, V S Zapasskii, D R Yakovlev, G G Kozlov, and M Bayer. Resources of polarimetric sensitivity in spin noise spectroscopy. *Phys. Rev. B*, 88:165314, 2013.
- [96] V G Lucivero, R Jimenez-Martinez, J Kong, and Morgan W Mitchell. Squeezed-light spin noise spectroscopy. *arXiv:1509.05653*, 2015.
- [97] M M Glazov, M A Semina, E Ya Sherman, and A V Kavokin. Spin noise of exciton polaritons in microcavities. *Phys. Rev. B*, 88:041309(R), 2013.
- [98] R Dabhashi, J Hübner, F Berski, J Wiegand, X Marie, K Pierz, H W Schumacher, and M Oestreich. Measurement of heavy-hole spin dephasing in (InGa)As quantum dots. *Appl. Phys. Lett.*, 100:031906, 2012.
- [99] M Oestreich, R Dabhashi, F Berski, and J Hübner. Spin noise spectroscopy: hole spin dynamics in semiconductor quantum dots. *Proc. SPIE*, 8461:846105, 2012.
- [100] I A Merkulov, A L Efros, and M Rosen. Electron spin relaxation by nuclei in semiconductor quantum dots. *Phys. Rev. B*, 65:205309, 2002.
- [101] K A Al-Hassanieh, V V Dobrovitski, E Dagotto, and B N Harmon. Numerical modeling of the central spin problem using the spin-coherent-state p representation. *Phys. Rev. Lett.*, 97:037204, 2006.
- [102] A Faribault and D Schurichts. Spin decoherence due to a randomly fluctuating spin bath. *Phys. Rev. B*, 88:085323, 2013.
- [103] N A Sinitsyn, Y Li, S A Crooker, A Saxena, and D L Smith. Role of nuclear quadrupole coupling on decoherence and relaxation of central spins in quantum dots. *Phys. Rev. Lett.*, 109:166605, 2012.
- [104] R Dabhashi, J Hübner, F Berski, K Pierz, and M Oestreich. Optical spin noise of a single hole spin localized in an (InGa)As quantum dot. *Phys. Rev. Lett.*, 112:156601, 2014.
- [105] P Maletinski, M Kroner, and A Imamoglu. Breakdown of the nuclear-spin-temperature approach in quantum-dot demagnetization experiments. *Nature Physics*, 5:407, 2009.
- [106] J. Hackmann, Ph. Glasenapp, A. Greulich, M. Bayer, and F. B. Anders. Influence of the nuclear electric quadrupolar interaction on the coherence time of hole and electron spins confined in semiconductor quantum dots. *Phys. Rev. Lett.*, 115:207401, 2015.
- [107] A Bechtold, D Rauch, F Li, T Simmet, P-L Ardelt, A Regler, K Müller, N A Sinitsyn, and J J Finley. Three stage decoherence dynamics of an electron spin qubit in an optically active quantum dot. *Nature Physics*, 11:1005, 2015.
- [108] H Horn, A Balocchi, X Marie, A Bakin, A Waag, M Oestreich, and J Hübner. Spin noise spectroscopy of donor-bound electrons in ZnO. *Phys. Rev. B*, 87:045312, 2013.
- [109] D Scalbert and S Cronenberger. Manganese spin noise spectroscopy in CdTe. *Proceeding Int. Conf. Spin physics, spin chemistry and spin technology, St. Petersburg, Russia*, page <http://spinconf.com>, July 2015.
- [110] A L Balk, M D Stiles, and S Unguris. Critical behavior of zero-field magnetic fluctuations in perpendicularly magnetized thin films. *Phys. Rev. B*, 90:184404, 2014.
- [111] S-W Chen and R-B Liu. Faraday rotation echo spectroscopy and detection of quantum fluctuations. *Scientific Reports*, 4:4695, 2014.
- [112] H Barkhausen. Zwei mit hilfe der neuen verstrker entdeckte erscheinungen. *Phys. Z.*, 20:401, 1919.
- [113] J Catty, P Fleischmann, J Chicois, and A Le Brun. Barkhausen noise analysis by surrounding coil. *Review of Progress in Quantitative Nondestructive Evaluation, Plenum Press, New York*, 14:1693, 1995.
- [114] J Magnusson, P Nordblad, and P Svedlindh. Flux noise in $\text{Bi}_2\text{Sr}_2\text{CaCu}_2\text{O}_8$ displaying the paramagnetic Meissner effect: Evidence of spontaneous magnetic moments. *Phys. Rev. B*, 57:10929, 1998.
- [115] W Reim, R H Koch, A P Malozemoff, M B Ketchen, and H Maletta. Magnetic equilibrium noise in spin-glasses: $\text{Eu}_{0.4}\text{Sr}_{0.6}\text{S}$. *Phys. Rev. Lett.*, 57:905, 1986.
- [116] P Svedlindh, K Gunnarsson, P Nordblad, L Lundgren, H Aruga, and A Ito. Equilibrium magnetic fluctuations of a short-range Ising spin glass. *Phys. Rev. B*, 40:7162, 1989.
- [117] I Mušević, A Kityk, M Škarabot, and R Blinc. Polarization noise in a ferroelectric liquid crystal. *Phys. Rev. Lett.*, 79:1062, 1997.
- [118] T Jonsson, P Nordblad, and P Svedlindh. Dynamic study of dipole-dipole interaction effects in a magnetic nanoparticle system. *Phys. Rev. B*, 57:497, 1998.
- [119] A De. Ising-Glauber spin cluster model for temperature-dependent magnetization noise in SQUIDS. *Phys. Rev. Lett.*, 113:217002, 2014.
- [120] Z Chen and C C Yu. Comparison of Ising spin glass noise to flux and inductance noise in SQUIDS. *Phys. Rev. Lett.*, 104:247204, 2010.
- [121] T S Grigera and N E Israeloff. Observation of fluctuation-dissipation-theorem violations in a structural glass. *Phys. Rev. Lett.*, 83:5038, 1999.
- [122] L Faoro, L Ioffe, and A Kitaev. Dissipationless dynamics of randomly coupled spins at high temperatures. *Phys. Rev. B*, 86:134414, 2012.
- [123] B C Stipe, H J Mamin, T D Stowe, T W Kenny, and D Rugar. Magnetic dissipation and fluctuations in individual nanomagnets measured by ultrasensitive cantilever magnetometry. *Phys. Rev. Lett.*, 86:2874, 2001.
- [124] P Peddibhotla, R Xue, H I T Hauge, A Assali, E P A M Bakkers, and M Poggio. Harnessing nuclear spin polarization fluctuations in a semiconductor nanowire. *Nature Physics*, 9:631, 2013.

- [125] A V Balatsky, M Nishijima, and Y Manassen. Electron spin resonance-scanning tunneling microscopy. *Adv. Phys.*, 61:117, 2012.
- [126] J Fransson, O Eriksson, and A V Balatsky. Theory of spin-polarized scanning tunneling microscopy applied to local spins. *Phys. Rev. B*, 81:115454, 2010.
- [127] Y M Galperin, V I Kozub, and V M Vinokur. Low-frequency noise in tunneling through a single spin. *Phys. Rev. B*, 70:033405, 2004.
- [128] A V Balatsky, J Fransson, D Mozyrsky, and Y Manassen. STM NMR and nuclear spin noise. *Phys. Rev. B*, 73:184429, 2006.
- [129] J Fernández-Rossier. Theory of single-spin inelastic tunneling spectroscopy. *Phys. Rev. Lett.*, 102:256802, 2009.
- [130] O G Shpyrko, E D Isaacs, J M Logan, Y Feng, G Aeppli, R Jaramillo, H C Kim, T F Rosenbaum, P Zschack, M Sprung, S Narayanan, and A R Sandy. Direct measurement of antiferromagnetic domain fluctuations. *Nature*, 447:68, 2007.
- [131] V L R Jacques, E Pinsolle, S Ravy, G Abramovici, and D Le Bolloc'h. Charge- and spin-density waves observed through their spatial fluctuations by coherent and simultaneous x -ray diffraction. *Phys. Rev. B*, 89:245127, 2014.
- [132] J Christopher Dainty. Laser speckle and related phenomena. In *Berlin and New York, Springer-Verlag (Topics in Applied Physics. Volume 9), 1975. 298 p*, volume 9, 1975.
- [133] J W Goodman. Some fundamental properties of speckle. *JOSA*, 66:1145, 1976.
- [134] O Adam, A V Andreev, and B Spivak. Statistics of speckle patterns. *Phys. Rev. Lett.*, 97:223901, 2006.
- [135] C L Degen, M Poggio, H J Mamin, and D Rugar. Role of spin noise in the detection of nanoscale ensembles of nuclear spins. *Phys. Rev. Lett.*, 99:250601, 2007.
- [136] K Chandra, J Schlaglweit, C Wohlschlager, A Jerschow, and N Müller. Spin-noise-detected two-dimensional Fourier-transform NMR spectroscopy. *J. Phys. Chem. Lett.*, 4:3853, 2013.
- [137] T Sleator, E L Hahn, C Hilbert, and J Clarke. Nuclear-spin noise. *Phys. Rev. Lett.*, 55:1742, 1985.
- [138] N Zhao, J Honert, B Schmid, Michael Klas, J Isoya, M Markham, D Twitchen, F Jelezko, R-B Liu, H Fedder, and J Wrachtrup. Sensing single remote nuclear spins. *Nature Nanotechnology*, 7:657, 2012.
- [139] O E Dial, M D Shulman, S P Harvey, H Bluhm, V Umansky, and A Yacoby. Charge noise spectroscopy using coherent exchange oscillations in a singlet-triplet qubit. *Phys. Rev. Lett.*, 110:146804, 2013.
- [140] D S Smirnov. Spin noise of localized electrons interacting with optically cooled nuclei. *Phys. Rev. B*, 91:205301, 2015.
- [141] A Peres. Quantum theory: Concepts and methods. (*New York: Kluwer*), 2002.
- [142] R-B Liu, S-H Fung, H-K Fung, A N Korotkov, and L J Sham. Dynamics revealed by correlations of time-distributed weak measurements of a single spin. *New J. Phys.*, 12:013018, 2010.
- [143] A A Clerk, M H Devoret, S M Girvin, F Marquardt, and R J Schoelkopf. Introduction to quantum noise, measurement, and amplification. *Rev. Mod. Phys.*, 82:1155, 2010.
- [144] A Bednorz, W Belzig, and A Nitzan. Nonclassical time correlation functions in continuous quantum measurement. *New J. Phys.*, 14:013009, 2012.
- [145] A Bednorz, C Bruder, B Reulet, and W Belzig. Nonsymmetrized correlations in quantum noninvasive measurements. *Phys. Rev. Lett.*, 110:250404, 2013.
- [146] M Reed and B Simon. Methods of modern mathematical physics. *Academic Press*, vol. II, 1975.
- [147] H S Bennett and E A Stern. Faraday effect in solids. *Phys. Rev.*, 137:A448, 1965.
- [148] J Sinova, D Culcer, Q Niu, N A Sinitsyn, T Jungwirth, and A H MacDonald. Universal intrinsic spin-Hall effect. *Phys. Rev. Lett.*, 92:126603, 2004.
- [149] W-K Tse, A Saxena, D L Smith, and N A Sinitsyn. Spin and valley noise in two-dimensional Dirac materials. *Phys. Rev. Lett.*, 113:046602, 2014.
- [150] K F Mak, C Lee, J Hone, J Shan, and T F Heinz. Atomically thin MoS₂: A new direct-gap semiconductor. *Phys. Rev. Lett.*, 105:136805, 2010.
- [151] N A Sinitsyn, J E Hill, H Min, J Sinova, and A H MacDonald. Charge and spin Hall conductivity in metallic graphene. *Phys. Rev. Lett.*, 97:106804, 2006.
- [152] L Yang, N A Sinitsyn, W Chen, J Yuan, J Zhang, J Lou, and S A Crooker. Long-lived nanosecond spin relaxation and spin coherence of electrons in monolayer MoS₂ and WS₂. *Nature Physics*, 11:830, 2015.
- [153] C Testelin, F Bernardot, B Eble, and M Chamarro. Hole-spin dephasing time associated with hyperfine interaction in quantum dots. *Phys. Rev. B*, 79:195440, 2009.
- [154] C Sun and N A Sinitsyn. Exact transition probabilities for a linear sweep through a Kramers-Kronig resonance. *J. Phys. A: Math. and Th.*, 48:505202, 2015.
- [155] A V Kuhlmann, J Houel, A Ludwig, L Greuter, D Reuter, A D Wieck, M Poggio, and R J Warburton. Charge noise and spin noise in a semiconductor quantum device. *Nature Physics*, 9:570, 2013.
- [156] L Yang, P Glasenapp, A Grelich, D Reuter, A D Wieck, D R Yakovlev, M Bayer, and S A Crooker. Two-colour spin noise spectroscopy and fluctuation correlations reveal homogeneous linewidths within quantum-dot ensembles. *Nature Communications*, 5:4949, 2014.
- [157] G Semerjian, L F Cugliandolo, and A Montanari. On the stochastic dynamics of disordered spin models. *J. Stat. Phys.*, 115:493, 2004.
- [158] G N Bochkov and Yu E Kuzovlev. Nonlinear fluctuation-dissipation relations and stochastic models in nonequilibrium thermodynamics: I. Generalized fluctuation-dissipation theorem. *Physica A*, 106:443, 1981.
- [159] C Jarzynski. Nonequilibrium equality for free energy differences. *Phys. Rev. Lett.*, 78:2690, 1997.
- [160] N A Sinitsyn, A Akimov, and V Y Chernyak. Supersymmetry and fluctuation relations for currents in networks. *Phys. Rev. E*, 83:021107, 2011.
- [161] V Y Chernyak, M Chertkov, and N A Sinitsyn. The geometric universality of currents. *J. Stat. Mech.*, 2011:P09006, 2011.
- [162] N A Sinitsyn. Fluctuation relation for heat engines. *J. Phys. A: Math. Theor.*, 44:405001, 2011.
- [163] C Wang and D E Feldman. Fluctuation relations for spin currentst. *Phys. Rev. B*, 92:064406, 2015.
- [164] S Ganeshan and N A Sinitsyn. Fluctuation relations for current components in mesoscopic electric circuits. *Phys. Rev. B*, 84:245405, 2011.
- [165] R L Stratonovich. Nonlinear nonequilibrium thermodynamics I: Linear and nonlinear fluctuation-dissipation theorems. *Springer Series in Synergetics*, 1992.
- [166] R L Stratonovich. Nonlinear nonequilibrium thermodynamics II: Advanced theory. *Springer Series in Synergetics*, 1994.
- [167] V Y Chernyak and N A Sinitsyn. Pumping-restriction theorem for stochastic networks. *Phys. Rev. Lett.*, 101:160601, 2008.
- [168] S Rahav, J Horowitz, and C Jarzynski. Directed flow in nonadiabatic stochastic pumps. *Phys. Rev. Lett.*, 101:140602, 2008.
- [169] S Bandopadhyay, D Chaudhuri, and A M Jayannavar.

- Stochastic thermodynamics of macrospins with fluctuating amplitude and direction. *Phys. Rev. E*, 92:032143, 2015.
- [170] M Braun and J König. Faraday-rotation fluctuation spectroscopy with static and oscillating magnetic fields. *Phys. Rev. B*, 75:085310, 2007.
- [171] C W Gardiner. *Handbook of Stochastic Methods*. Springer; 4th ed. 2009 edition, Heidelberg, 2009.
- [172] Y V Pershin, V A Slipko, D Roy, and N A Sinitsyn. Two-beam spin noise spectroscopy. *Appl. Phys. Lett.*, 102:202405, 2013.
- [173] S Kos, A V Balatsky, P B Littlewood, and D L Smith. Spin noise of itinerant fermions. *Phys. Rev. B*, 81:064407, 2010.
- [174] Y V Pershin and V A Slipko. Radial spin helix in two-dimensional electron systems with Rashba spin-orbit coupling. *arXiv:1007.0853v1*, 2010.
- [175] F Reif. *Fundamentals of Statistical and Thermal Physics*. McGraw-Hill, 1965.
- [176] M I Dyakonov and V I Perel'. Spin relaxation of conduction electrons in noncentrosymmetric semiconductors. *Sov. Phys. Solid State*, 13:3023, 1972.
- [177] M I Dyakonov and V Y Kachorovskii. Spin relaxation of two-dimensional electrons in noncentrosymmetric semiconductors. *Sov. Phys. Semicond.*, 20:110, 1986.
- [178] G Dresselhaus. Spin-orbit coupling effects in zinc blende structures. *Phys. Rev.*, 100:580, 1955.
- [179] M M Glazov and E Ya Sherman. Theory of spin noise in nanowires. *Phys. Rev. Lett.*, 107:156602, 2011.
- [180] A V Poshakinskiy and S A Tarasenko. Spatiotemporal spin fluctuations caused by spin-orbit-coupled Brownian motion. *Phys. Rev. B*, 92:045308, 2015.
- [181] M V Sadovskii. *Diagrammatics: Lectures on Selected Problems in Condensed Matter Theory*. World Scientific Publishing Company, 2006.
- [182] A A Burkov and L Balents. Spin relaxation in a two-dimensional electron gas in a perpendicular magnetic field. *Phys. Rev. B*, 69:245312, 2004.
- [183] N A Sinitsyn, A H MacDonald, T Jungwirth, V K Dugaev, and J Sinova. Anomalous Hall effect in 2D Dirac band: link between Kubo-Streda formula and semiclassical Boltzmann equation approach. *Phys. Rev. B*, 75:045315, 2007.
- [184] T S Nunner, N A Sinitsyn, M F Borunda, Ar Abanov, C Timm, T Jungwirth, J Inoue, V K Dugaev, A H MacDonald, and J Sinova. Anomalous Hall effect in two-dimensional electron gas. *Phys. Rev. B*, 76:235312, 2007.
- [185] N A Sinitsyn. Semiclassical theories of the anomalous Hall effect. *J. Physics: Cond. Matt.*, 20:023201, 2008.
- [186] D Culcer and S Das Sarma. Anomalous Hall response of topological insulators. *Phys. Rev. B*, 83:245441, 2011.
- [187] J Swiebodzinski, A Chudnovskiy, T Dunn, and A Kamenev. Spin torque dynamics with noise in magnetic nanosystems. *Phys. Rev. B*, 82:144404, 2010.
- [188] K E Nagaev. Cascade Boltzmann-Langevin approach to higher-order current correlations in diffusive metal contacts. *Phys. Rev. B*, 66:075334, 2002.
- [189] J K Luo, H Thomas, D V Morgan, D Westwood, and R H Williams. The electrical breakdown properties of GaAs layers grown by molecular beam epitaxy at low temperature. *Semicond. Sci. Technol.*, 9:2199, 1994.
- [190] J S Blakemore. Semiconducting and other major properties of gallium arsenide. *J. Appl. Phys*, 53:R123, 1982.
- [191] M M Glazov. Spin fluctuations of non-equilibrium electrons and excitons in semiconductors. *JETP (in press); arXiv1511.07661*, 2015.
- [192] L S Levitov and G B Lesovik. Charge distribution in quantum shot noise. *JETP Lett.*, 58:230, 1993.
- [193] A Komnik and A O Gogolin. Full counting statistics for the Kondo dot. *Phys. Rev. Lett.*, 94:216601, 2005.
- [194] A G Abanov and D A Ivanov. Factorization of quantum charge transport for noninteracting fermions. *Phys. Rev. B*, 79:205315, 2009.
- [195] K Schonhammer. Full counting statistics for noninteracting fermions: Exact results and the Levitov-Lesovik formula. *Phys. Rev. B*, 75:205329, 2007.
- [196] T L Schmidt, A Komnik, and A O Gogolin. Hanbury Brown-Twiss correlations and noise in the charge transfer statistics through a multiterminal Kondo dot. *Phys. Rev. Lett.*, 98:056603, 2007.
- [197] F Li and N A Sinitsyn. Universality in higher order spin noise spectroscopy. *Phys. Rev. Lett.*, 116:026601, 2016.
- [198] S Pilgram, A N Jordan, E V Sukhorukov, and M Büttiker. Stochastic path integral formulation of full counting statistics. *Phys. Rev. Lett.*, 90:206801, 2003.
- [199] M Borunda, T S Nunner, T Luck, N A Sinitsyn, C Timm, J Wunderlich, T Jungwirth, A H MacDonald, and J Sinova. Absence of skew scattering mechanism in two dimensional systems: a test of anomalous Hall effect theory. *Phys. Rev. Lett.*, 99:066604, 2007.
- [200] N A Sinitsyn, N Hengartner, and I Nemenman. Adiabatic coarse-graining and simulations of stochastic biochemical networks. *Proceed. Nat. Acad. Sci. U.S.A.*, 106:10546, 2009.
- [201] F Li, A Saxena, D Smith, and N A Sinitsyn. Higher order spin noise statistics. *New. J. Phys.*, 15:113038, 2013.
- [202] A Chantasri, J Dressel, and A N Jordan. Action principle for continuous quantum measurement. *Phys. Rev. A*, 88:042110, 2013.
- [203] A Chantasri and A N Jordan. Stochastic path-integral formalism for continuous quantum measurement. *Phys. Rev. A*, 92:032125, 2015.
- [204] W D Rice, W Liu, T A Baker, N A Sinitsyn, V I Klimov, and S A Crooker. Revealing giant internal magnetic fields due to spin fluctuations in magnetically doped colloidal nanocrystals. *Nature Nanotechnology*, 11:137, 2016.
- [205] S M Ryabchenko and Y G Semenov. Spin-correlation effects for a large-radius electron center in a magnetically mixed semiconductor. *JETP*, 57:825, 1983.
- [206] L Cywiński, V V Dobrovitski, and S Das Sarma. Spin echo decay at low magnetic fields in a nuclear spin bath. *Phys. Rev. B*, 82:035315, 2010.
- [207] L D Landau and L M Lifshitz. Quantum mechanics. non-relativistic theory. *Butterworth-Heinemann; 3 edition*, 1981.
- [208] D S Smirnov. Spin noise of localized electrons interacting with optically cooled nuclei. *Phys. Rev. B*, 91:205301, 2015.
- [209] A Faribault and D Schurichts. Integrability based analysis of the hyperfine interaction induced decoherence in quantum dots. *Phys. Rev. Lett.*, 110:040405, 2013.
- [210] J Hackmann and F B Anders. Spin noise in the anisotropic central spin model. *Phys. Rev. B*, 89:045317, 2014.
- [211] G S Uhrig, J Hackmann, D Stanek, J Stolze, and F B Anders. Conservation laws protect dynamic spin correlations from decay: Limited role of integrability in the central spin model. *Phys. Rev. B*, 90:060301(R), 2014.
- [212] R Dekeyser and M H Lee. Time-dependent correlations for spin Van der Waals systems. *Phys. Rev. B*, 19:265, 1979.
- [213] M Chertkov and I Kolokolov. Equilibrium dynamics of a paramagnetic cluster. *Phys. Rev. B*, 51:3974(R), 1995.
- [214] D S Smirnov, M M Glazov, and E L Ivchenko. Effect of exchange interaction on the spin fluctuations of localized electrons. *Physics of the Solid State*, 56:254, 2014.

- [215] J Hackmann, D S Smirnov, M M Glazov, and F B Anders. Spin noise in a quantum dot ensemble: From a quantum mechanical to a semi-classical description. *physica status solidi (b)*, 251:1270, 2014.
- [216] M M Glazov and E L Ivchenko. Spin noise in quantum dot ensembles. *Phys. Rev. B*, 86:115308, 2012.
- [217] M M Glazov. Spin noise of localized electrons: Interplay of hopping and hyperfine interaction. *Phys. Rev. B*, 91:195301, 2015.
- [218] Y V Pershin and V Privman. Spin relaxation of conduction electrons in semiconductors due to interaction with nuclear spins. *Nano Letters*, 3:695–700, 2003.
- [219] V V Mkhitarian and V V Dobrovitski. Hyperfine-induced spin relaxation of a diffusively moving carrier in low dimensions: Implications for spin transport in organic semiconductors. *Phys. Rev. B*, 92:054204, 2015.
- [220] D Roy, Y Li, A Grelich, Yu V Pershin, A Saxena, and N A Sinitsyn. Spin noise spectroscopy of quantum dot molecules. *Phys. Rev. B*, 88:045320, 2013.
- [221] A G Sykes, D Solenov, and D Mozyrsky. Bloch-Redfield theory of high-temperature magnetic fluctuations in interacting spin systems. *Phys. Rev. B*, 85:174419, 2012.
- [222] K Agarwal, E Demler, and I Martin. $1/f^\alpha$ noise and generalized diffusion in random heisenberg spin systems. *Phys. Rev. B*, 92:184203, 2015.
- [223] V N Vapnik. Statistical learning theory. *Wiley-Interscience*, 1998.
- [224] S Kay. Fundamentals of statistical signal processing: Estimation theory. *Prentice Hall*, 1993.
- [225] P I Hurtado and P L Garrido. Spontaneous symmetry breaking at the fluctuating level. *Phys. Rev. Lett.*, 107:180601, 2011.
- [226] I Lesanovsky, M van Horssen, M Guță, and J P Garrahan. Characterization of dynamical phase transitions in quantum jump trajectories beyond the properties of the stationary state. *Phys. Rev. Lett.*, 110:150401, 2013.
- [227] C P Espigares, P L Garrido, and P I Hurtado. Dynamical phase transition for current statistics in a simple driven diffusive system. *Phys. Rev. E*, 87:032115, 2013.
- [228] D A Ivanov and A G Abanov. Characterizing correlations with full counting statistics: Classical Ising and quantum XY spin chains. *Phys. Rev. E*, 87:022114, 2013.
- [229] B-B Wei and R-B Liu. Lee-Yang zeros and critical times in decoherence of a probe spin coupled to a bath. *Phys. Rev. Lett.*, 109:185701, 2012.
- [230] J Ren and N A Sinitsyn. Braid group and topological phase transitions in stochastic dynamics. *Phys. Rev. E*, 87:050101(R), 2013.
- [231] T D Lee and C N Yang. Statistical theory of equations of state and phase transitions. ii. Lattice gas and Ising model. *Phys. Rev.*, 87:410, 1952.
- [232] T D Lee and C N Yang. Statistical theory of equations of state and phase transitions. i. Theory of condensation. *Phys. Rev.*, 87:404, 1952.
- [233] X Peng, H Zhou, B-B Wei, J Cui, J Du, and R-B Liu. Experimental observation of Lee-Yang zeros. *Phys. Rev. Lett.*, 114:010601, 2015.
- [234] C Flindt and J P Garrahan. Trajectory phase transitions, Lee-Yang zeros, and high-order cumulants in full counting statistics. *Phys. Rev. Lett.*, 110:050601, 2013.
- [235] J M Hickey, C Flindt, and J P Garrahan. Trajectory phase transitions and dynamical Lee-Yang zeros of the Glauber-Ising chain. *Phys. Rev. E*, 88:012119, 2013.
- [236] F Li, J Ren, and N A Sinitsyn. Quantum Zeno effect as a topological phase transition in full counting statistics and spin noise spectroscopy. *Europhys. Lett.*, 105:27001, 2014.
- [237] A G Kofman and G Kurizki. Acceleration of quantum decay processes by frequent observations. *Nature*, 405:546, 2000.
- [238] G J Milburn and M J Gagen. Rydberg-atom phase-sensitive detection and the quantum Zeno effect. *Phys. Rev. A*, 46:1578, 1992.
- [239] E P Danieli, G A Alvarez, P R Levsteinand, and H M Pastawski. Quantum dynamical phase transition in a system with many-body interactions. *Solid State Comm.*, 141:422, 2007.
- [240] B Misra and E C G Sudarshan. The Zeno's paradox in quantum theory. *J. Math. Phys.*, 18:756, 1977.
- [241] J Wolters, M Strauss, R S Schoenfeld, and O Benson. Quantum Zeno phenomenon on a single solid-state spin. *Phys. Rev. A*, 88:020101(R), 2013.
- [242] H F Song, S Rachel, C Flindt, I Klich, N Laflorencie, and K Le Hur. Bipartite fluctuations as a probe of many-body entanglement. *Phys. Rev. B*, 85:035409, 2012.
- [243] S V Isakov, M B Hastings, and R G Melko. Topological entanglement entropy of a Bose-Hubbard spin liquid. *Nature Phys.*, 7:772, 2011.
- [244] D A Abanin and E Demler. Measuring entanglement entropy of a generic many-body system with a quantum switch. *Phys. Rev. Lett.*, 109:020504, 2012.
- [245] O A Castro-Alvaredo and B Doyon. Entanglement entropy of highly degenerate states and fractal dimensions. *Phys. Rev. Lett.*, 108:120401, 2012.
- [246] Y Zhang, T Grover, and A Vishwanath. Entanglement entropy of critical spin liquids. *Phys. Rev. Lett.*, 107:067202, 2011.
- [247] P Calabrese, M Mintchev, and E Vicari. Entanglement entropy of one-dimensional gases. *Phys. Rev. Lett.*, 107:020601, 2011.
- [248] M P Zaletel, J H Bardarson, and J E Moore. Logarithmic terms in entanglement entropies of 2D quantum critical points and shannon entropies of spin chains. *Phys. Rev. Lett.*, 107:020402, 2011.
- [249] M P Hertzberg and F Wilczek. Some calculable contributions to entanglement entropy. *Phys. Rev. Lett.*, 106:050404, 2011.
- [250] C Nadal, S N Majumdar, and M Vergassola. Phase transitions in the distribution of bipartite entanglement of a random pure state. *Phys. Rev. Lett.*, 104:110501, 2010.
- [251] A Kitaev and J Preskill. Topological entanglement entropy. *Phys. Rev. Lett.*, 96:110404, 2006.
- [252] E Fradkin and J E Moore. Entanglement entropy of 2D conformal quantum critical points: Hearing the shape of a quantum drum. *Phys. Rev. Lett.*, 97:050404, 2006.
- [253] J Eisert and T J Osborne. General entanglement scaling laws from time evolution. *Phys. Rev. Lett.*, 97:150404, 2006.
- [254] A T Bollinger, G Dubuis, J Yoon, D Pavuna, J Misewich, and I Božović. Superconductor-insulator transition in $\text{La}_2\text{xSrxCuO}_4$ at the pair quantum resistance. *Nature*, 472:458, 2011.
- [255] M Wiesniak, V Vedral, and C Brukner. Magnetic susceptibility as a macroscopic entanglement witness. *New J. Phys.*, 7:258, 2005.
- [256] G Tóth, C Knapp, O Gühne, and H J Briegel. Optimal spin squeezing inequalities detect bound entanglement in spin models. *Phys. Rev. Lett.*, 99:250405, 2007.
- [257] A S Sørensen and K Mølmer. Entanglement and extreme spin squeezing. *Phys. Rev. Lett.*, 86:4431, 2001.
- [258] P Hauke, M Heyl, L Tagliacozzo, and P Zoller. Measuring multipartite entanglement through dynamic susceptibilities. *Nature Physics (published online)*, 2016.
- [259] T Kuroiwa. Faraday rotation of ferromagnetic (Ga,Mn)As. *Electronics Letters*, 34:190, 1998.
- [260] C Sun and V L Pokrovsky. Spin correlations in quantum

- wires. *Phys. Rev. B*, 91:161305(R), 2015.
- [261] O A Tretiakov, K S Tikhonov, and V L Pokrovsky. Spin resonance in Luttinger liquid with spin-orbit interaction. *Phys. Rev. B*, 88:125143, 2013.
- [262] Luis G. G. V. Dias da Silva and Rogério de Sousa. Spin versus charge noise from Kondo traps. *Phys. Rev. B*, 92:085123, 2015.
- [263] D Roy, R Singh, and R Moessner. Probing many-body localization by spin noise spectroscopy. *Phys. Rev. B*, 92:180205(R), 2015.
- [264] F Li, W M Saslow, and V L Pokrovsky. Phase diagram for magnon condensate in yttrium iron garnet film. *Scientific Reports*, 3:1372, 2013.
- [265] C Nisoli, R Wang, J Li, W F McConville, P E Lammert, P Schiffer, and V H Crespi. Ground state lost but degeneracy found: The effective thermodynamics of artificial spin ice. *Phys. Rev. Lett.*, 98:217203, 2007.
- [266] C Nisoli, R Moessner, and P Schiffer. Colloquium: Artificial spin ice: Designing and imaging magnetic frustration. *Rev. Mod. Phys.*, 85:1473, 2013.
- [267] M I Dyakonov and V I Perel. Current induced spin orientation of electrons in semiconductors. *Phys. Lett. A*, 35:459, 1971.
- [268] J E Hirsch. Spin Hall effect. *Phys. Rev. Lett.*, 83:1834, 1999.
- [269] N A Sinitsyn, E M Hankiewicz, W Teizer, and J Sinova. Spin Hall and spin-diagonal conductivity in the presence of Rashba and Dresselhaus spin-orbit coupling. *Phys. Rev. B*, 70:081312(R), 2004.
- [270] Y A Bychkov and E I Rashba. Properties of a 2D electron-gas with lifted spectral degeneracy. *JETP Lett.*, 39:78, 1984.
- [271] Y V Pershin and M Di Ventra. A voltage probe of the spin Hall effect. *J. Phys.: Cond. Matt.*, 20:025204, 2007.
- [272] H Noh, S-J Lee, and S H Chun. Hall voltages without a magnetic field in a non-uniform two-dimensional electron system. *J. Phys.: Cond. Matt.*, 25:045301, 2013.